

DEFECT STRUCTURE AND ELECTRICAL PROPERTIES
OF CaO-STABILIZED ZrO₂

BY

NORMAN MAN-PAK LOW

B. Sc., The University of British Columbia, 1961

A THESIS SUBMITTED IN PARTIAL FULFILMENT OF
THE REQUIREMENT FOR THE DEGREE OF
MASTER OF SCIENCE
in the Department
of
METALLURGY

We accept this thesis as conforming to the
standard required from candidates for the degree
of MASTER OF SCIENCE

Members of the Department
of Metallurgy

THE UNIVERSITY OF BRITISH COLUMBIA

April, 1967

In presenting this thesis in partial fulfilment of the requirements for an advanced degree at the University of British Columbia, I agree that the Library shall make it freely available for reference and study. I further agree that permission for extensive copying of this thesis for scholarly purposes may be granted by the Head of my Department or by his representatives. It is understood that copying or publication of this thesis for financial gain shall not be allowed without my written permission.

Department of Metallurgy

The University of British Columbia
Vancouver 8, Canada

Date: April 26, 1967

ABSTRACT

The cubic fluorite-type solid solution of ZrO_2 containing 15 mole % CaO has been prepared by the hot-pressing process. The effects of annealing on the change of lattice parameter, electrical properties, and density of the solid solution have been investigated.

The lattice parameter of the cubic solid solution was found to depend on the heat treatment of the specimens. The decrease of lattice parameter with annealing temperature and time has been interpreted either in terms of the removal of interstitial oxygen ions from the lattice or in terms of the inhomogeneous distribution of the CaO in the ZrO_2 lattice.

The activation energy for conduction was also found to depend on the heat treatment of the specimens. The variation of activation energy with annealing temperature has been interpreted in terms of pairing and clustering of the oxygen vacancies with the substitutional Ca ions in the solid solution. The minimum activation energy obtained in the present investigation corresponded to the theoretically predicted activation energy for the migration of oxygen vacancies.

ACKNOWLEDGEMENT

The author is grateful for the advice and encouragement given by his research director, Dr. A. C. D. Chaklader.

Thanks are extended to Dr. E. Peters for his criticisms and suggestions in the kinetic analysis, to Mr. A. G. Fowler of the Computing Centre, University of British Columbia for his assistance in setting up the FORTRAN computer programme, and to Mr. P. Bruin for his technical assistance.

He also wishes to thank the various members of the faculty and fellow graduate students for many helpful discussions.

Financial assistance which was provided by the National Research Council of Canada under Grant No. A-2461 is gratefully acknowledged.

TABLE OF CONTENTS

	<u>Page</u>
I. INTRODUCTION AND REVIEW OF LITERATURE	1
(A) Introduction	1
(B) Review of Literature	3
1. Phase Transformation and Stabilization of Zirconia ..	3
a. Phase Transformation of ZrO_2	3
b. Stabilization of ZrO_2	4
2. Crystalline Structure and Relationship of Lattice Parameter With Compositions in the $CaO-ZrO_2$ System ..	7
a. Crystalline Structure	7
b. Relationship of Lattice Parameter With Compositions	8
3. Cation and Anion Diffusion in the $CaO-ZrO_2$ System ..	11
a. Anion (Oxygen Ion) Diffusion	11
b. Cation Diffusion	12
4. Infrared Absorption Spectroscopy of Pure ZrO_2 and CaO -stabilized ZrO_2	14
5. Internal Friction in ZrO_2 Containing CaO	15
6. Electrical Conductivity in the $CaO-ZrO_2$ Solid Solutions	19
a. Electrical Conductivity Kinetics	19
b. Ionic Conductivity.....	20
c. Electronic Conductivity.....	22
d. Relationship of Electrical Conductivity and Diffusion Coefficient	24
II. EXPERIMENTAL PROCEDURE	25
(A) Materials and Specimen Preparation	25
1. Materials Preparation	25

TABLE OF CONTENTS (cont'd)

	<u>Page</u>
2. Specimen Preparation	25
(B) Phase Identification	26
(C) Annealing Procedure	26
(D) Precise Lattice Parameter Measurement	27
1. Experimental Procedure	27
2. Lattice Parameter Calculation	28
(E) Infrared Absorption Spectroscopy	28
(F) Electrical Conductivity Measurements	29
1. Specimen Preparation	29
2. Apparatus and Equipment	29
3. Measurement Procedure	30
(G) Porosity and True Density Measurements	32
III. EXPERIMENTAL RESULTS	33
(A) Phase Identification of the $Zr_{0.85}Ca_{0.15}O_{1.85}$ Solid Solution	33
1. X-ray Diffraction	33
2. Infrared Absorption Spectra	35
(B) Precise Lattice Parameter of the $Zr_{0.85}Ca_{0.15}O_{1.85}$ Solid Solution	38
1. Effect of Annealing Temperature on the Lattice Parameter	38
2. Relationship Between Lattice Parameter and Band Frequency of the Infrared Absorption Spectra	43
3. Effect of Annealing Time on the Lattice Parameter ..	44
(C) Electrical Conductivity of the $Zr_{0.85}Ca_{0.15}O_{1.85}$ Solid Solution	46
1. Electrical Conductivity as a Function of Temperature	46
2. Calculation of the Oxygen Ion Diffusion Coefficients From Electrical Conductivity Data	53

TABLE OF CONTENTS (cont'd)

	<u>Page</u>
(D) Porosity and True Density of the $Zr_{0.85}Ca_{0.15}O_{1.85}$ Solid Solution	58
1. Apparent Porosity of the Hot-pressed Specimens	58
2. True Density of the $Zr_{0.85}Ca_{0.15}O_{1.85}$ Solid Solution	60
(E) Chemical Analysis of the Hot-pressed $CaO-ZrO_2$ Specimens.	60
 IV. DISCUSSION	 62
(A) Lattice Contraction or Shrinkage of the Cubic Unit Cell in the $Zr_{0.85}Ca_{0.15}O_{1.85}$ Solid Solution	62
(B) Effect of Annealing on the Electrical Properties of the $Zr_{0.85}Ca_{0.15}O_{1.85}$ Solid Solution	70
(C) Effect of Heat Treatment on the Oxygen Ion Diffusion in the $CaO-ZrO_2$ Solid Solution	77
 V. SUMMARY AND CONCLUSIONS	 79
 VI. SUGGESTIONS FOR FUTURE WORK	 81
 VII. APPENDICES	 82
APPENDIX I : Experimental Data for Precise Lattice Parameter Measurements	82
APPENDIX II : Experimental Data for Electrical Conductivity Measurements	87
APPENDIX III : Experimental Data for Porosity and True Density Measurements	93
APPENDIX IV : Estimation of Error	96
APPENDIX V : Cohen's Method for Precise Lattice Parameter Calculation	98
APPENDIX VI : Derivation of the Nernst-Einstein Equation for Diffusion Coefficient Calculation from Electrical Conductivity Data	101

TABLE OF CONTENTS (cont'd)

	<u>Page</u>
APPENDIX VII : Apparent Porosity and Bulk Density Determination	103
APPENDIX VIII : True Density Determination	104
APPENDIX IX : Theoretical Density Calculation of the CaO-ZrO ₂ Solid Solutions for the Oxygen Vacancy Model and the Oxygen Interstitial Model	105
VIII. BIBLIOGRAPHY	106

LIST OF FIGURES

<u>No.</u>	<u>Page</u>
1. Phase equilibrium diagram for the CaO-ZrO ₂ system	6
2. Fluorite-type structure of the CaO-ZrO ₂ cubic solid solutions.	6
3. Change of densities with CaO content in the CaO-ZrO ₂ solid solutions after annealing at high temperatures	9
4. Change of lattice parameter with CaO content in the CaO-ZrO ₂ solid solutions	10
5. Infrared absorption spectra of monoclinic ZrO ₂ and CaO-stabilized ZrO ₂	16
6. Schematic diagram of the high temperature electrical conductivity furnace and sample holder	31
7. X-ray diffraction patterns of the unreacted and reacted CaO-ZrO ₂ compositions	34
8. Infrared absorption spectra of the monoclinic ZrO ₂ and partially CaO-stabilized ZrO ₂	36
9. Infrared absorption spectra of the completely CaO-stabilized ZrO ₂ after heat treatment	37
10. Typical X-ray diffraction pattern of powdered samples of the Zr _{0.85} Ca _{0.15} O _{1.85} solid solution	40
11. Decrease of lattice parameter as a function of annealing temperature	41
12. Decrease of lattice parameter as a function of annealing temperature (over-all data with mean values)	42
13. Relationship between lattice parameter and peak band frequency of the infrared absorption spectra for the CaO-stabilized ZrO ₂ solid solution after heat treatment.....	45
14. Decrease of lattice parameter as a function of annealing time.	47
15. Arrhenius plot of electrical conductivity and temperature.	48
16. Change of activation energy for electrical conduction with annealing temperature	49
17. Comparison between the electrical conductivity data from the literature and the present data for the Zr _{0.85} Ca _{0.15} O _{1.85} solid solution	51

LIST OF FIGURES (cont'd)

<u>No.</u>	<u>Page</u>
18. Variation of electrical conductivity as measured immediately and after 30-45 minutes of soaking at the same temperature	52
19. Change of electrical conductivity as measured during the heating and cooling cycles (specimen annealed @900°C).....	54
20. Change of electrical conductivity as measured during the heating and cooling cycles (specimen annealed @1400°C)....	55
21. Arrhenius plot of oxygen ion diffusion coefficients and temperature	56
22. Change of activation energy for oxygen ion diffusion with annealing temperature	57
23. Comparison between the oxygen ion diffusion coefficient data in the literature and the present data in the CaO-ZrO ₂ system	59
24. Change of densities with annealing temperatures	61
25. Relative decrease of lattice parameter with annealing time....	67
26. Arrhenius plot of the rate of relative decrease of lattice parameter and temperature	69
27. Change of excess energy for conduction with annealing temperature	74

LIST OF TABLES

<u>No.</u>		<u>Page</u>
I	X-ray diffraction peaks of several compounds in the 27°-33° of 2θ values	33
II	Infrared absorption band frequencies of the monoclinic ZrO ₂ and CaO-stabilized ZrO ₂	38
III	Chemical analysis of the CaO-ZrO ₂ solid solutions	62
IV	Energies of oxygen vacancy motion and dissociation in the CaO-ZrO ₂ system	73

I. INTRODUCTION AND REVIEW OF LITERATURE

(A) Introduction

During the past ten years there have been numerous outstanding developments in aircraft propulsion, nuclear systems, metallurgical research, and other closely allied fields. To meet the requirements of these fields, considerable efforts have been directed toward the investigation and development of new refractory compounds and combinations. Over the years, the chemistry of ZrO_2 has attracted the attention of both the theoretical scientist and the practical industrialist interested in high-temperature materials. Zirconia (ZrO_2) is considered as one of the most refractory oxides. It has not only a high melting point ($2700^\circ C$) but also other distinctive properties, such as chemical inertness, corrosion resistance to oxidizing and reducing atmospheres and low neutron capture cross section. Zirconia also is polymorphic and possesses a complex crystal structure. Thus, extensive research has been done in studying its structure, polymorphism and refractory properties.

The application of pure ZrO_2 is limited due to the disruptive volume change associated with its polymorphic transformation. However, this limitation can be overcome by the addition of certain foreign oxides with which ZrO_2 forms solid solutions. The addition of a small amount of Calcia (CaO) to ZrO_2 results in the formation of stabilized cubic solid solutions which remain stable at temperatures up to $2000^\circ C$. Because of the stabilization, ZrO_2 -based solid solutions have been used as a heat exchanger of ceramic-heated blowdown jets and other aerodynamic devices, as potential fuels incorporated with urania and thoria for nuclear power.

application, and as heating elements in high temperature furnaces. The CaO-ZrO₂ cubic solid solutions also possess rather unique electrical properties, and as a result have considerable usefulness as solid electrolytes in galvanic and fuel cells. Electromotive force measurements on galvanic cells which utilize the solid electrolyte of CaO-ZrO₂ have proved to be a valued and accepted technique for obtaining useful thermodynamic data, particularly for the determination of elevated-temperature thermodynamic properties of metallic oxides.

The solid solutions of CaO-ZrO₂ used in each potential application are generally custom-made products. The voluminous literature reporting the properties of these solid solutions, particularly on the electrical properties, frequently show disagreement between workers. This inconsistency is generally inherent to the purity of the starting material and the technique used in preparation. The common method for preparing CaO-ZrO₂ solid solutions is the method of partially reacting CaCO₃ and ZrO₂ at temperatures between 1300-1400°C and then sintering the reacted material at higher temperatures, followed by a long period of annealing at low temperature. The CaO-ZrO₂ cubic solid solutions are nonstoichiometric and their electrical properties are structure sensitive. The temperature of specimen preparation and subsequent annealing may have a bearing on the defect-structure.

The purpose of the present investigation is two-fold:

1. to prepare a 15 mole % CaO + 85 mole % ZrO₂ cubic solid solution by the hot-pressing technique and to anneal the specimens at various temperatures; and
2. to observe any change in the crystalline structure and the electrical

conductivity with annealing temperature and time. The choice of the composition, 15 mole % CaO + 85 mole % ZrO₂, is dictated by the available data in the literature on this particular solid solution as it provides adequate data for comparison.

(B) Review of Literature

(1). Phase Transformation and Stabilization of Zirconia

a. Phase Transformation

The existence of two structural modifications of zirconia was first reported by Van Arkel¹ in 1924. Several years later Ruff and Ebert² definitely established the phenomenon of polymorphism in this material by measuring the lattice constants and densities of both the monoclinic (density = 5.68 gm/cc) and tetragonal (density = 6.10 gm/cc) forms. The existence of a modification of zirconia with hexagonal symmetry reported a decade later by Cohn³ has never been confirmed. The reversible reaction of monoclinic ZrO₂ \rightleftharpoons tetragonal ZrO₂ has been observed to occur in the range 1100-1200°C. All attempts to stabilize the high-temperature tetragonal modification by rapid quenching have been unsuccessful to date^{4,5}. Prior to 1962, it was generally assumed that a cubic modification of chemically pure zirconia could not exist^{6,7,8}. Recent data have indicated, however, that above 2200°C the reversible formation of a cubic form of ZrO₂ is indeed possible^{9,10}.

The monoclinic \rightleftharpoons tetragonal transformation in zirconia occurs at a definite temperature and pressure, possesses a latent heat of (endothermic) reaction, involves a change of structural ordering, and has a large

disruptive volume change. This indicates that the monoclinic \rightleftharpoons tetragonal transformation is a phase transition "of the first order"¹¹. Furthermore, Wolten¹² has pointed out that the ZrO_2 transformation is indeed both diffusionless, (ie., all atoms have the same neighbours in either phase,) and of the martensitic type.

b. Stabilization of Zirconia

The stabilization of ZrO_2 has been an important subject of research for many years. Since the discovery of the reversible transformation of ZrO_2 , Geller and Yavorsky¹³ confirmed and extended earlier findings which indicated that during the transformation a large and rapid volume change occurred and that the phase transformation could be suppressed by the addition of certain oxides which resulted in the formation of solid solutions having a cubic lattice. A considerable amount of research work has been carried out in studying the reaction of ZrO_2 with various oxides. Roth¹⁴ has formulated a general set of rules which can be used for the reaction of ZrO_2 in various binary oxide systems. These rules govern the solid-state reaction of ZrO_2 with oxides of the divalent, trivalent, tetravalent, and pentavalent ions.

Duvez, Odell and Brown¹⁵ were among the earlier researchers on the subject of stabilization of ZrO_2 with other oxides. They established the phase diagram for the binary system of $CaO-ZrO_2$, (Fig. 1), and the binary system of $MgO-ZrO_2$. Webber, Garrett, Mauer and Schwartz¹⁶ later extended the earlier studies to cover more binary and ternary systems. Hoch and Mathur¹⁷ have studied the formation of cubic ZrO_2 with transition

metals of group V and VI and their oxides. Smoot and Ryan¹⁸ have investigated the initial temperatures of the ZrO_2 phase change and the reactions for the formation of solid solution using X-ray diffraction. The study of the reaction of the ZrO_2 with other oxides or transition metals remains an open field in research.

A small amount of CaO will form a solid solution with ZrO_2 possessing cubic fluorite-type structure. An equal molar mixture of CaO and ZrO_2 will form a $CaZrO_3$ compound rather than a solid solution. Duwez et al showed that solid solutions containing 16 to 30 mole % CaO have cubic symmetry when quenched from 2000°C. On the other hand, Hund¹⁹ found that the cubic phase existed only from 10 to 20 mole % CaO in specimens prepared at 1460°C. Dietzel and Tober²⁰ reported that cubic solid solutions of ZrO_2 extended from 7 to 24 mole % CaO at 1800°C and from 14 to 20 mole % CaO at 1400°C. A recent Russian investigation²¹ placed the cubic phase field between 10 and 40 mole % CaO in specimens prepared at 1500°C. Tien and Subbarao²² delineated the cubic phase boundaries by careful X-ray diffraction studies and observed that the cubic phase existed from 12-13 mole % to 20-23 mole % CaO in specimens prepared at 2000°C and quenched from 1400°C. Cocco²³ has investigated, by reflection microscopy, the composition limits at high temperature of the cubic phase of $CaO-ZrO_2$ and reported a cubic phase composed of 5-10 mole % CaO and 90-95 mole % ZrO_2 . Thus, considerable disagreement exists concerning the cubic phase boundaries in the $CaO-ZrO_2$ system. These variations can be most probably attributed to the varying purity of the materials, the method of preparation, and finally to the reaction temperatures used in preparing the solid solution.

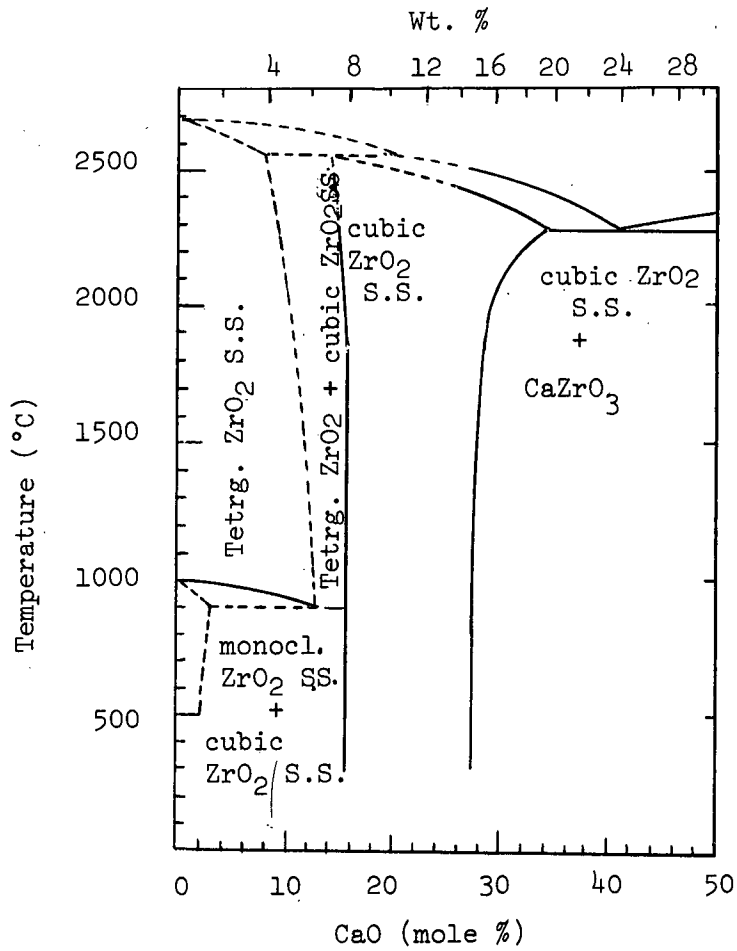


Figure 1. Phase Equilibrium Diagram for the CaO-ZrO₂ system. (after Duwez and Odell⁸)

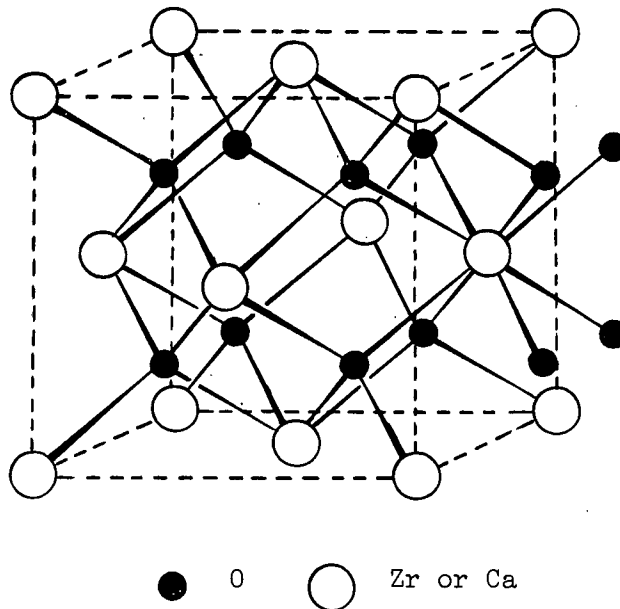


Figure 2. Fluorite-Type Structure of CaO-ZrO₂ Cubic Solid Solutions. (after Kingery⁵³)

In spite of these variations in the cubic phase boundaries, the composition of 15 mole % CaO and 85 mole % ZrO₂ is definitely within the single cubic phase region. This is probably the determining factor which prompts most research workers to choose this composition for their investigations.

(2) Crystal Structure and Relationship with Compositions for the CaO-ZrO₂ Cubic Solid Solutions

a. Crystal Structure

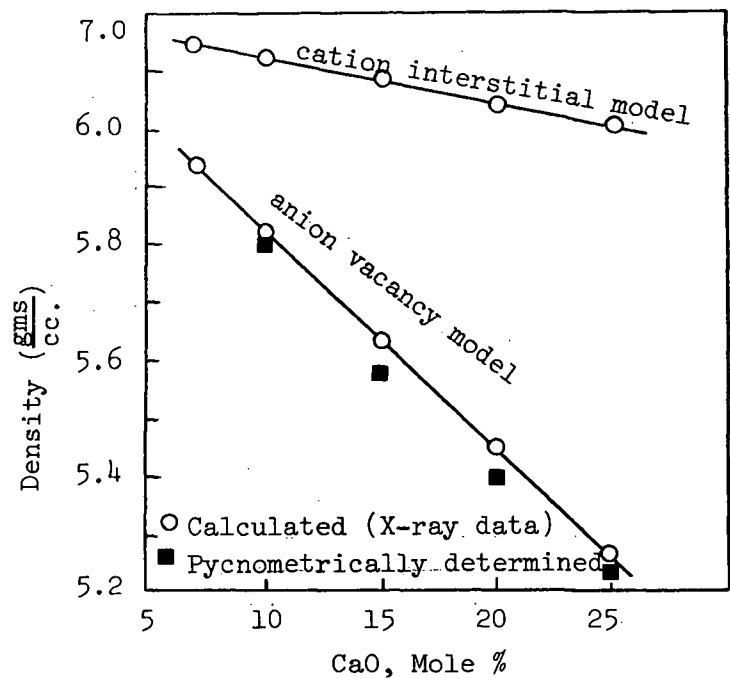
The CaO-ZrO₂ solid solutions crystallize with the cubic fluorite structure of the space group Fm3m¹⁹. In the fluorite structure the anions are in simple cubic packing with half the interstices filled by cations. This gives rise to a unit cell ^{with} ~~in which~~ a space at the center of the unit cell corresponding to unfilled interstices in the simple cubic anion lattice. The atomic arrangement in a fluorite-type structure is given in Fig. 2.

Hund¹⁹ established by density measurements that the cation lattice sites were completely filled with Zr⁴⁺ and Ca²⁺ ions and that enough oxygen vacancies were created to provide charge compensation distributed at random over the oxygen sites in order to preserve electrical neutrality. Using X-ray intensity studies, Tien and Subbarao²² have confirmed the structural model with Zr⁴⁺ and Ca²⁺ ions completely filling the cation lattice sites, and oxygen ion sites, equal in number to the mole % CaO added, being vacant. The formation of a cubic fluorite-type structure of CaO-ZrO₂ is assumed to be a random substitutional solid solution. The Zr⁴⁺ ions are randomly replaced by the added Ca²⁺ ions.

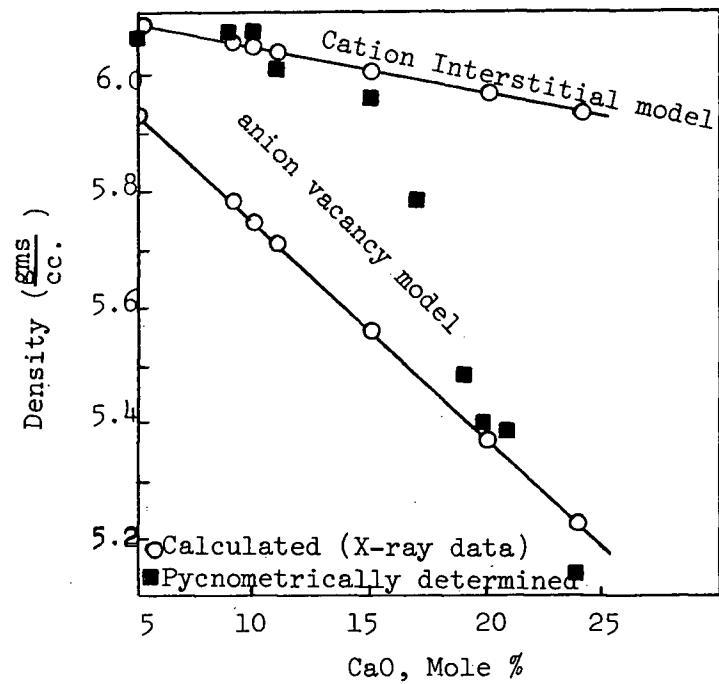
Recently, Diness and Roy²⁴ reported that there is evidence that the predominantly oxygen vacancy model changes to a cation interstitial model at higher temperatures. According to their data, when the CaO-ZrO₂ solid solutions were equilibrated at 1600°C and 1800°C respectively and were then quenched at about 1000°C/second, the pycnometer density measurements and X-ray data on the lattice parameter showed significantly different results. In the 1600°C data, the measurements confirmed the classically accepted model for an effectively "pure" anion vacancy defect for that material. From the 1800°C data, it was observed that in the low CaO concentration region (up to at least 15 mole%) the measured densities indicated a predominantly cation interstitial model, as shown in Fig. 3. However, they concluded that at this stage of the work the results had not defined the equilibrium concentration of defects at any temperature with great precision since they could not be sure that the "quenching" perfectly reproduced the high temperature defect character. No subsequent work has been published to support their observations.

b. Relationship of Compositions with Lattice Parameter

The relationship between the lattice parameter and compositions of the cubic solid solutions of CaO-ZrO₂ was first investigated by Hund¹⁹, who observed that the lattice parameter increased as the mole % of CaO added to mixture increased. A linear relationship was obtained in a plot between lattice parameter and mole % CaO with the lattice parameter increasing from $5.1137 \pm 0.0007 \text{ \AA}$ (10.3 mole % CaO) to $5.1276 \pm 0.0005 \text{ \AA}$ (23.9 mole % CaO), as shown in Fig. 4b. Tien and Subbarao²² extended the earlier investigation and also observed that a linear relationship existed between lattice parameter and mole% CaO in the cubic field as shown in Fig. 4a. The lattice parameter obtained in Tien and Subbarao's investigation varied from $5.129 \pm 0.005 \text{ \AA}$ (12 mole% CaO) to $5.143 \pm 0.005 \text{ \AA}$ (22 mole % CaO). It can be seen that although the change of lattice parameter between the

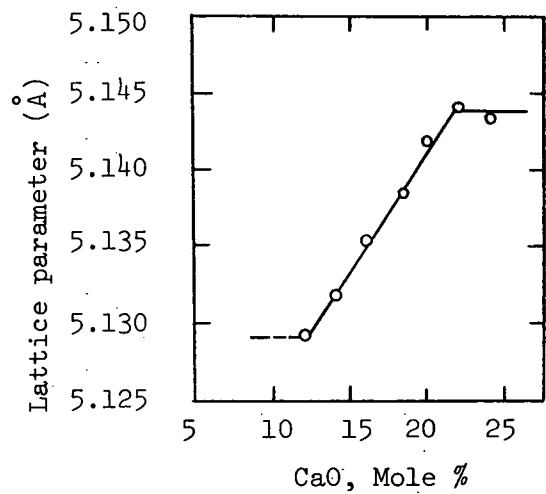


Comparison of densities determined by X-ray and pycnometric methods for the CaO-ZrO₂ crystalline solutions quenched from 1600°C

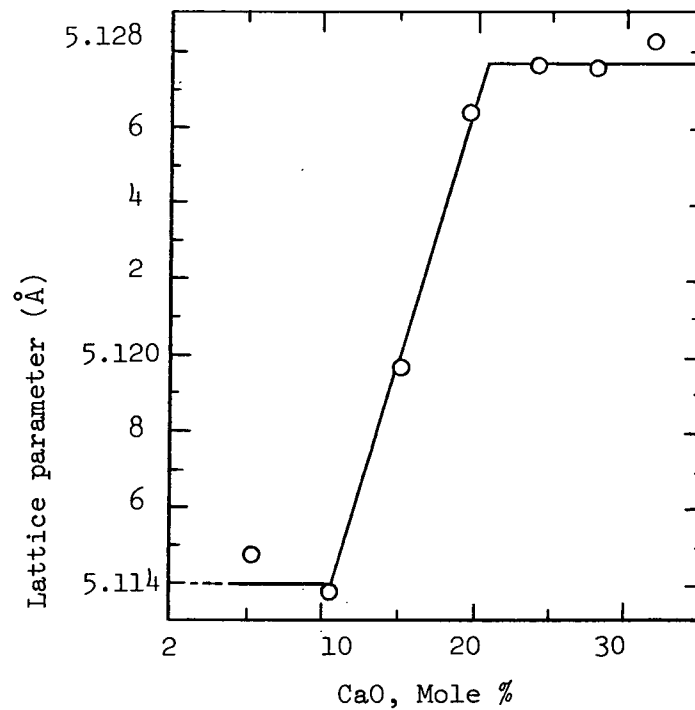


Comparison of Densities determined by X-ray and pycnometric methods for the CaO-ZrO₂ crystalline solutions quenched from 1800°C

Figure 3. Change of Densities with CaO Content in the CaO-ZrO₂ Solid Solutions after Annealing at High Temperatures Followed by Quenching. (After Diness and Roy²⁴).



a. (after Tien and Subbarao²²)



b. (after Hund¹⁹)

Figure 4. Change of Lattice Parameter with CaO Content in the CaO-ZrO₂ Cubic Solid Solutions.

phase boundaries in these two investigations was very similar, the position of the phase boundaries in these two cases was significantly different.

For the composition 15 mole% CaO and 85 mole% ZrO₂, the lattice parameter obtained in Hund's work was about 5.119 Å, whereas that obtained in Tien and Subbarao's work was about 5.133Å. The experimental accuracy, the purity of the ZrO₂ and the temperature used in specimen preparation in these two studies may account for the different results. Hund did not report the purity of his ZrO₂ and used ordinary X-ray diffractometer techniques, while Tien and Subbarao used 99.9% pure ZrO₂ and employed the back reflection region of the diffraction on powder samples. ZrO₂ of 99.9% purity and back reflection focusing camera were used in the present investigation in order to check these discrepancies.

(3) Cation and Anion (Oxygen Ion) Diffusion in the CaO-ZrO₂ System

a. Anion (Oxygen Ion) Diffusion

The oxygen ion mobility in the cubic solid solutions of CaO-ZrO₂ was first investigated by Kinergy, Pappis, Dotty and Hill²⁵ by direct measurement of the rate of exchange of oxygen between a gas phase and heated spherical particles assuming instantaneous equilibrium at the solid surface. A decrease of [O¹⁸] in the constant volume gas phase was determined using an isotope ratio mass spectrometer. The temperature dependence of the oxygen ion diffusion coefficients between 700°C and 1100°C, can be expressed as: $D = 1.0 \times 10^{-2} \exp \left(\frac{-1.22}{KT} \right)$, in which the activation energy is 1.22 ev. They further claimed that the diffusion coefficients calculated from the electrical conductivity measurements were in good agreement with

those determined by the isotopic exchange technique. Hagel²⁶ redetermined the oxygen diffusion coefficients on well-spheroidized arc-melted specimens and obtained values appreciably lower than those calculated from the electrical conductivity data. Because of these discrepancies, Simpson and Carter²⁷ commented that the correlation factor in diffusion must be included when calculating diffusion coefficients from electrical conductivity data. The correlation factor in diffusion for the fluorite-type structure has been calculated to be about 0.65²⁸. Carter and Simpson extended their studies on the subject of oxygen diffusion to include oxygen exchange in the CaO-ZrO₂ system by the conventional sectioning technique and employed a solid source mass spectrometer to determine the diffusion profile. They presented a theoretical model based on the observation that the large gas volume maintained the boundary conditions at a constant composition of the gas phase²⁹, from which the diffusion profile could be expressed by the relation:

$$C = C_o \operatorname{erfc} \left(\frac{X}{2\sqrt{Dt}} \right)$$

Where C = ratio of $\frac{O^{18}}{O^{16} + O^{18}}$ at depth X at time t ,

C_o = ratio of $\frac{O^{18}}{O^{16} + O^{18}}$ in the gas,

D = diffusion coefficient provided there is instantaneous equilibrium at the solid-gas interface.

The oxygen surface exchange coefficient can be defined by the expression:

$$\alpha(C_o - C_s) = -D \frac{\partial C}{\partial x}$$

Where C_s is the surface ratio of $\frac{O^{18}}{O^{16} + O^{18}}$

From their experimental data over the temperature range 800-1097°C, the diffusion coefficients were expressed by the Arrhenius relation:

$$D = 0.018 \begin{matrix} +0.098 \\ -0.015 \end{matrix} \exp \left(\frac{-31,200 \pm 4300}{RT} \right) \text{ cm}^2/\text{sec}$$

in which the activation energy for diffusion is about 1.34 eV. They also reported that the diffusion coefficients are the same for both single crystal and polycrystalline specimens, and were in good agreement with those results³⁰ calculated from their electrical conductivity data. If correlation factor in diffusion was used, Kingery's result for the activation energy is about 1.32 eV in agreement with that obtained by Simpson and Carter.

The oxygen surface exchange coefficients in the same temperature range were found to fit the relation as:

$$\alpha = 0.078 \begin{matrix} +0.443 \\ -0.066 \end{matrix} \exp \left(\frac{-22,800 \pm 4400}{RT} \right) \text{ cm/sec}$$

in which the activation energy is about 0.99 eV, which is smaller than the activation energy for diffusion.

b. Cation Diffusion

Investigations on the cation diffusion in the cubic solid solutions of the CaO-ZrO₂ system are limited. Carter and Rhode³¹ have done some initial studies and reported the following experimental data :

$$D_L = (\text{Zr in Zr}_{0.88} \text{Ca}_{0.12} \text{O}_{1.88}) = 2.95 \times 10^{-3} \exp \left(\frac{-82,900}{RT} \right) \text{ cm}^2/\text{sec}$$

$$D_L = (\text{Zr in Zr}_{0.84} \text{Ca}_{0.16} \text{O}_{1.84}) = 1.97 \exp \left(\frac{-109,000}{RT} \right) \text{ cm}^2/\text{sec}$$

$$D_L = (\text{Ca in Zr}_{0.84} \text{Ca}_{0.16} \text{O}_{1.84}) = 3.65 \exp \left(\frac{-109,000}{RT} \right) \text{ cm}^2/\text{sec}$$

Data on cation diffusion studies were also cited in the work by Witzman, Molbius and Gerlach³², who have investigated the cation diffusion and its temperature dependence by using radioisotopes.

The cation diffusion in the CaO-ZrO₂ system is considerably slower than the oxygen ion diffusion, as this can be seen from the following comparison of diffusion coefficients.

In a solid solution of Zr_{0.84} Ca_{0.16} O_{1.84} at 1000°C³¹

$$D_{Ca^{2+}} = 10^{-19} \text{ cm}^2/\text{sec}$$

$$D_{Zr^{4+}} = 10^{-17} \text{ cm}^2/\text{sec}$$

In a solid solution of Zr_{0.858} Ca_{0.142} O_{1.858}²⁷

$$D_{O^{2-}} \text{ (single crystal @960°C)} = 7.8 \times 10^{-8} \text{ cm}^2/\text{sec}$$

$$D_{O^{2-}} \text{ (polycrystals @1002°C)} = 5.9 \times 10^{-8} \text{ cm}^2/\text{sec}$$

(4) Infrared Absorption Spectroscopy of Zirconia

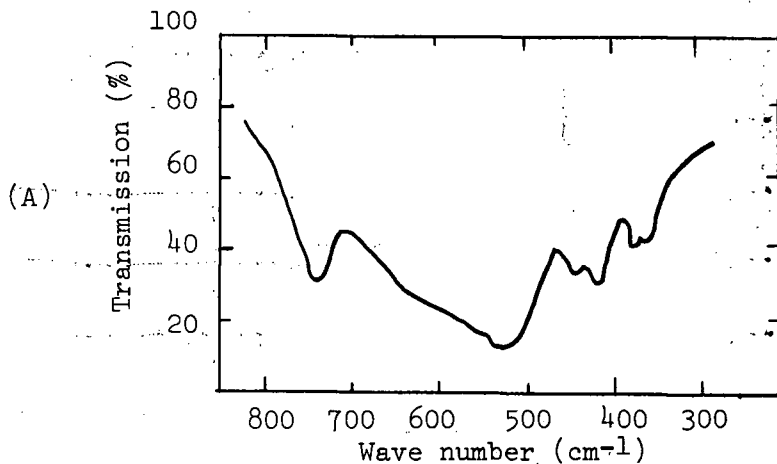
Infrared absorption spectroscopy is a powerful tool for studying aqueous solutions. But in the past few years its use has been extended to solid state systems. Baun and McDevitt³³ have reported infrared absorption data for some rare-earth oxides in the region 800-240 cm⁻¹. They found that the rare-earth oxides give individualistic infrared absorption bands and that all type C (cubic) oxides give spectra which are different from the spectra obtained from type A (hexagonal) and type B (monoclinic) oxides. It was observed that the band of the spectra is affected by changing the cation in the lattice of type C oxides and that the peak frequency is lowered if the unit cell of a type C oxide increases its dimensions. A linear

relationship was obtained from a plot of unit cell dimensions and the peak band frequency. Later, they reported further experimental data on pure ZrO_2 and CaO-stabilized ZrO_2 ³⁴. The monoclinic ZrO_2 appeared to absorb strongly in the 800-300 cm^{-1} region and the spectrum has six characteristic absorption peaks with a broad band shoulder at about 620 cm^{-1} , as shown in Fig. 5A. In the low frequency region, 300-50 cm^{-1} , the spectrum of the monoclinic ZrO_2 shows two absorption peaks, one at 270 cm^{-1} and the other one at 230 cm^{-1} , as shown in Fig. 5B.

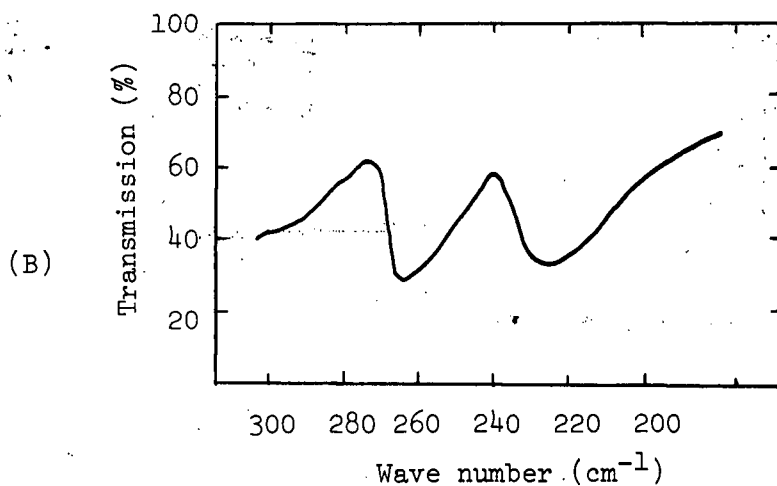
In sharp contrast to the monoclinic ZrO_2 spectrum, the cubic solid solutions of CaO-stabilized ZrO_2 gave only one broad band in the 800-300 cm^{-1} region, as shown in Fig. 5C. This was obtained from a commercial cubic ZrO_2 sample which was stabilized with 15 mole % CaO. This broad band showed a peak frequency at about 470 cm^{-1} . When an equivalent amount of CaO was added in a KBr pellet, they reported that no apparent absorption bands were found and that the transmission spectrum of the cubic CaO- ZrO_2 in the low frequency region was quite transparent. This broad band is, therefore, not contributed by any single ZrO_2 band or by the CaO band but a band with several frequencies superimposed. This broad band may be considered as a characteristic absorption band for the CaO-stabilized ZrO_2 . From these experimental results it can be seen that the infrared absorption spectra of solids are strongly dependent on the crystal structure and also on the symmetry of the unit cell.

(5) Internal Friction in ZrO_2 Containing CaO

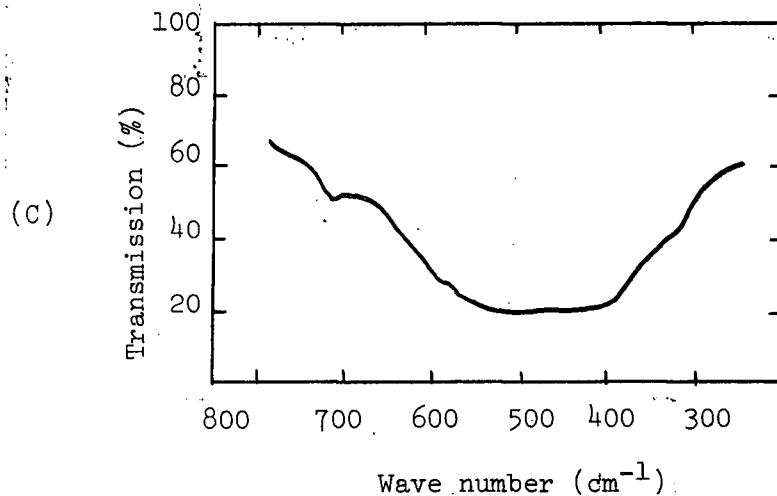
A homogeneous stress or an electric field acting upon a point defect can, under certain conditions, cause reorientation of the defect



(A) Infrared Absorption Spectrum of Monoclinic ZrO_2 (KBr pressed disk, 0.67wt.% ZrO_2)



(B) Lower Frequency Infrared Absorption Spectrum of Monoclinic ZrO_2 (Nujol mull, CsI plates)



(C) Infrared Absorption Spectrum of Cubic CaO-Stabilized ZrO_2 (commercial material)

Figure 5. Infrared Absorption Spectra of Monoclinic ZrO_2 and CaO-Stabilized ZrO_2 (after Baun and McDevitt³⁴)

and produce a corresponding mechanical or electrical relaxation. Measurements of the internal friction peak or dielectric loss peak can then be used to study the variation of point defect concentration with composition and heat treatment.

An internal friction peak was first found by Dew³⁵ in commercial ZrO_2 partially stabilized with CaO and its existence was confirmed in two subsequent investigations, by Wachtman, Tefft, Lam and Stinchfield³⁶ and by Chang³⁷. Dew suggested plastic deformation as a possible cause; Chang suggested the motion of twin boundaries; and Wachtman et al suggested the motion of oxygen vacancies. Recently, Wachtman and Corwin³⁸ carried out a further investigation on the internal friction of ZrO_2 containing CaO. In the cubic field of 10 to 20 mole % CaO added, they observed a symmetrical internal friction peak with its maximum at about 300°C at 1 kHz; and in the two phase field, below 10 mole % CaO, a nonsymmetrical peak occurred at a somewhat higher temperature. The symmetrical peaks in as-sintered specimens were also observed to have the same dependence on CaO content as that reported for electrical conductivity at 1000°C.

Wachtman and Corwin interpreted this observation to indicate that the nonsymmetrical internal friction peak in partially stabilized ZrO_2 might be associated with Chang's mechanism of twin boundary motion in tetragonal grains, but the symmetrical peak occurring in the cubic field could not be associated with tetragonal grains. The similarity of peak height dependence and electrical conductivity dependence on CaO content suggested that the symmetrical peak was associated with oxygen vacancy motion. Accordingly, they have proposed three defect models to illustrate the motion of oxygen vacancies.

First, consider a single oxygen vacancy in an otherwise perfect fluorite structure. This vacancy would move under an electric field but not under homogeneous stress. It would therefore contribute to the frequency independent part of the electrical conductivity but would not contribute to internal friction or dielectric relaxation.

Second, consider an oxygen vacancy neighbouring a Ca^{2+} ion at (0,0,0) and constrained by electrostatic attraction to the eight nearest neighbour oxygen sites at $(\pm 1/4, \pm 1/4, \pm 1/4)$. Either the homogeneous stress or the electric field will cause a preferred distribution so that this oxygen vacancy will make no contribution to the frequency independent electrical conductivity but will contribute both to internal friction and to dielectric relaxation.

Third, consider two oxygen vacancies at $(1/4, 1/4, 1/4)$ and $(1/4, 1/4, -1/4)$ neighbouring two Ca^{2+} ions at (0,0,0) and $(1/2, 1/2, 0)$. Two defects of the second type should have electrostatic attraction of the dipole-dipole type tending to cause this defect to form. The oxygen vacancies in this defect will make no contribution to the frequency independent part of the electrical conductivity, the dielectric relaxation, or the internal friction.

They concluded, however, that these models used to explain the motion of oxygen vacancies in the CaO-ZrO_2 solid solutions were only partially correct, and that the detailed models are likely to be complex due to the fact that oxygen vacancies in the $\text{CaO-stabilized ZrO}_2$ exist in several states of binding. It can be seen that the dynamical behavior of oxygen vacancies in the cubic field of the CaO-ZrO_2 system is a complicated subject.

(6) Electrical Conductivity in the CaO-ZrO₂ Cubic Solid Solutions

a. Electrical Conductivity Kinetics

Measured electrical conductivity in oxide systems is the sum of ionic and electronic contributions. The electronic contribution will consist of excess electrons and electron-holes. Even if the concentrations of electrons or electron-holes are small, they still make a substantial contribution to the conductivity since their mobility is high. The total conductivity can therefore be expressed as:

$$\sigma = \sigma_{ion} + F \mu_{\ominus} C_{\ominus} + F \mu_{\oplus} C_{\oplus} \dots\dots\dots(1)$$

where σ = total conductivity

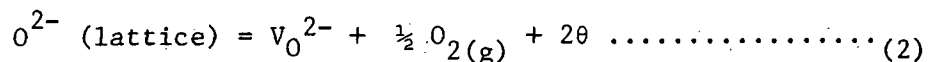
σ_{ion} = conductivity due to motion of ions

$\mu_{\ominus}, \mu_{\oplus}$ = mobility of the electrons and electron-holes, respectively (cm. sec.⁻¹ per volt cm⁻¹).

C_{\ominus}, C_{\oplus} = concentration of the electrons and electron-holes, respectively.

F = Faraday Constant

In a system in which there is a large concentration of oxygen vacancies fixed by composition and independent of oxygen pressure the ionic contribution will not be pressure dependent. However, as the oxygen pressure is changed there may be a change in the electronic contribution to the total conductivity. The formation of conduction electrons can then be expressed as follows²⁵:



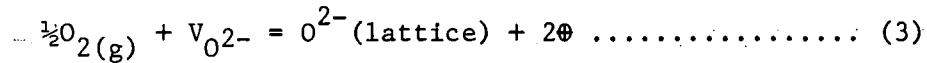
where $O^{2-}(\text{lattice})$ = oxygen ion in a normal lattice site

V_O^{2-} = oxygen ion vacancy

$O_2(g)$ = oxygen liberated as gas

θ = excess electrons

Similarly one might fill in normally vacant sites and form electron-holes \oplus according to the relation:



The concentrations of the excess electrons or electron-holes are therefore dependent on the oxygen pressure. Assuming that association or interaction effects are small at the low concentrations, the mass action equation for equations (2) and (3) can be expressed as:

$$k_1 = \frac{[\oplus]^2 P_{O_2}^{1/2} [V_{O^{2-}}]}{[O^{2-}]} \dots\dots\dots (4)$$

$$k_2 = \frac{[\oplus]^2 [O^{2-}]}{P_{O_2} [V_{O^{2-}}]} \dots\dots\dots (5)$$

Since $[V_{O^{2-}}]$ and $[O^{2-}]$ are fixed by the composition, the concentrations of electrons and electron-holes are given by:

$$[\oplus] = k_1 P_{O_2}^{-1/4} \dots\dots\dots (6)$$

$$[\oplus] = k_2 P_{O_2}^{1/4} \dots\dots\dots (7)$$

The total conductivity is then related to the oxygen pressure by

$$\sigma = \sigma_{ion} + k_1 P_{O_2}^{-1/4} + k_2 P_{O_2}^{1/4} \dots\dots\dots (8)$$

This expression indicates that the total conductivity would be oxygen pressure dependent if there is an appreciable contribution from the electronic conduction.

b. Ionic Conductivity

The works of Wagner and Kiukkola³⁹ have established that the electrical conductivity of the cubic solid solutions of CaO-ZrO₂ is due entirely to the migration of oxygen ion vacancies. Subsequently, the electrical conductivity as a function of temperature and of CaO content

for this system has been extensively investigated by a large number of workers^{19,22,25,30,31,40-46}. The possibility of grain boundary conductivity in the CaO-ZrO₂ ceramics was also recently studied by Tien⁴⁷. Most experimental results for the conductivity-temperature data over the temperature range 500-1800°C for the CaO-ZrO₂ cubic solid solutions were generally observed to follow an Arrhenius relation:

$$\sigma = \sigma_0 \exp\left(\frac{-E}{KT}\right) \dots\dots\dots (9)$$

σ = electrical conductivity

σ_0 = Pre-exponential term

E = activation energy

K = Boltzman's constant

T = Absolute temperature

For a fixed composition, such as 15 mole % CaO and 85 mole % ZrO₂, the activation energy for conduction obtained by most investigators was in fair agreement. However, the conductivity values at a given temperature, such as at 1000°C, varied greatly between different workers. (See Table 5, APPENDIX II).

The experimental results showed that with increasing CaO content the activation energy increased and the conductivity decreased for a given temperature. Tien and Subbarao²² have proposed the following model to account for the observed dependence of conductivity on CaO content: The oxygen ion, which is the charge carrier, has to pass between two metal ions to reach an adjacent anion site. These metal ions may be two Zr⁴⁺ ions, one Zr⁴⁺ ion and one Ca²⁺ ion or two Ca²⁺ ions. In as much as the Ca²⁺ ion (0.99Å) is approximately 25% larger than the Zr⁴⁺ ion (0.78Å), it is expected that the energy required for an oxygen

ion to pass between two Ca^{2+} ions would be the largest, while that for the case of two Zr^{4+} ions would be the smallest. Each oxygen ion is surrounded by four metal ions in the fluorite-type lattice. As the CaO content increases from 13 to 20 Mole %, the probability of having one Ca^{2+} ion as a nearest neighbour to an oxygen ion increases from 34% to 41% and the probability of having two Ca^{2+} ions as nearest neighbours to an oxygen ion increases from 7.7% to 17%. Therefore, the activation energy for conduction increases and, consequently, the conductivity at a given temperature decreases with increasing CaO content.

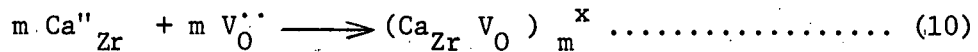
c. Electronic Conductivity

The electronic conductivity in an oxide system is oxygen partial pressure dependent as indicated by the following two equations:

$$1) \quad \theta = k_1 P_{\text{O}_2}^{-1/4} \qquad 2) \quad \theta = k_2 P_{\text{O}_2}^{1/4}$$

Kiukkola and Wagner³⁹ in their measurements on galvanic cells involving solid electrolytes observed that the electrical conductivity of the electrolyte $\text{Zr}_{0.85} \text{Ca}_{0.15} \text{O}_{1.85}$ was virtually constant when the oxygen partial pressure was varied over a wide limit from 10^0 to $10^{-22.5}$ atmospheres. Weissbärt and Ruka⁴⁸ reported that the electronic contribution to the total conductivity in this system is perhaps less than 2%. At $P_{\text{O}_2} < 10^{-22.5}$ atmosphere, Schmalzried⁴⁹ and Alcock and Steele⁵⁰ observed that the electronic (n-type) conduction becomes predominant, with $\sigma_e \propto P_{\text{O}_2}^{-1/4}$. Vest and Tallan⁵¹ found that incorporation of 2 mole % vanadium + 1.4 mole% Al gives rise to dominant electronic conduction at oxygen partial pressures up to 10^{-16} atmosphere, where $\sigma_e \propto P_{\text{O}_2}^{-1/n}$ with $n = 5.8 \pm 1.0$.

Very recently, Kroger⁵² has introduced the concept of charged free, as opposed to associated neutral, imperfections to account for the observed variations of the electronic conductivity of stabilized ZrO₂. He proposed two imperfection models, one for Zr_{0.85}Ca_{0.15}O_{1.85}V_{0.15} and one for donor-doped stabilized ZrO₂. In the former model, he suggested that most of the Ca is present in a neutral form. The doubly charged imperfections originally thought to be present might exist as neutral centers which are pairs or clusters formed according to the following relation and only a small portion of them existed in the free, double charged form.



where $m = 1$ for pairs

Ca''_{Zr} = a Ca ion occupied a Zr ion site with effective double negative charge

$\text{V}_\text{O}^{\bullet\bullet}$ = An oxygen vacant site with effective double positive charge

$(\text{Ca}_{\text{Zr}} \text{V}_\text{O})_m^x$ = charged free, or associated neutral cluster

with $k_{p(m)} = \frac{[\text{Ca}_{\text{Zr}} \text{V}_\text{O}]_m^x}{[\text{Ca}''_{\text{Zr}}]^m [\text{V}_\text{O}^{\bullet\bullet}]^m} \dots\dots\dots (11)$

He also considered the quasi-chemical reactions which describe the formation and ionization of defects in the crystal and the incorporation or removal of oxygen into and from the crystal respectively, the law of mass action to these relations, and the complementary relations obtained with a neutrality condition and a calcium balance equation, from which Kroger arrived at a schematic solution for the concentration of the various imperfections as a function of oxygen partial pressure at a high temperature. Owing to the large concentration of oxygen vacancies

present in the neutral centers which increase the ionic current, he concluded that electronic p-type or n-type conduction will become noticeable only at extremely high or extremely low oxygen partial pressures. Since the extremely low pressures are more easily established than the extremely high oxygen pressures, only n-type conduction has been observed in a pressure of less than $P_{O_2}^{-22.5}$ atmosphere in the cubic solid solutions of CaO-ZrO₂.

d. Relationship Between Electrical Conductivity and Diffusion Coefficient

When electrical conductivity is entirely due to ionic mobility, the electrical conductivity and the transfer number (fraction of the total current carried by each charged particle) are related to the ionic diffusion coefficient by the Nernst-Einstein equation⁵³:

$$\sigma_i = t_i \sigma = \frac{D_i n_i (Z_i e)^2}{KT} \dots\dots\dots(11)$$

When the measured volume conductivity, the macroscopic tracer diffusion coefficient, and the correlation factor in diffusion are combined, the Nernst-Einstein equation can be rearranged and expressed in the following relation⁵⁴. (Derivations are given in APPENDIX VI)

$$\frac{D}{\sigma} = \frac{f t_i k T}{N (Z_i e)^2} \dots\dots\dots(12)$$

Electrical conductivity measurement has been proved to be a reliable method of determining the oxygen diffusion coefficients in the CaO-ZrO₂ system and also in other oxide systems.

II. EXPERIMENTAL PROCEDURE

(A) Materials and Specimen Preparation

1. Materials Preparation

Reagent grade calcium carbonate (Allied Chemical Co., U.S.A.) and 99.9% pure ZrO_2 (Koch-Light Laboratory Ltd., England) were used to prepare the 15 mole% CaO and 85 mole % ZrO_2 composition. The weighed mixtures were wet blended for two hours in a ball-mill with calcia-stabilized zirconia pebbles using acetone as the mixing agent. The blended mixtures were then filtered and dried in an oven at $100^\circ C$ for 20 hours.

2. Specimen Preparation

The mixtures of $CaCO_3$ and ZrO_2 powders were loaded into a right circular cylindrical graphite die ($3/8''$ diameter in bore and 3" in length) with graphite plungers inserted from both sides. The graphite die assembly was placed on a mechanical jack (the pressure of which was controlled by a compressed gas cylinder) and was heated by a LEPEL induction generator. The temperature was brought up rapidly to $1550^\circ C$ in about 15 minutes. The powders inside the graphite die were allowed to heat at this temperature under argon atmosphere for 15 minutes and were then hot-pressed at 4600 p.s.i. for another 15 minutes. The graphite die assembly was allowed to cool to room temperature under full pressure in the argon atmosphere in about 60 minutes before removing the specimen from the die assembly. The temperature was measured with a W-W + 26% Re thermocouple at a distance of about $1/8''$ from the top level of the powder inside the graphite die. The true temperature of reaction

during hot-pressing was measured and found to be about 200°C higher than the recorded temperature (1550°C) in the plunger. This implied that the actual reaction temperature is about 1750°C. The ends and surface of each pellet were polished in a wet-belt grinding wheel with very fine sand paper. The polished specimens were later heated in air in an oven at about 800°C for one hour. This short period of heating was intended to burn out any carbon remaining on the surface of the specimens.

(B) Phase Identification

The phases in each hot-pressed pellet ^{here} ~~was~~ identified by X-ray diffraction. A Norelco diffraction unit using Ni-filtered Cu radiation was employed. A fast-scan pattern, one degree per minute, was made between 27° and 33° of 2θ values. The diffraction pattern was limited to this narrow region because this interval includes the two most prominent monoclinic peaks (1 1 1) and (1 1 $\bar{1}$), the most intense tetragonal peak (1 1 1), and the solid-solution cubic peak (1 1 1) of ZrO₂. The strongest peaks of the CaCO₃ and CaZrO₃ compounds also occur in this region. Thus, a fast scan of the diffraction pattern in this region indicated the phases present in the specimen. To check the uniformity of the phase in the specimen, diffraction patterns were made on both ends of the pellet.

(C) Annealing Procedure

The annealing specimens were placed in a high purity recrystallized alumina tube and were heated in air in a Super-Kanthal furnace under normal atmospheric conditions. The temperature was measured with a Pt-Pt+40% Rh thermocouple, which was placed in contact with the annealing specimens inside the alumina tube. Thus, the recorded temperature was the true annealing

temperature. After annealing, the specimens were allowed to cool slowly to room temperature. This was done over a period of 30 minutes by gradually withdrawing the alumina tube from the hot zone of the furnace.

(D) Precise Lattice Parameter Measurement

1. Experimental Procedure

The precise lattice parameter measurement was made by obtaining X-ray diffraction photographs on powdered samples.

A Norelco Precision Symmetrical Back Reflection Focusing Camera was used. This camera has an effective camera diameter of 12 cm and provides excellent resolution between $\theta = 59^\circ$ and $\theta = 88.74^\circ$. The camera mounted with a powdered sample was exposed to Ni-filtered Cu radiation on the standard Norelco diffraction unit. The average exposure time for each diffraction photograph was about two hours at 35 Kv and 15 ma.

The powdered sample used for the X-ray diffraction photograph was prepared by the following procedure: A small portion of each annealed specimen was ground to a fine powder in an agate mortar and subsequently passed through a 200 mesh screen. The screened powder was then dusted onto a piece of thick paper which has been covered with a layer of Dow-Corning silicone grease. The sample was then inserted into the camera with the powder coating facing inwards.

"No-screen medical X-ray safety" films were used. On development the outer surface of the film was covered with a piece of flatback paper tape, which was stripped off before the film was immersed in

the fixing solution. If this is not done, the lines will appear on both sides of the film, with possible loss of apparent resolution and loss of precision in determining the line positions.

The positions of the $K\alpha_1\alpha_2$ doublet diffracted lines and the camera knife-edge marks for film shrinkage corrections were measured using a Norelco Film-Measuring device with accuracy to ± 0.05 mm. The true positions and observed positions of the camera knife-edge marks were compared and the necessary corrections for film shrinkage in each film were made through a FORTRAN computer programme.

2. Lattice Parameter Calculation

The precise lattice parameter was calculated according to Cohen's method⁵⁵ (APPENDIX V). A FORTRAN computer programme based on this calculation was written and all experimental data were computed by running this programme and the data in an IBM 7040 computer. The computer output printed the lattice parameter value and the drift-constant in 5 significant figures. The reproducibility was about ± 0.0001 Å and the drift-constant on all output results varied from 0.0001 to 0.0003. The drift-constant is a measure of the total systematic error involved in the determination.

(E) Infrared Absorption Spectroscopy Measurement

Infrared absorption spectra have been obtained for the 99.9% pure monoclinic ZrO_2 , and the partially and completely CaO-stabilized ZrO_2 . The effect of annealing temperature on the infrared absorption spectra for completely CaO-stabilized ZrO_2 has also been studied. A Perkin-Elmer Model 521 Grating Infrared Spectrophotometer was used for obtaining spectra in the region 1000 to 300 cm^{-1} in potassium bromide (KBr) pellets.

Both monoclinic ZrO_2 and CaO-stabilized ZrO_2 powders were first passed through a 200 mesh screen and were then ground to a finer powder in an agate mortar for about 5 minutes before dispersing in potassium bromide. The powders were thoroughly mixed by further grinding in the agate mortar. Disks of about 1.6 cm in diameter and 1 mm thick were prepared by vacuum pressing at about 10,000 p.s.i.. The disks contained about 0.5 wt.% ZrO_2 or CaO- ZrO_2 in KBr. Duplicate runs with less sample material in the KBr. pellet were made in each specimen.

(F) Electrical Conductivity Measurement

1. Specimen Preparation

Specimens used in electrical conductivity measurements were right circular cylindrical pellets of about 10 mm in diameter and 10 mm in length. Before annealing, the ends and surface of each pellet were further polished in a wet-belt grinding wheel with very fine sand paper. Two small holes, about 0.05 mm in diameter, 3 mm deep and approximately 5 mm apart were drilled on the surface of the pellet by an ultrasonic drill. These holes were used to house the measuring potential leads. After annealing, these holes were coated with a thin layer of Hanovia liquid platinum paste (Platinum Paste No. 6082). The application of this platinum paste improved the electrical contact between the potential lead wires and the specimen. The electrode separation and the diameter of each specimen were measured by a micrometer and the average value over ten measurements was used for calculation. The accuracy of these measurements was about ± 0.1 mm.

2. Apparatus and Equipments

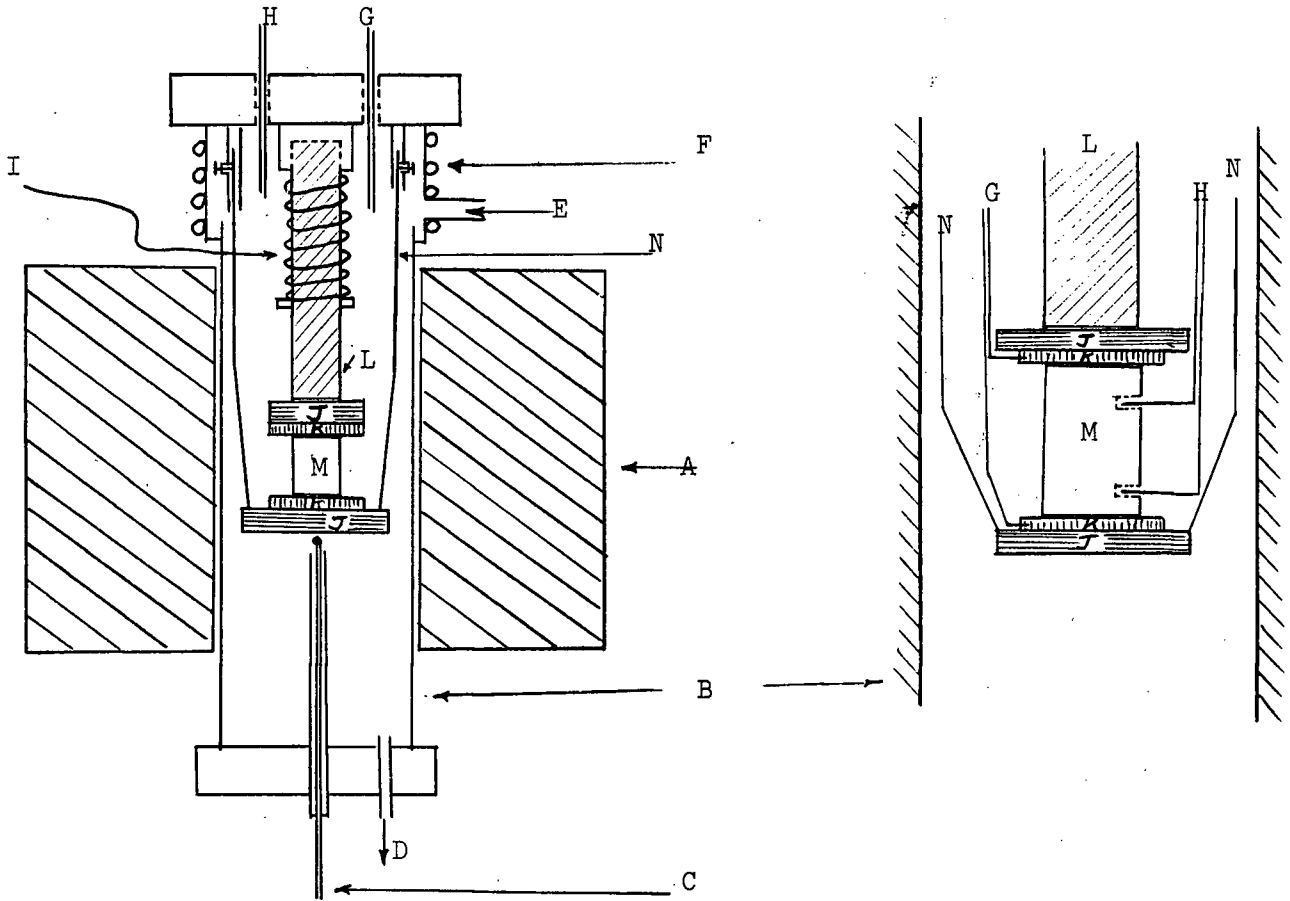
The specimen holder used for electrical conductivity

measurement was a four-terminal spring-loading device. The specimen was placed between two platinum plate electrodes to which a pair of 0.020" diameter platinum wires ^{were} ~~was~~ attached serving as current leads. Two pieces of high-purity alumina plates were put on the platinum plates for protection. The platinum and alumina plates were held together under compression by a spring and an alumina rod. A second pair of 0.02" platinum wires was used as potential leads for measuring the voltage drop across the sample. The potential lead wires were securely inserted into the two small holes which have been coated with platinum paste. A schematic diagram is given in Fig. 6.

An A-C source of 1000 cps was supplied from a Heatkit Oscillator. The voltage drop across the sample and across a standard resistor (Type 510 Decade-Resistance Unit) which was connected in series with the sample was measured by a Hewlett Packard Model 400D VTVM (Vacuum-Tube-Volt-Meter). The standard resistor connected in series with the specimen was used to measure the current passing through the specimen.

3. Measurement Procedure

The conductivity measurement assembly was inserted into an open-end alumina tube and heated in a Glo-bar furnace. A steady stream of helium gas was always passed in order to maintain a neutral atmosphere during the entire period of measurement. A Pt-Pt+10% Rh thermocouple which was placed directly underneath the bottom alumina plate served as both temperature-recording and temperature-controlling thermocouple. The rate of heating was about 8°C per minute in the 500-1000°C range and about 4°C per minute in the 1100-1400°C range. The voltage drop across the specimen and across the standard resistor was measured every two hundred degrees. Readings were taken immediately after



High Temperature Electrical Conductivity Furnace

Details of sample position

- A - Glo-bar furnace
- B - Recrystallized alumina tube
- C - pt - pt + 10% Rh thermocouple wires
- D - Helium gas outlet
- E - Helium gas inlet
- F - Water Cooling Coil
- G - 0.02" platinum wires as current leads
- H - 0.02" platinum wires as potential leads
- I - Steel-spring coil
- J - High-purity alumina plates
- K - Platinum Thin plates
- L - Recrystallized alumina rod
- M - sample
- N - Shielded molybdenum wires

Figure 6. Schematic diagram of High-Temperature Electrical Conductivity Furnace and Sample Holder.

the desired temperature was reached and also after 30 to 45 minutes of soaking at the same temperature. The conductivity of each specimen was measured both during the heating and cooling cycles in the temperature range of 500-1400°C.

4. Electrical Conductivity Calculation

The electrical conductivity was calculated according to the following relation⁵⁶:

$$\sigma = \frac{I L}{V A}$$

where σ = Electrical conductivity ($\text{ohm}^{-1} \cdot \text{cm}^{-1}$)

I = Current (Ampere)

V = Voltage drop (volts)

L = Electrode separation (cm)

A = Cross-sectional area of specimen (cm^2)

for a 4-terminal method of measurement

$$I \text{ (Amps)} = \frac{\text{voltage drop across standard resistor (volt)}}{\text{Resistance in standard resistor (ohms)}}$$

V = voltage drop across the specimen between potential leads

(G) Porosity and Density Measurements

The porosities of the hot-pressed and annealed specimens were determined by following the ASTM-C 20-46 water-absorption procedure⁵⁷.

The true specific gravity of a series of specimens which have been annealed at various temperatures for a fixed period of time was determined by following the ASTM-C135-47 pycnometer bottle procedure using powder samples⁵⁷. The annealed specimens were ground to fine powders passing through a 100 mesh screen. A constant temperature bath of 25°C with fluctuation of about $\pm 0.1^\circ\text{C}$ was used and all weighings were carried out at room temperature of about 20-22°C.

III. EXPERIMENTAL RESULTS

(A) Phase Identification of the $Zr_{0.85}Ca_{0.15}O_{1.85}$ Solid Solution

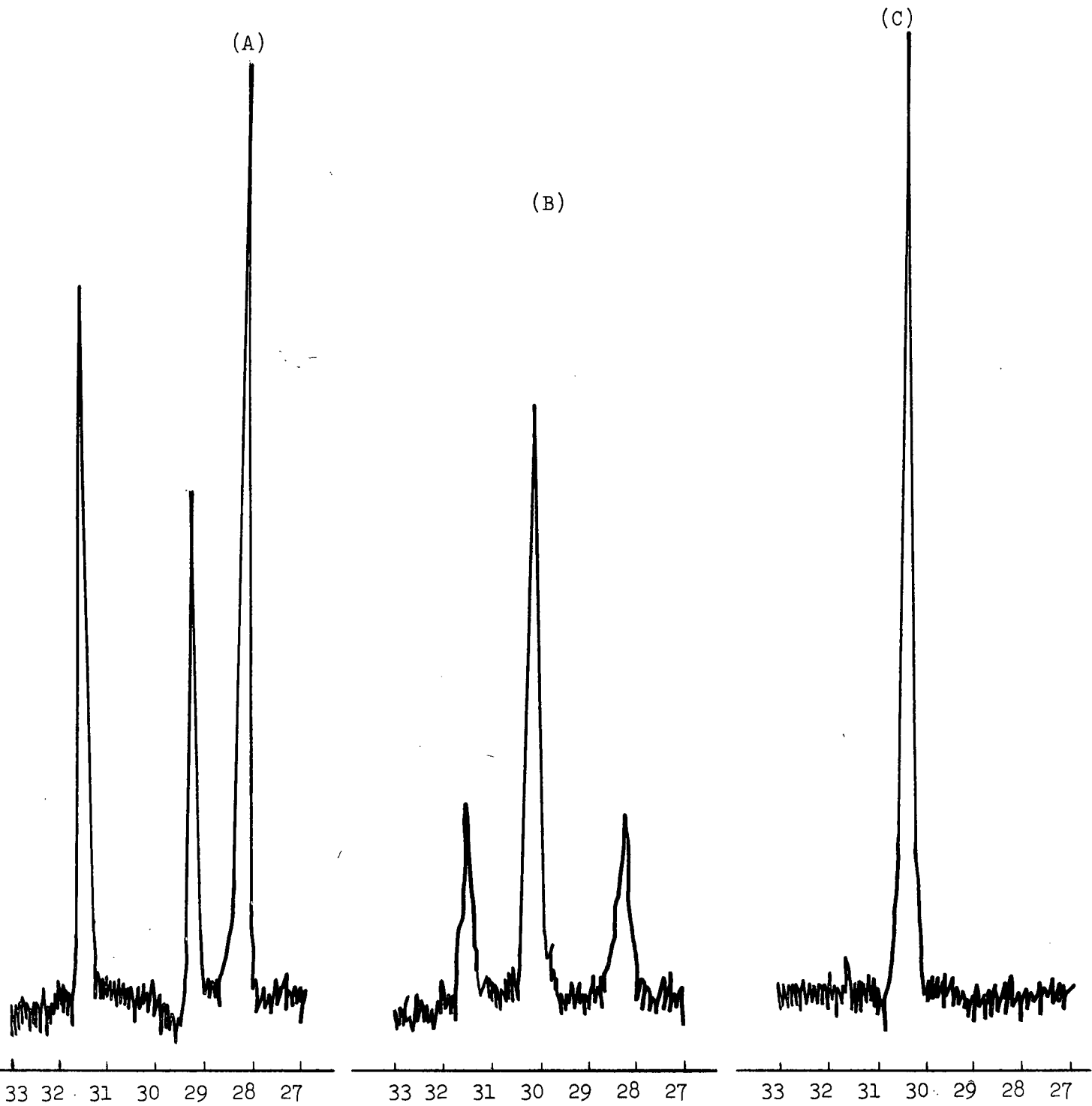
1. X-Ray Diffraction

In the interval 27° - 33° of 2θ values, six X-ray diffraction peaks can occur for the binary system of CaO-ZrO₂ as summarized in Table I:

Table I
X-ray Diffraction Peaks of Several Compounds in the 27° - 33° Interval

Compound	2θ	$\frac{I}{I_0}$	(hkl)
ZrO ₂ (monoclinic)	28.20	100	(111)
	31.58	65	(11 $\bar{1}$)
ZrO ₂ (high-temp. tetragonal)	30.26	100	(111)
ZrO ₂ (cubic solid-solution)	30.58	100	(111)
CaCO ₃ (calcite)	29.36	100	(104)
CaZrO ₃ (orthorhombic)	31.58	100	(220) (022)

The X-ray diffraction pattern for the unreacted mixtures of CaCO₃ and ZrO₂ used in this study showed three diffraction peaks at $2\theta = 28.3^{\circ}$, 29.3° , and 31.5° , as shown in Fig. 7A. These peaks were identified as the two prominent monoclinic ZrO₂ peaks at (111) and (11 $\bar{1}$) and the most intense peak of CaCO₃ at (104). After hot-pressing at 1500°C and under 4600 psi for 30 minutes, the reacted material gave three peaks with a strongest peak at $2\theta = 30.4^{\circ}$ and two small peaks at 28.2° and 31.5° as shown in Fig. 7B. The strongest peak was identified as the cubic solid solution at (111), and the two small peaks were the monoclinic ZrO₂ peaks. This indicated that the ZrO₂ was not completely stabilized with CaO or completely converted into the cubic phase. However, when the mixtures were heated at a recorded temperature of 1550°C for 15 minutes, followed by further hot-pressing at 1550°C and 4600 psi pressure for another



(A) Monoclinic ZrO_2+CaCO_3
Mixtures

(B) Partially CaO-Stabilized
 ZrO_2

(C) Completely CaO-Stabilized
 ZrO_2

Figure 7. X-Ray Diffraction Patterns of Unreacted and Reacted CaO- ZrO_2 Compositions.

15 minutes, the reacted material gave only one diffraction peak at $2\theta = 30.5^\circ$, as shown in Fig. 7C. This peak was identified as the cubic solid solution peak at (111). This indicated that the ZrO_2 was completely stabilized with CaO at these reaction conditions. The possibility of the existence of tetragonal ZrO_2 in the reacted material can be ruled out, since the tetragonal phase has never been detected previously at room temperature. The hot-pressed material was considered to be a homogeneous cubic solid solution of CaO- ZrO_2 having the composition of 15 mole% CaO + 85 mole% ZrO_2 .

2. Infrared Absorption Spectra

The 99.9% pure monoclinic ZrO_2 gave six bands in the region $800-300\text{ cm}^{-1}$ in the infrared absorption spectrum as shown in Fig. 8A. The strongest absorption band occurred at 530 cm^{-1} . The partially CaO-stabilized ZrO_2 gave similar absorption spectrum as the monoclinic ZrO_2 . The strongest absorption band remained at the 530 cm^{-1} but the side bands showed gradual disappearance as shown in Fig. 8B. The completely CaO-stabilized ZrO_2 or cubic solid solution of CaO- ZrO_2 gave a single broad band which is completely different from the absorption spectrum of the monoclinic ZrO_2 , as shown in Fig. 9. The peak frequency of this broad band appeared to shift depending on the heat treatment of the specimen. For example, when the sample was annealed at 800°C for 1 hour, the peak frequency of the absorption band occurred at about 440 cm^{-1} ; whereas when the same sample was annealed at 1500°C for 24 hours, the peak frequency of the absorption band appeared at about 455 cm^{-1} . The shift of the peak frequency of the broad band may be due to the complexity of grouping the cations and oxygen ions and vacancies in the

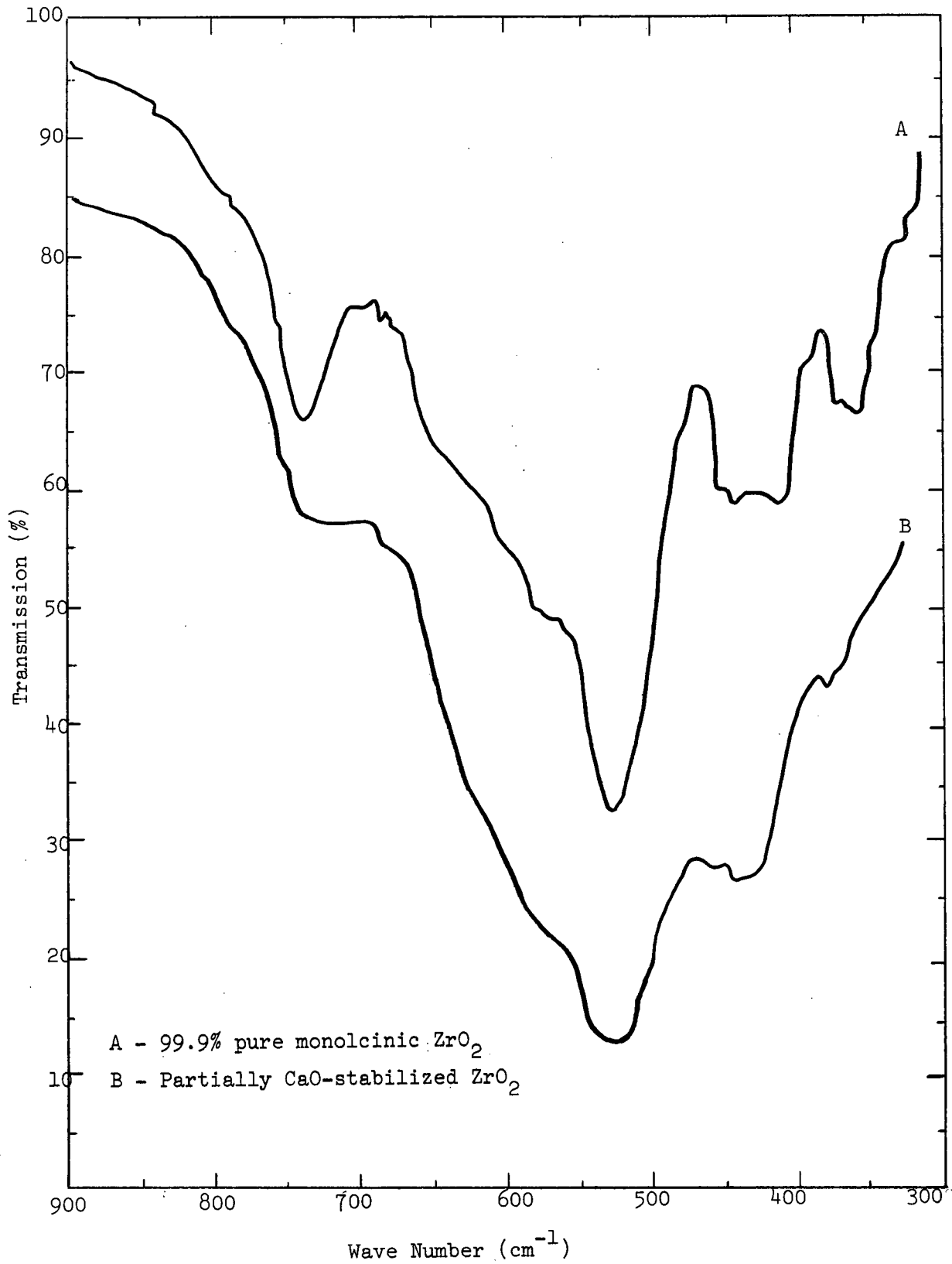


Figure 8. Infrared Absorption Spectra of Monoclinic ZrO₂ and Partially CaO-Stabilized ZrO₂.

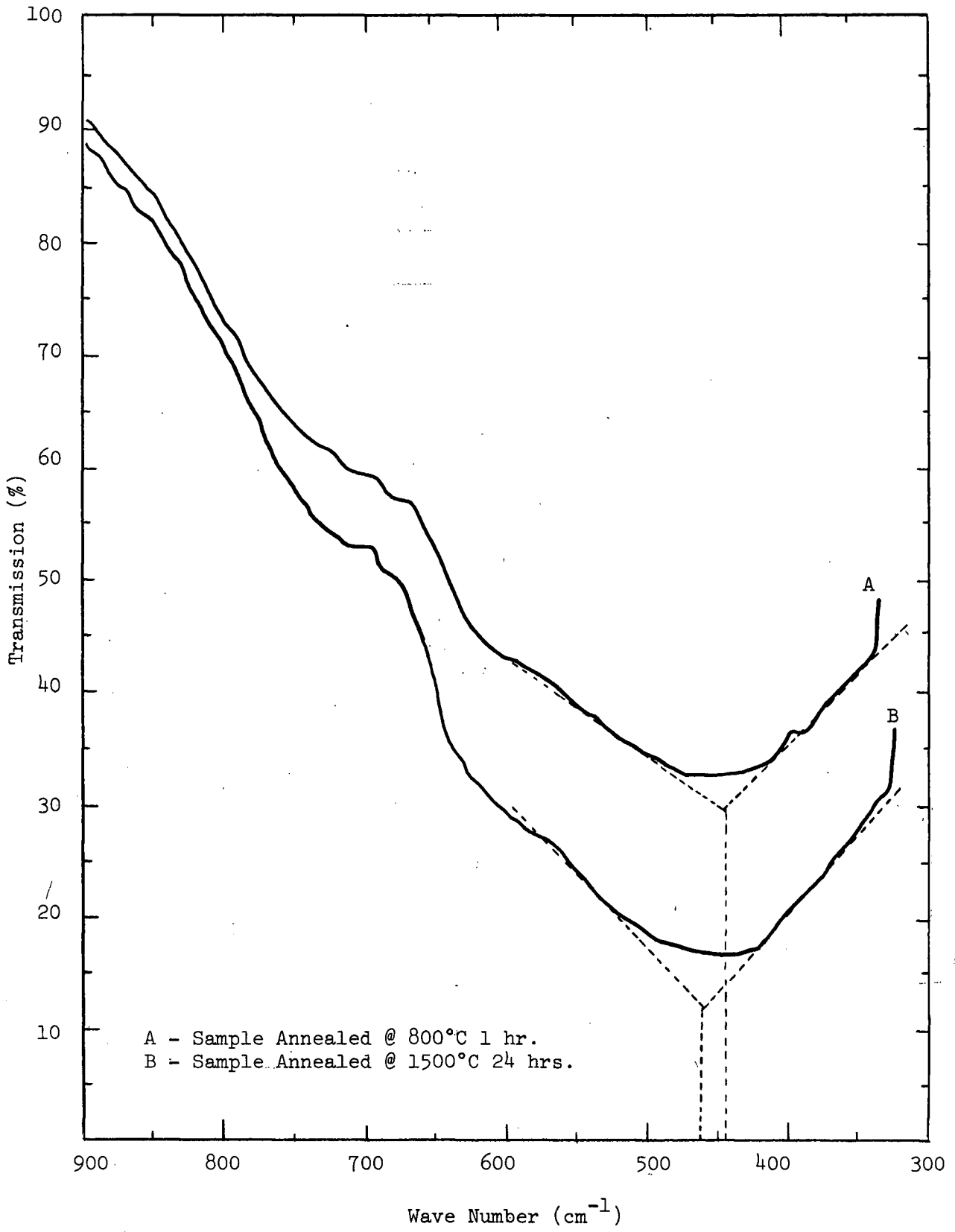


Figure 9. Infrared Absorption Spectra of Completely CaO-Stabilized ZrO₂ After Heat Treatment.

solid solution.

In general, the infrared absorption spectra obtained in the present investigation are in good agreement with those reported by Baun and McDevitt³⁴. This can be seen by comparing the data given in Figs. 5A,B,C and Fig. 9. The band frequencies of the infrared absorption spectra obtained in these two investigations are given in Table II.

Table II

Infrared Absorption Band Frequencies of Monoclinic ZrO_2 and CaO-Stabilized ZrO_2

<u>Compound</u>	<u>Band Frequencies (cm⁻¹)</u>	
	<u>Baun & McDevitt</u>	<u>Present Invest.</u>
monoclinic ZrO_2	740	740
	620	600
	530	530
	460	450
	430	420
	370	360
commercial CaO-stabilized ZrO_2	470	-
hot-pressed CaO- ZrO_2	-	440-455
(both CaO- ZrO_2 materials are of the same composition 15 mole% CaO + 85 Mole% ZrO_2)		

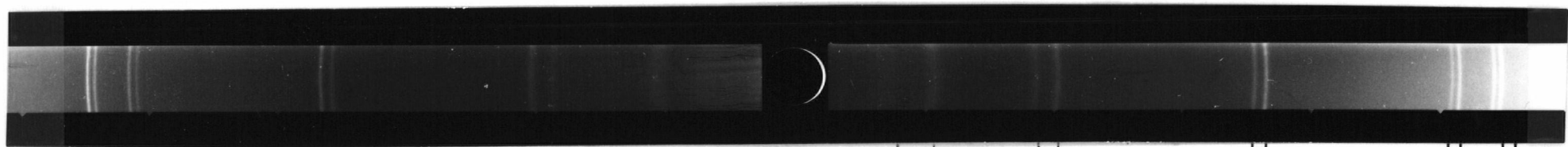
(B) Precise Lattice Parameter of the $Zr_{0.85}Ca_{0.15}O_{1.85}$
Cubic Solid Solution

1. Effect of Annealing Temperature on the Lattice Parameter

The relationship between the lattice parameter of the cubic unit cell of the $Zr_{0.85}Ca_{0.15}O_{1.85}$ solid solution and the annealing temperature has been systematically investigated. More than 60 X-ray diffraction photographs have been obtained and a typical example of the X-ray diffraction pattern of a powdered specimen is given in Fig. 10. The annealing temperatures ranged from 800°C to 1500°C. All samples were heated and cooled under identical conditions. The experimental data are given in Tables 1 and 2, APPENDIX I.

Figure 11 shows the linear relationship between the lattice parameter and the annealing temperature for three separate series of samples. Each series of samples was obtained from a single specimen. It is quite evident that the lattice parameter of the cubic unit cell of the $CaO-ZrO_2$ solid solution decreased as the annealing temperature increased from 800°C to 1500°C. The lattice parameter of three separate specimens before annealing at high temperature appeared to vary slightly from one specimen to another. However, these lattice parameter values seemed to converge to an approximately constant value as specimens were annealed at temperatures higher than 1500°C.

Figure 12 shows the least squares fit plot of the mean values of the lattice parameter of all samples measured as a function of annealing temperature. The lattice parameter decreased from a mean value of 5.1363Å at 800°C to a mean value of 5.1349Å at 1500°C. The experimental data of Figs. 11 and 12, therefore, indicate that a lattice contraction was experienced in the $Zr_{0.85}Ca_{0.15}O_{1.85}$ cubic solid solution as the material was subjected to high temperature heat treatment after hot-pressing.



Cu K $\alpha_1\alpha_2$ =	α_1 α_2				
(hkl) =	(622)	(533)	(620)	(442)	(531)
θ_{α_1} =	84.7	79.9	71.7	64.3	62.6
α_2 =	86.8	80.7	71.1	64.6	62.7

Figure 10. Typical X-Ray Diffraction Pattern of Powdered Sample of $Zr_{0.85}Ca_{0.15}O_{1.85}$ Solid Solution.

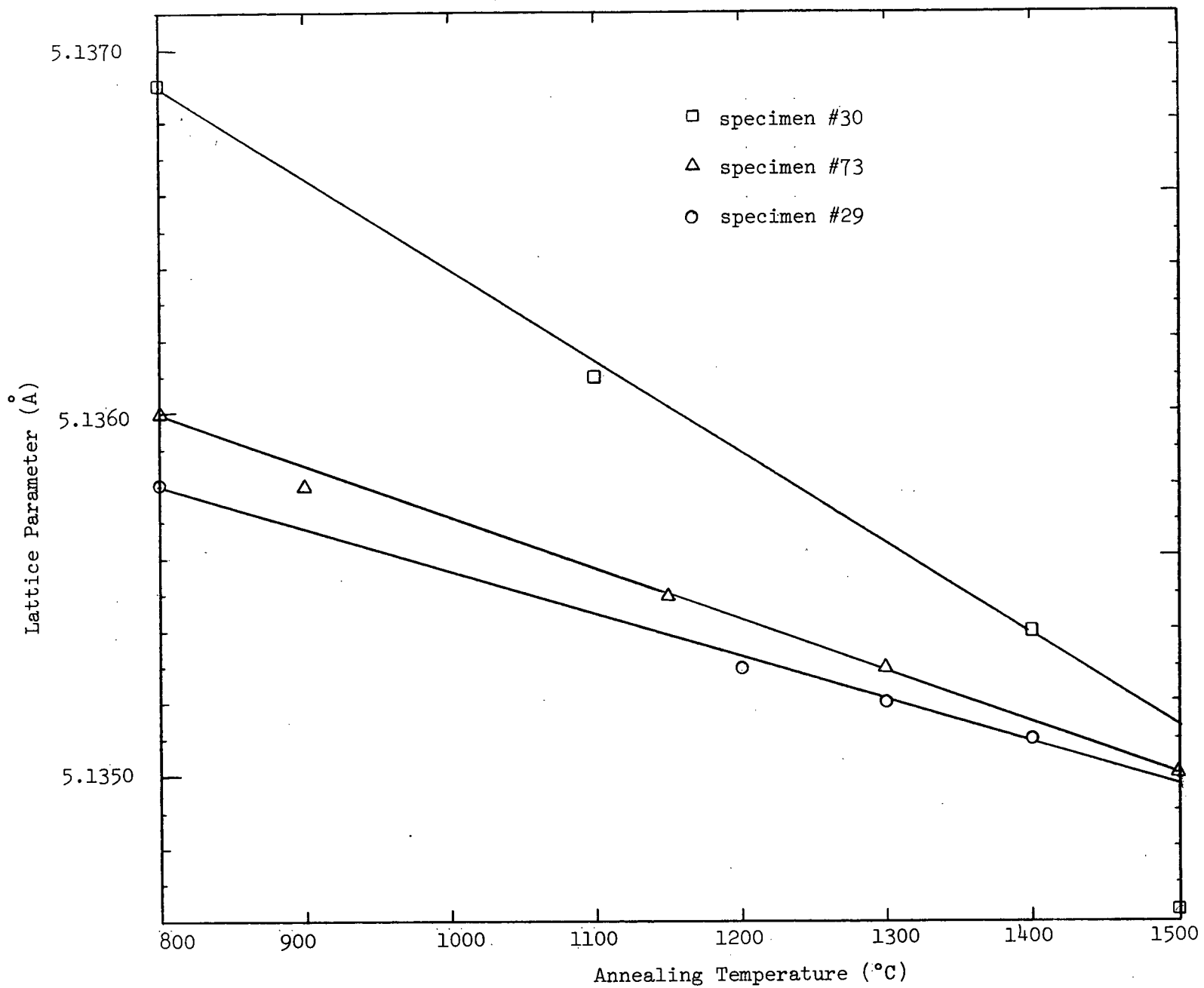


Figure 11. Decrease of Lattice Parameter as a Function of Annealing Temperature.

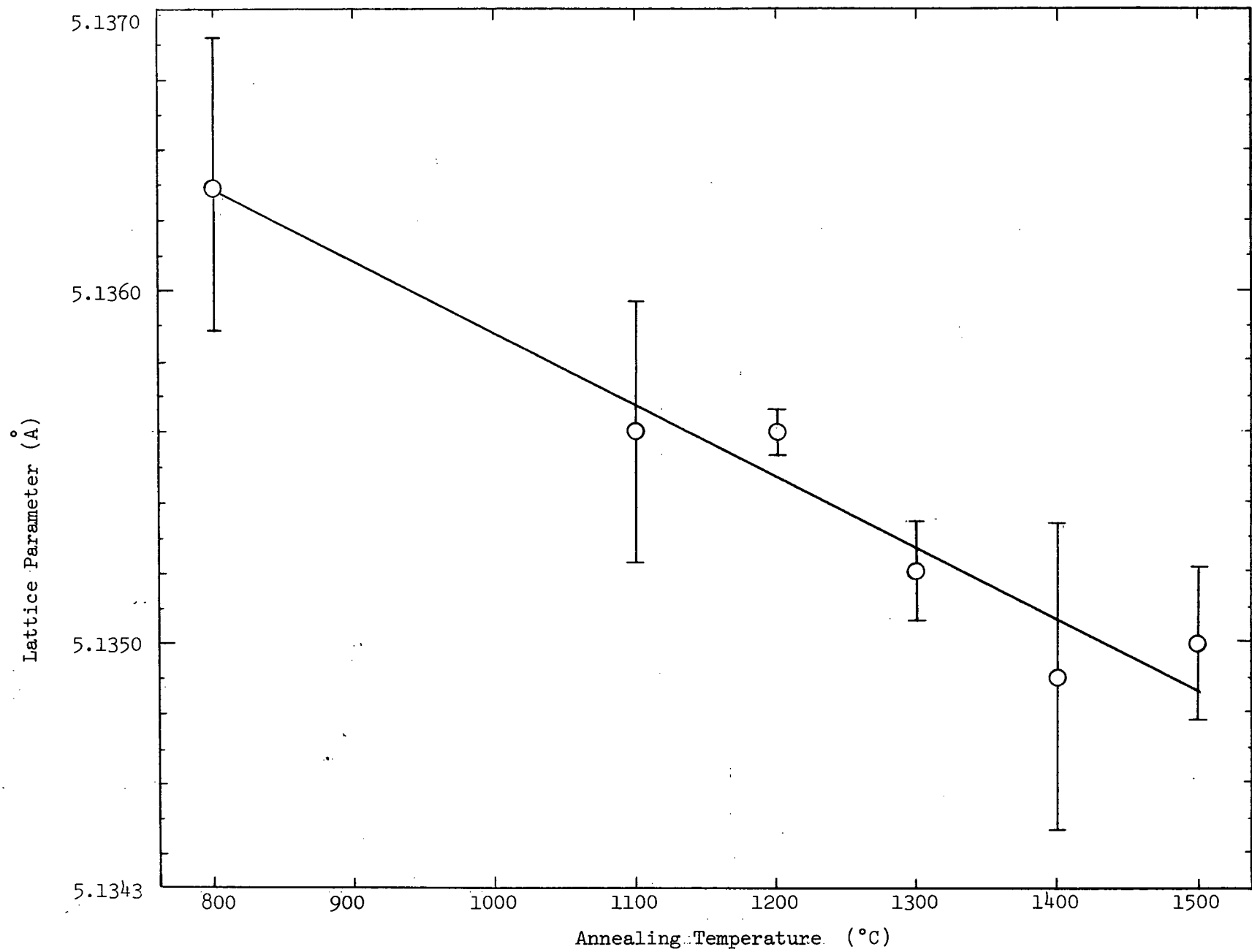


Figure 12. Decrease of Lattice Parameter as a Function of Annealing Temperature.
(over-all data with mean values).

Thus far in the literature, only a few workers have reported their lattice parameter values for the $Zr_{0.85}Ca_{0.15}O_{1.85}$ cubic solid solution and these values vary widely. For this composition, Kingery et al.²⁵ reported that the lattice parameter is 5.131Å. Their sample was prepared by calcining the $CaCO_3$ and ZrO_2 mixtures at 1300°C to form solid solution. The reacted mixtures were then cold-pressed and sintered at 2000°C for 7 hours. For the same composition, Tien and Subbarao²² reported a lattice parameter of 5.133Å for their sample which was prepared by reacting the $CaCO_3$ and ZrO_2 mixtures at 1350°C for 24 hours. The reacted mixtures were then compacted and sintered at 2000°C in an oxygen atmosphere for 2 hours and later annealed at 1400°C for one week. Roy and Diness²⁴ have reported that the lattice parameter for the $Zr_{0.85}Ca_{0.15}O_{1.85}$ solid solution, changed from 5.144Å to 5.134Å when it was heated to 1600°C and 1800°C respectively and then subsequently quenched at about 1000°C per second. The lattice parameter of the same composition obtained in the present study is 5.1350Å when the sample was annealed at 1500°C for 24 hours after hot-pressing.

In view of the experimental results obtained in the present investigation together with those reported by other workers, it can be inferred that the lattice parameter of the cubic unit cell of the $Zr_{0.85}Ca_{0.15}O_{1.85}$ solid solution significantly depends on the heat treatment of the material.

2. Relationship Between Lattice Parameter and Band Frequency of the Infrared Absorption Spectra

The relationship between lattice parameter and peak band frequency of the infrared absorption spectra for the $Zr_{0.85}Ca_{0.15}O_{1.85}$

solid solution was obtained from X-ray diffraction and infrared absorption spectroscopy data which are given in Table 3, APPENDIX I.

The solid solutions of CaO-stabilized ZrO_2 gave a broad band in the infrared absorption spectra, as shown in Fig. 9. The peak frequency of the absorption bands was obtained by taking the intersecting point of two straight lines which were drawn parallel to the spectral tracing.

Figure 13 is a least squares fit plot which shows a linear relationship between lattice parameter and peak band frequency of the infrared absorption spectra for the $Zr_{0.85}Ca_{0.15}O_{1.85}$ solid solution. It is quite evident that the value of the peak band frequency is raised from 440 cm^{-1} to 455 cm^{-1} as the lattice parameter is reduced from 5.1369 \AA to 5.1344 \AA . This observation is in accord with the postulation made by Baun and McDevitt³³, in which they stated that, as the unit cell of a type C (cubic) oxide increases in size, the frequency of the band is lowered and a linear relation can be obtained from plot of unit cell dimension and band frequency.

From all these observations it appeared that there is a definite lattice contraction or shrinkage of the cubic unit cell in the $Zr_{0.85}Ca_{0.15}O_{1.85}$ solid solution after heat treatment.

3. Effect of Annealing Time on the Lattice Parameter

The effect of annealing time on the lattice parameter values of the $Zr_{0.85}Ca_{0.15}O_{1.85}$ solid solution has been studied at 1100°C , 1300°C , 1400°C , and 1500°C . Four series of samples from four separate specimens were used. The annealing time varied from 5 hours to 70 hours at each temperature. The experimental data are given in Table 4,

APPENDIX I.

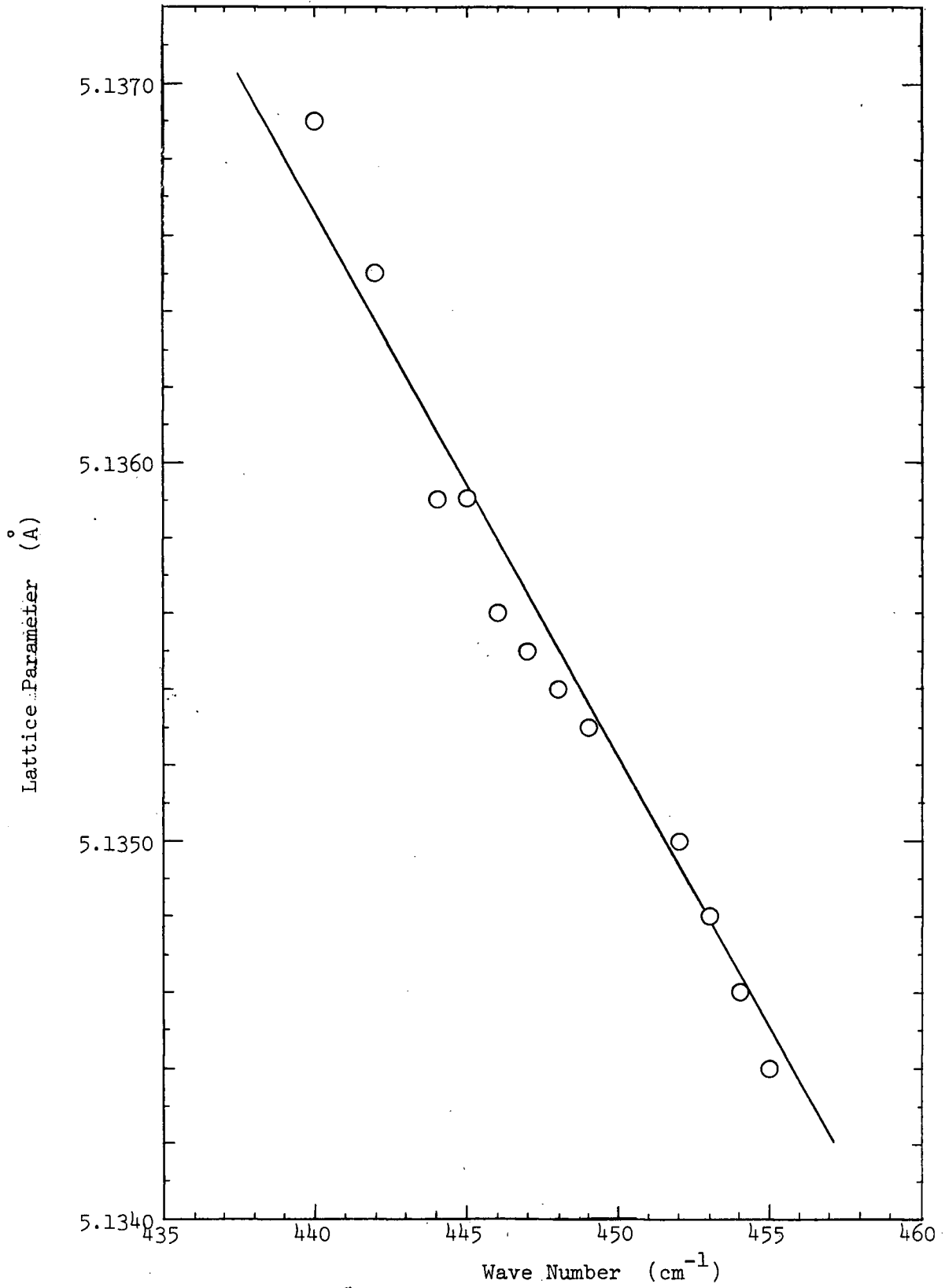


Figure 13. Relationship Between Lattice Parameter and Peak Band Frequency of the Infrared Absorption Spectra of the CaO-stabilized ZrO₂ Solid Solution After Heat Treatment.

Figure 14 shows the variation of lattice parameter values as a function of annealing time at each temperature. From these plots, it can be seen that the lattice parameter values decreased rapidly with annealing time during the early stage of annealing. At 1100°C and 1300°C, the lattice parameter reached a constant value after 16 hours of annealing time and remained constant on further annealing; whereas at 1400°C and 1500°C, the lattice parameter decreased and reached a constant value after 24 hours of annealing. No further change of lattice parameter was observed when these samples were subsequently annealed for a longer period at the same temperature.

(C) Electrical Conductivity of the $Zr_{0.85}Ca_{0.15}O_{1.85}$ Solid Solution:

1. Electrical Conductivity as a Function of Temperature

The electrical conductivity of the $Zr_{0.85}Ca_{0.15}O_{1.85}$ cubic solid solution has been measured over the temperature range of 500°-1400°C at 200°C intervals.

The conductivity-temperature data are given in Tables 1, 2, and 3, APPENDIX II. Figure 15 shows the least squares fit of the Arrhenius relation for three of the eight measured specimens obtained at the temperatures after 30-45 minutes of soaking during the heating cycle.

The activation energy for conduction obtained from the Arrhenius relation is given in Table 4, APPENDIX II. Figure 16 shows the relation between activation energy and annealing temperature for data obtained at the equilibrated temperatures during heating cycle. From this plot it can be seen that the relation between the activation energy for electrical conduction and annealing temperature shows a minimum value at 1100°C.

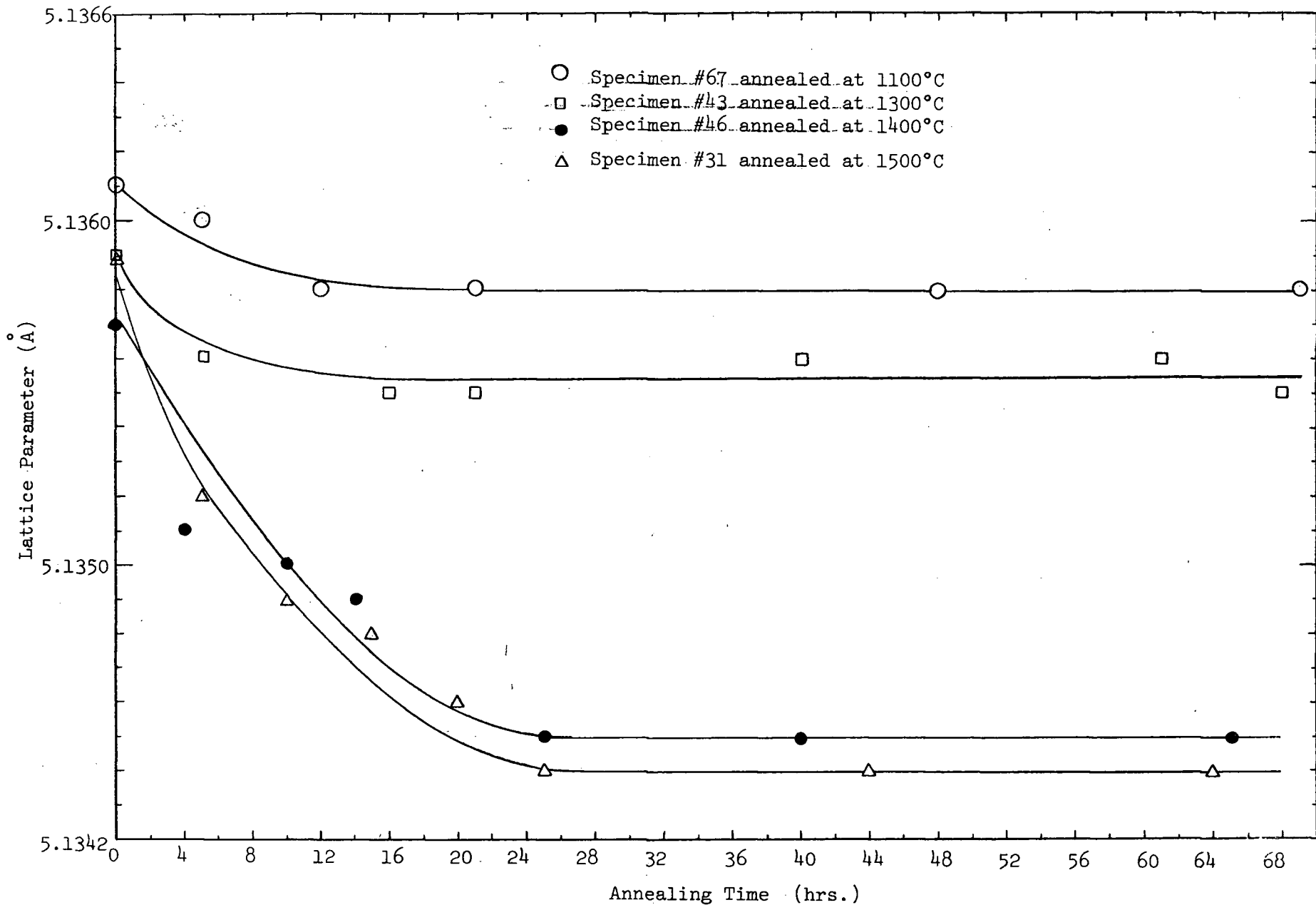


Figure 14. Decrease of Lattice Parameter as a Function of Annealing Time.

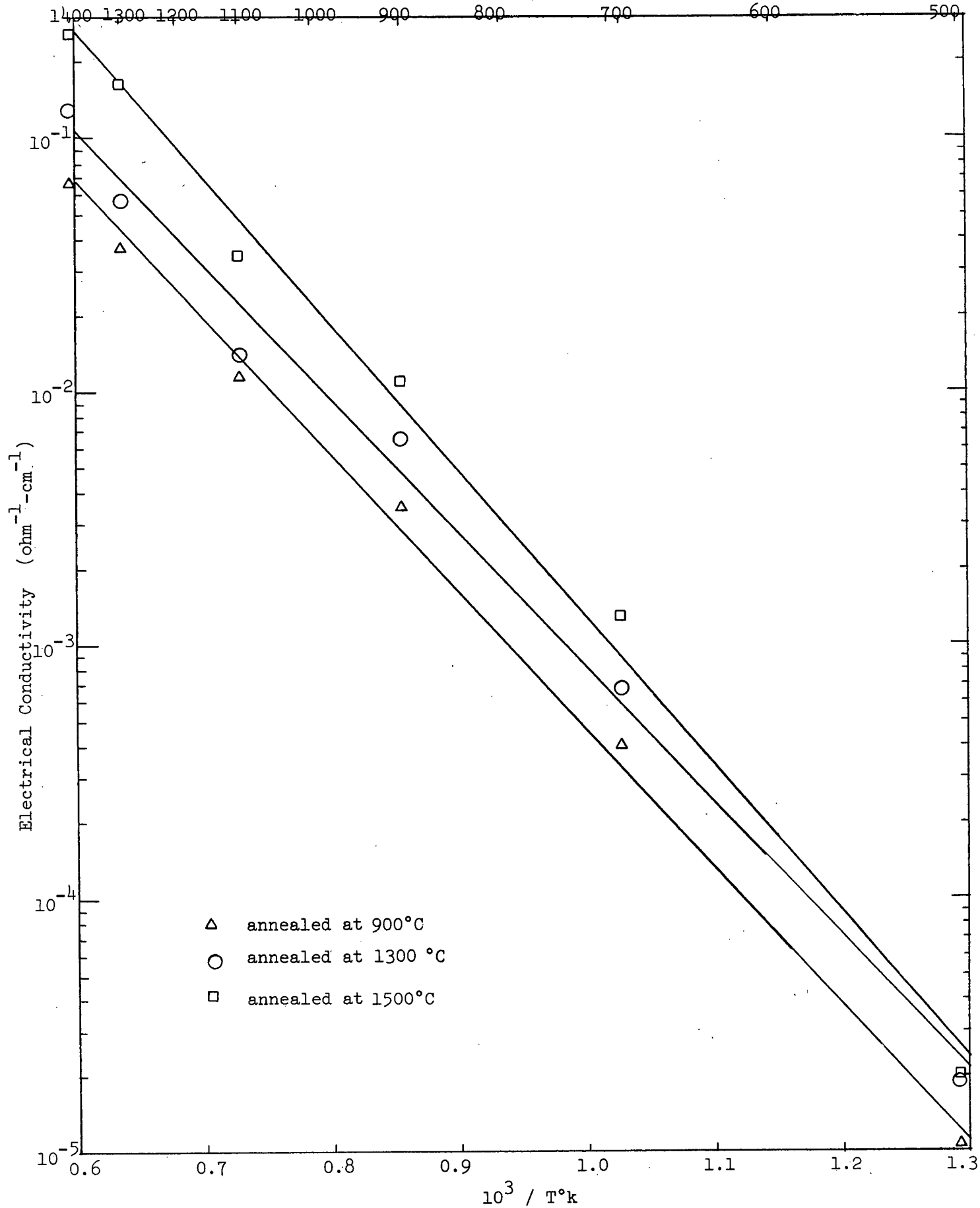


Figure 15. Arrhenius plot of Electrical Conductivity and Temperature.

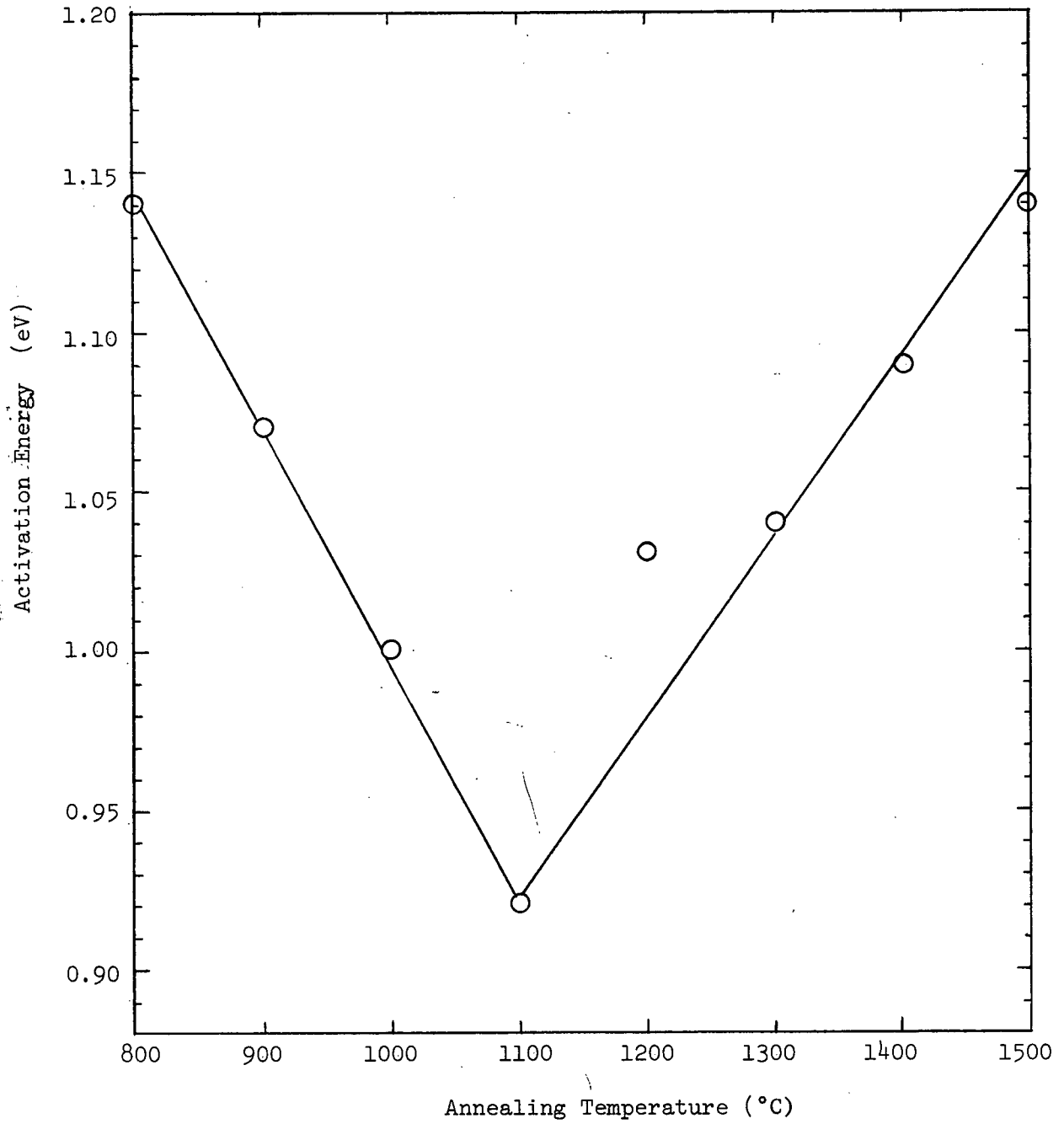


Figure 16. Change of Activation Energy for Electrical Conduction With Annealing Temperature.

This indicates that the electrical conductivity of the CaO-stabilized ZrO_2 solid solutions significantly depends on its thermal history.

The over-all electrical conductivity values obtained in the present investigation appeared to be in good agreement with those reported in the literature. For the purpose of comparison, the electrical conductivity data for the solid solution having composition of 15 mole% CaO and 85 mole % ZrO_2 obtained in the present investigation along with those reported by other workers are shown in Fig. 17 and the electrical conductivity at 1000°C together with the activation energy reported in the literature are given in Table 5, APPENDIX II. In general, the activation energy for conduction obtained in this study seemed to be slightly lower than most reported values. However, when specimens were annealed at higher temperatures, e.g. 1500°C, the specimens appeared to give higher activation energy values which are more comparable with the reported values.

The electrical conductivity of the specimens measured immediately after it reached the desired temperature and also after soaking for 30-45 minutes at the same temperature was the same, as shown in Fig. 18. This indicates that the 30-45 minutes of heat treatment of the specimens at a given temperature did not significantly affect the conductivity. The structural change associated with the heat treatment as reported earlier in the present investigation was very small (see Fig. 14) and did not cause any significant effect on the conductivity when carried out after 30-45 minutes of temperature equilibration.

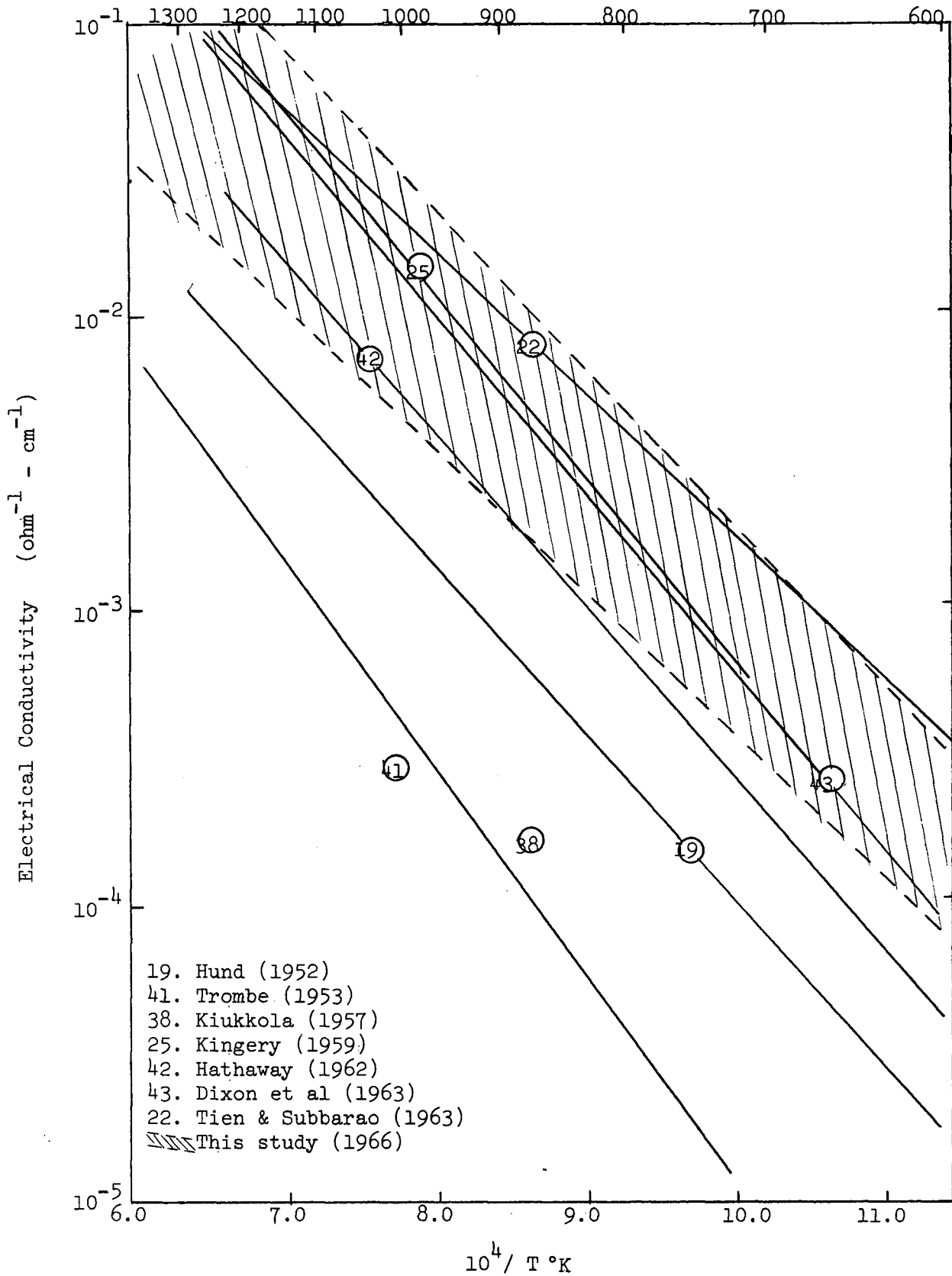


Figure 17. Comparison between the electrical conductivity data from the literature and the present data for the $\text{Zr}_{0.85}\text{Ca}_{0.15}\text{O}_{1.85}$ solid solution.

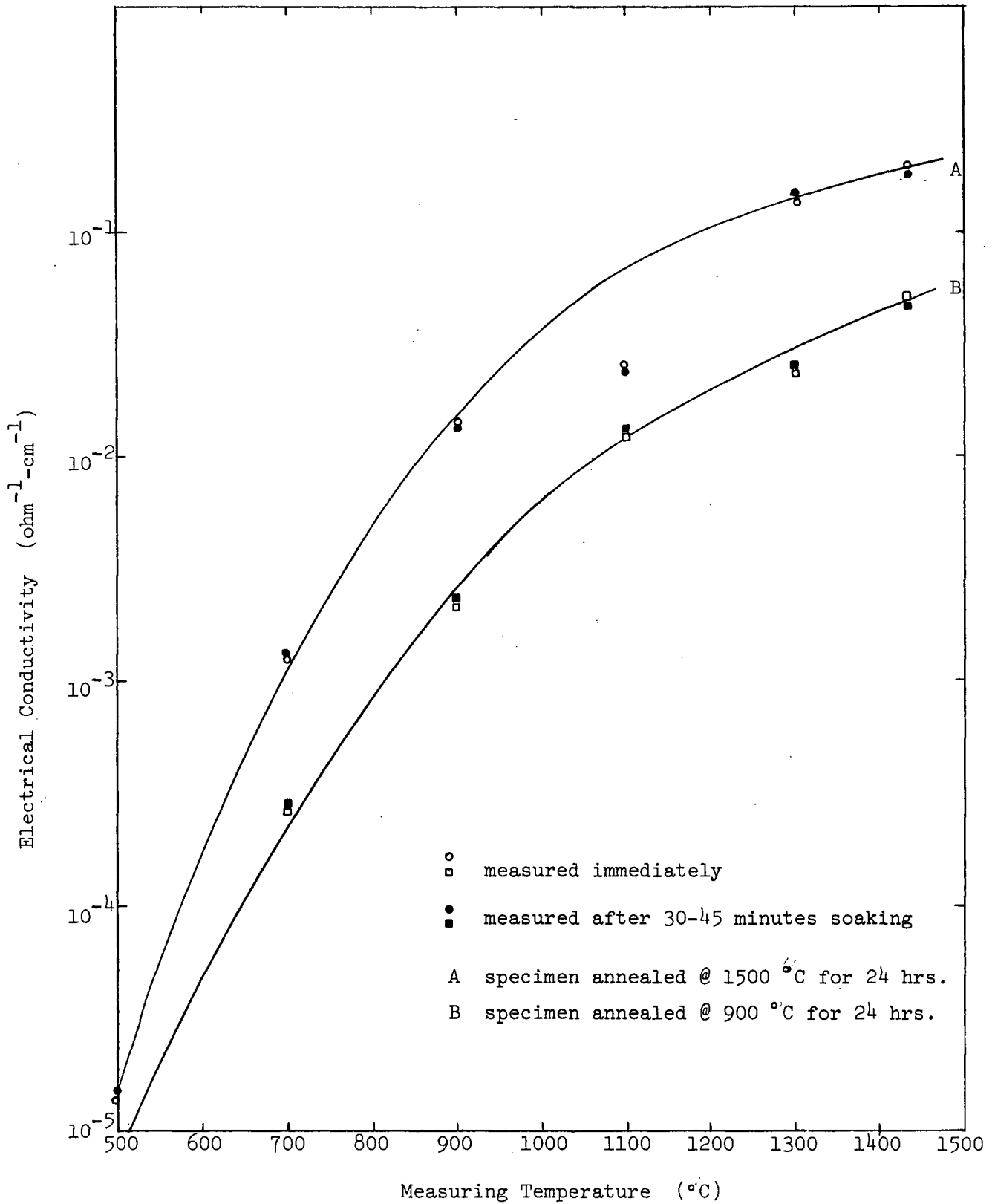


Figure 18. Variation of Electrical Conductivity as Measured Immediately and After 30-45 Minutes of Soaking at the Same Temperature.

The electrical conductivity measured during the heating and cooling cycles, however, showed some variations, as shown in Figs. 19 and 20 and also in Table 3, APPENDIX II. It was observed that when specimens were annealed at temperatures below 1000°C, the electrical conductivity values measured during the cooling cycle were higher than those measured during the corresponding heating cycle; whereas when specimens were annealed at temperatures above 1300°C, the electrical conductivity values measured during the cooling cycle were lower than those measured during the corresponding heating cycle.

2. Calculation of Oxygen Ion Diffusion Coefficients From Electrical Conductivity Measurements

As it has been shown by previous workers that the electrical conductivity of the CaO-ZrO_2 cubic solid solutions at high temperatures is due entirely to the migration of oxygen ions, the oxygen ion diffusion coefficients can be calculated from the electrical conductivity data by the Nernst-Einstein equation (see APPENDIX VI).

The diffusion coefficient-temperature data for the $\text{Zr}_{0.85}\text{Ca}_{0.15}\text{O}_{1.85}$ solid solution calculated from the conductivity data obtained in the present study are given in Table 6, APPENDIX II. Figure 21 shows the least squares fit of Arrhenius relation for three of the 8 specimens measured.

Figure 22 shows the relationship between the activation energy for oxygen ion diffusion and annealing temperature. From this plot it can be seen that there is a minimum activation energy at 1100°C. A similar trend was also observed between the activation energy for electrical

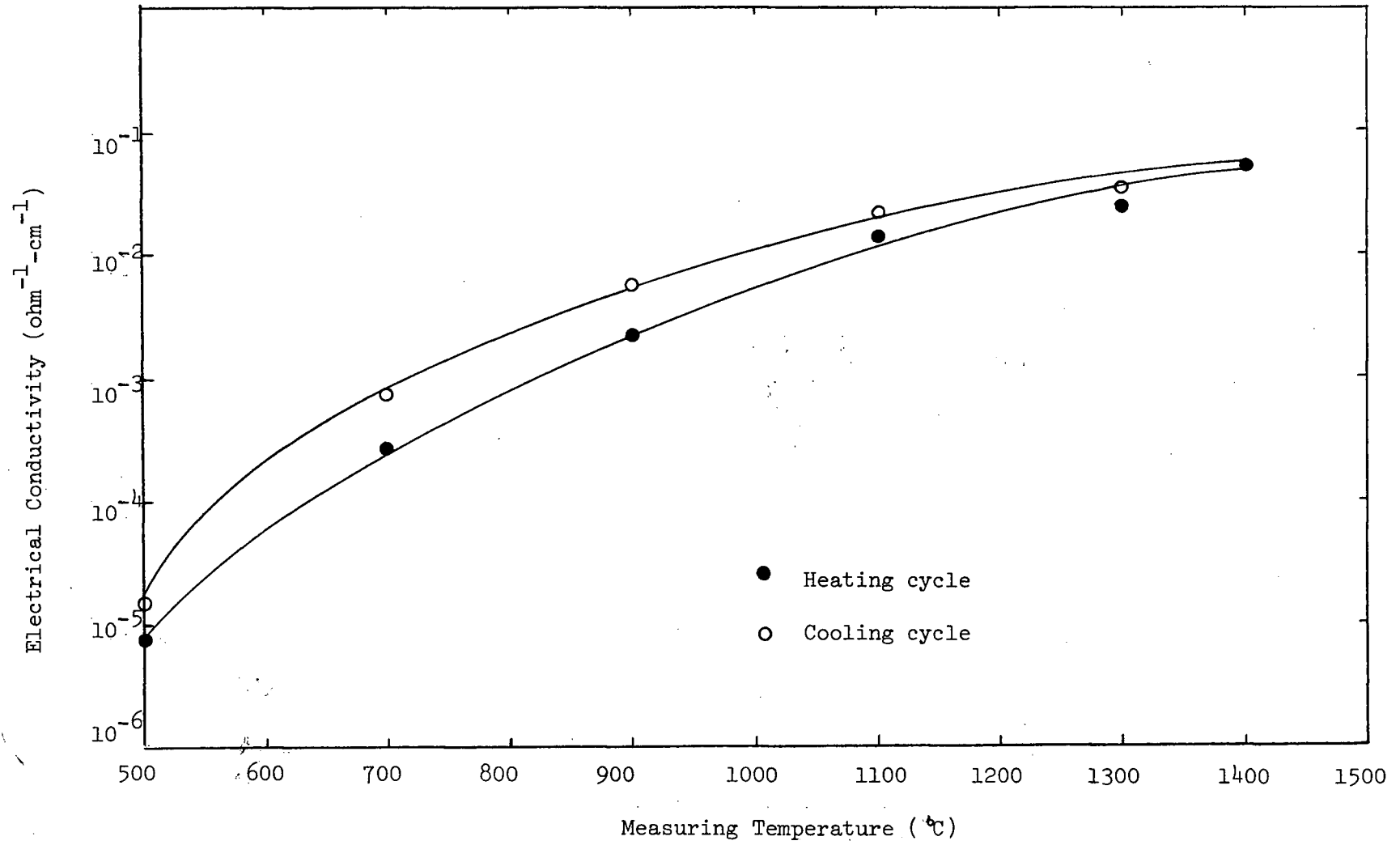


Figure 19. Change of Electrical Conductivity as Measured During the Heating and Cooling Cycles.
 (Specimen annealed at 900 °C)

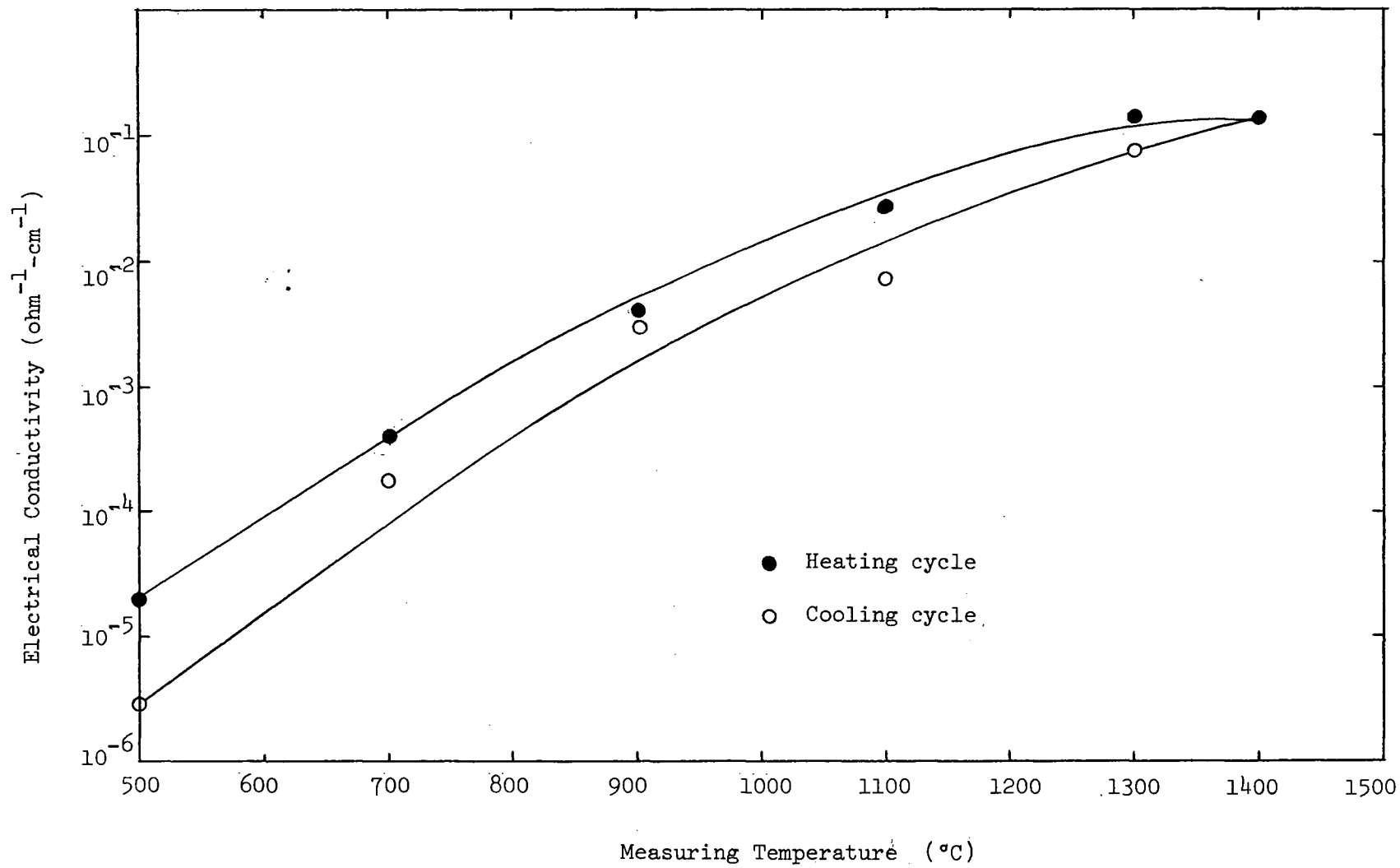


Figure 20. Change of Electrical Conductivity as Measured During the Heating and Cooling Cycles.
 (Specimen annealed at 1400 °C)

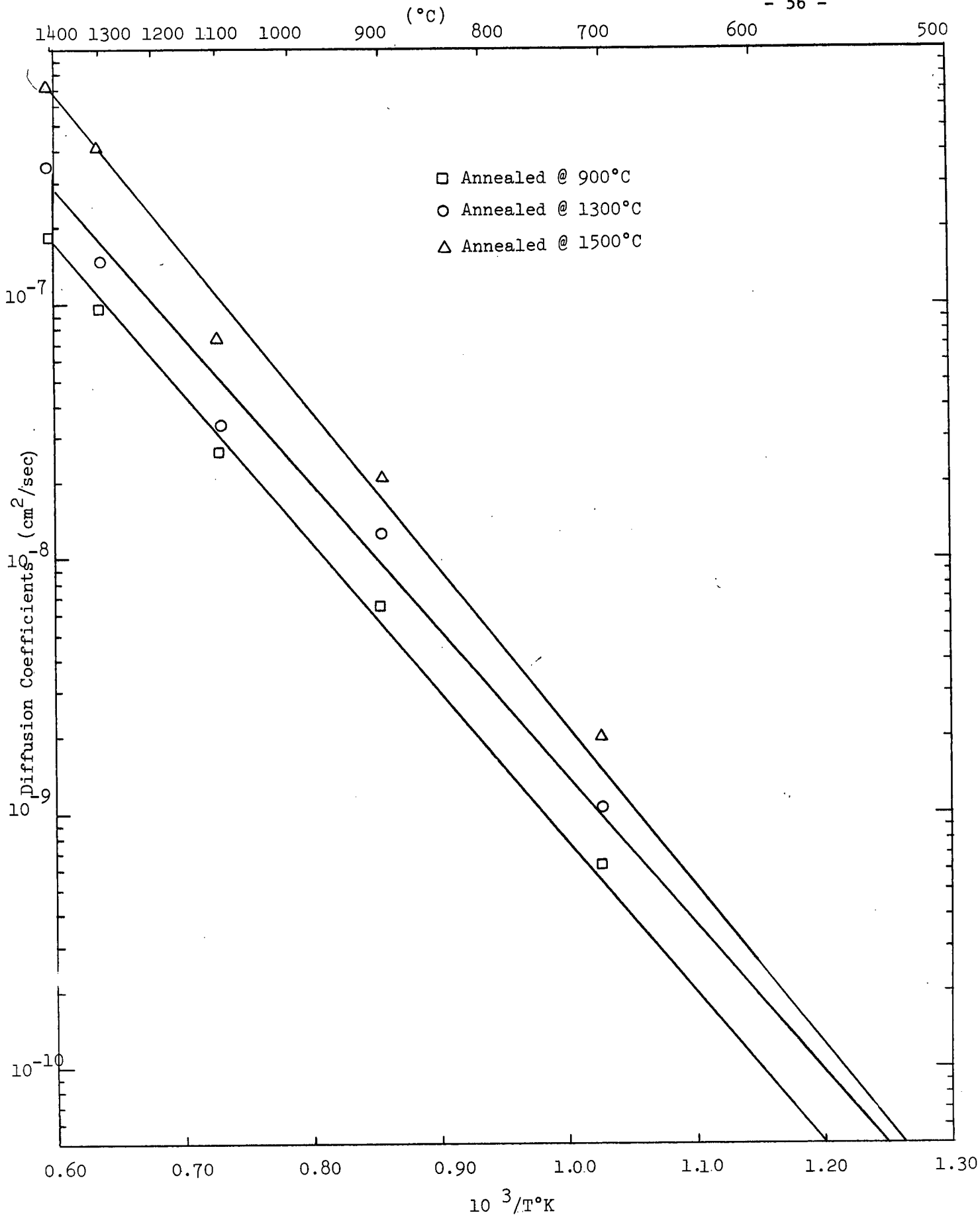


Figure 21. Arrhenius plot of Oxygen Ion Diffusion Coefficients and Temperatures.

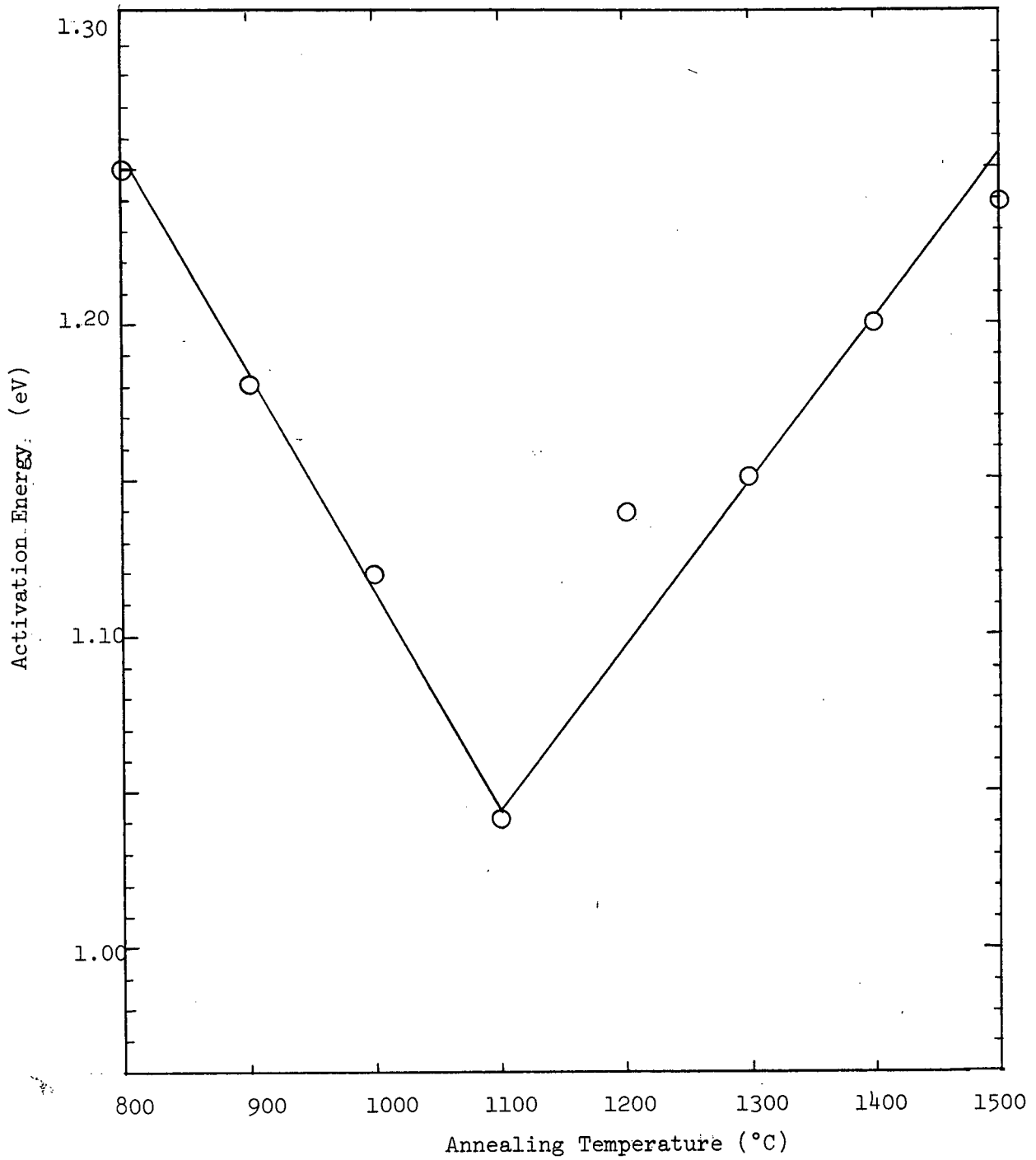


Figure 22. Change of Activation Energy for Oxygen Ion Diffusion with Annealing Temperature.

conduction versus annealing temperature, as shown in Fig. 16.

The oxygen ion diffusion coefficients calculated from the electrical conductivity data obtained in the present investigation appeared to be in good agreement with those reported by Kingery²⁵ and by Carter and Simpson²⁷, as shown in Fig. 23. However, the activation energy for oxygen ion diffusion obtained in this study seemed to be slightly lower than the value of 1.34 eV reported by Carter and Simpson and of 1.32 eV (after correction for the correlation factor in diffusion, the published value being 1.22 eV) by Kingery. The highest activation energy for diffusion obtained in this study is about 1.25 eV for a specimen annealed at 1500°C for 24 hours. The band plotted in Fig. 23 is the summary of experimental results obtained in the present study with the highest and lowest values as boundaries.

(D) Porosity and Density of the $Zr_{0.85}Ca_{0.15}O_{1.85}$ Solid Solution

1. Apparent Porosity of the Hot-pressed Specimens

The apparent porosity, which is expressed as a percentage for the volume of the open pores of the specimen to the exterior volume of the hot-pressed specimens before and after heat treatment has been determined by the water absorption procedure. The experimental data for the apparent porosity and bulk density of the measured specimens are given in Table 1, APPENDIX III.

The bulk density of most specimens was found to vary from 4.34 to 4.60 grams/cc which did not change with any heat treatment below 1400°C.

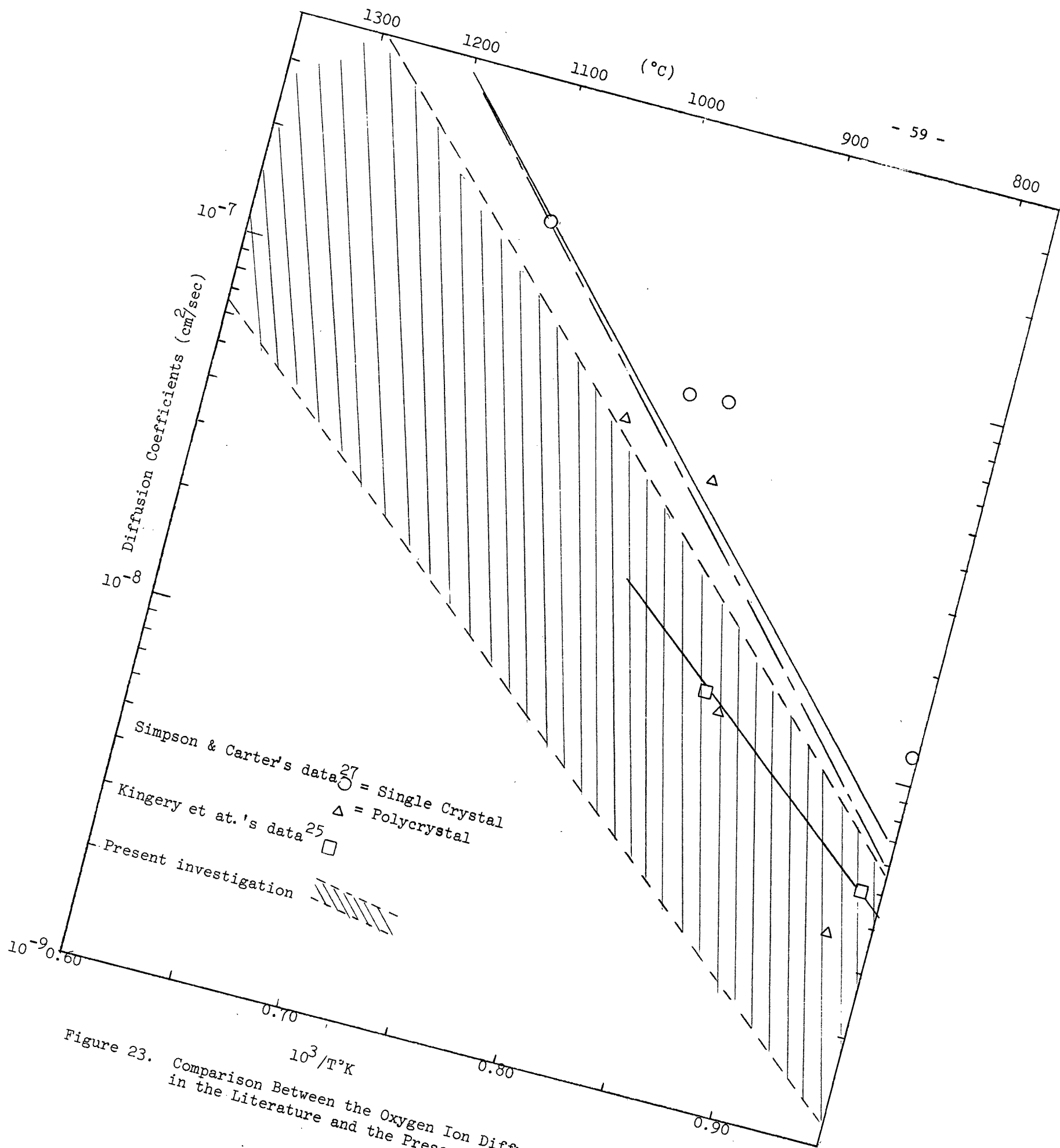


Figure 23. Comparison Between the Oxygen Ion Diffusion Coefficient Data in the Literature and the Present Data in the CaO-ZrO₂ System

2. True Density of the $Zr_{0.85}Ca_{0.15}O_{1.85}$ Solid Solution

The true density of the material was determined by the pycnometric method using ethyl alcohol, bromoform, and distilled water. The experimental data obtained from ethyl alcohol and bromoform were widely scattered and inconclusive. The data obtained from distilled water are given in Table 2, APPENDIX III. The theoretical density of the solid solution assuming both oxygen vacancy and oxygen interstitial models calculated from X-ray data is given in Table 3, APPENDIX III.

Figure 24 shows the relationship between the true density of the solid solution and the annealing temperature. It is evident that the true density of the material was affected by the annealing treatment. When the specimens were annealed below $1000^{\circ}C$ the true density appeared to be slightly higher than the theoretical density according to the oxygen vacancy model and lower than the oxygen interstitial model. When the specimens were annealed above $1000^{\circ}C$ for 24 hours the true density appeared to be comparable with the theoretical density of the oxygen vacancy model.

(E) Chemical Analysis of the Hot-pressed $CaO-ZrO_2$ Solid Solution

In the specimen preparation the solid solution was assumed to have the composition of 15 mole % CaO and 85 mole % ZrO_2 . In order to check whether the annealing treatment after hot-pressing has any effect on the change of the chemical constituents, chemical analyses for CaO and ZrO_2 contents in the sample have been carried out on four specimens. These four specimens have been annealed at $800^{\circ}C$, $1000^{\circ}C$, $1100^{\circ}C$, and $1400^{\circ}C$ respectively for about 24 hours. The chemical analyses were carried out.

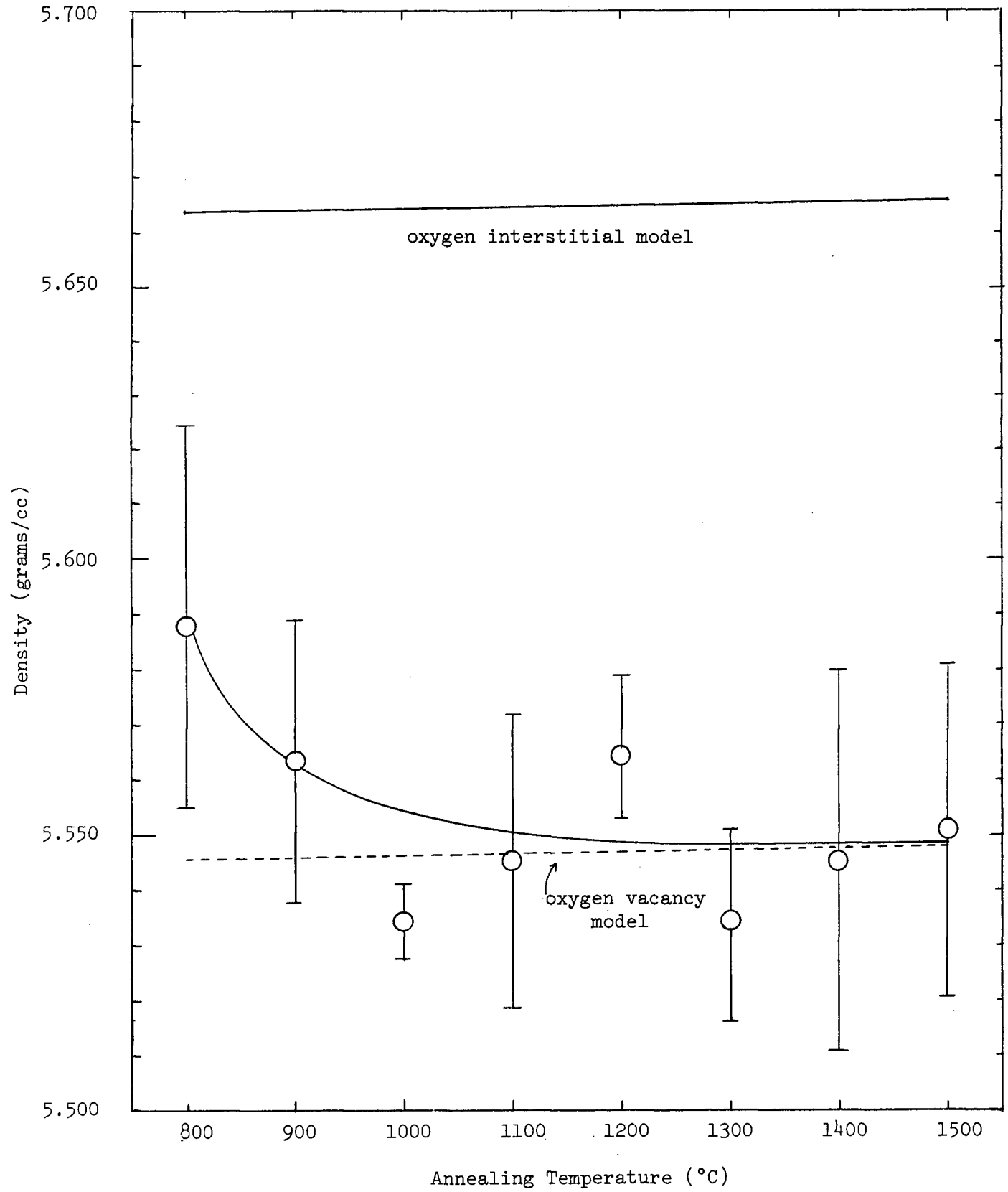


Figure 24. Change of Density with Annealing Temperatures.

by "Coast Eldridge Engineers and Chemists Ltd" in Vancouver. The experimental results are given in Table III.

Table III
Chemical Analysis of CaO-ZrO₂ Solid Solutions

Specimen No.	Annealing		ZrO ₂		CaO	
	Temp.	Time	Wt. %	Mole %	Wt. %	Mole %
56	800°C	26 hrs.	91.97	86.29	6.65	13.71
62	1000°C	25 hrs.	92.25	86.66	6.46	13.34
63	1100°C	24 hrs.	92.10	85.71	6.99	14.29
65	1400°C	25 hrs.	91.40	85.44	7.09	14.56
				86.02±0.5		13.98±0.5

According to the analyst, it was claimed that the accuracy of these analyses was about ± 1 wt.% for ZrO₂ and about ±0.4 wt.% for CaO. Accepting this accuracy for analysis, it appears that annealing of the specimens has no significant effect on the change of the chemical content (i.e. the amount of [Zr⁴⁺] and [Ca²⁺] in the solid solution).

IV. DISCUSSION

(A) Lattice Contraction or Shrinkage of the Cubic Unit Cell in the Zr_{0.85}Ca_{0.15}O_{1.85} Solid Solution

From the experimental results obtained in the present investigation, it is quite evident that annealing of the Zr_{0.85}Ca_{0.15}O_{1.85} solid solution after hot-pressing has a definite effect on its lattice parameter. As the annealing temperature was increased from 800 to 1500°C the lattice parameter of the solid solution decreased correspondingly in a linear relation. At a constant temperature of 1100, 1300, 1400, and 1500°C, the lattice parameter decreased asymptotically with annealing time and approached a constant value which varied with the

temperature. From a literature survey it is also apparent that there exists some relationship between the lattice parameter and the temperature of specimen preparation.

In the formation of the cubic phase solid solution of ZrO_2 with CaO the Ca atoms are assumed to enter into the ZrO_2 structure by replacing the Zr atoms thus causing a rearrangement of the atoms resulting in a fluorite-type structure. The substitution for Zr atoms with Ca atoms is assumed to be completely random and the distribution of CaO in the solid solution is homogeneous. The three models that have been postulated to account for the formation of a homogeneous solid solution are: the cation interstitial model, the anion (oxygen) vacancy model, and the oxygen interstitial model.

In the cation interstitial model it is assumed that the Ca atoms first enter into the ZrO_2 lattice without replacing the Zr atoms and thus become interstitials. If this mechanism is operative the lattice parameter of the cubic unit cell will be slightly larger than the true cubic unit cell and the density of the material will be increased. Diness and Roy²⁴ have reported that there is evidence indicating such a solid solution is possible by heating the material at 1800°C and then quenching at 1000°C/sec. According to their data, the theoretical density of a cation interstitial solid solution having composition of 15 mole % CaO + 85 mole % ZrO_2 would be in the order of about 6.00 grams/cc (see Fig. 3).

In the anion (oxygen ion) vacancy model it is assumed that the Ca atoms enter into the ZrO_2 lattice by replacing the Zr atoms with the

formation of an equal number of oxygen vacancies to maintain charge neutrality. This oxygen vacancy model is generally accepted by most workers^{19,21,24,25} as the predominant point defect-type structure in the fluorite-type crystalline solution field of the CaO-ZrO₂ system. According to the data by Diness and Roy for a composition of 15 mole % CaO + 85 mole % ZrO₂, the theoretical density is in the order of about 5.54 grams/cc. (see Fig. 3).

In the oxygen interstitial model it is assumed that the Ca atoms enter into the ZrO₂ lattice by replacing the Zr atoms with the formation of oxygen vacancies and oxygen ion interstitials. That is, instead of oxygen ions diffusing out from the lattice they may remain as interstitials. Buyers⁴¹ has mentioned that such a model is quite possible as indicated in his theoretical model for electrical conduction in the Ta/CaO-stabilized ZrO₂/W system. If this mechanism is operative the lattice parameter of the cubic unit cell would be slightly larger than the value without the oxygen interstitials. The density of the material would also be higher than that of the oxygen vacancy model but lower than that of the cation interstitial model, since the atomic weight of a Ca atom is much greater than that of an oxygen atom.

According to the X-ray data, the theoretical density of the Zr_{0.85} Ca_{0.15} O_{1.85} solid solution prepared in the present investigation was calculated to be in the range of 5.546-5.549 grams/cc for the pure oxygen vacancy model and in the range of 5.664-5.666 grams/cc for the pure oxygen interstitial model. The pycnometer measured density of the solid solution was found to be in the range 5.534-5.588 grams/cc which indicates that the cubic solid solution is conclusively not the cation interstitial

solid solution. The calculated and measured densities of the $Zr_{0.85}Ca_{0.15}O_{1.85}$ solid solution obtained in the present study are in good agreement with those reported by Diness and Roy²⁴ (see Fig. 3) for the oxygen vacancy model. However, the slightly higher density observed in the specimens annealed at low temperatures is indicative of the deviation from the pure oxygen vacancy model and could tentatively be interpreted as due to the presence of a small number of interstitial oxygen ions remaining in the lattice.

The minimum amount of CaO required to stabilize ZrO_2 in the cubic phase has been agreed upon by various workers to be in the range of 12-13 mole %. The solid solution prepared in this investigation contained about 15 mole % CaO, which is just over the cubic phase boundary. Although in the literature no experimental observations have been reported on the existence of any inhomogeneity in a solid solution of the CaO- ZrO_2 system, the possibility of a non-uniform distribution of CaO in the ZrO_2 lattice can not be completely disregarded. It is possible that the cubic phase of ZrO_2 exists with some areas enriched in CaO and some areas slightly deficient in CaO because of the slow rate of this solid state reaction thus resulting in the inhomogeneous distribution of Ca^{2+} ions; although the over-all solid solution remains in a stable cubic form. It has been observed by both Hund¹⁹ and Tien and Subbarao²², that the variation of lattice parameter with CaO content in the cubic field of CaO- ZrO_2 solid solutions was very small as compared with the dimension of the cubic unit cell. (see Fig. 4). When the CaO content in the cubic field varied about 1 mole % the change of the lattice parameter was in the order of about 0.001Å. The magnitude of change of the lattice parameter observed

in the present investigation was also in the same order. Thus, the possibility of the existence of inhomogeneity in the solid solution is not inconsistent with this observation.

The results of the density measurements appeared to rule out the possibility of extensive formation of thermally-induced vacancies, that is, the formation of more oxygen vacancies and cation vacancies (Schottky defects). Loss of Ca ions from the unit cell appeared to be unfavorable since no previous experimental observations have been reported on the loss of Ca^{2+} ions upon heat treatment of specimens of the CaO-ZrO_2 solid solutions. De-stabilization of the cubic CaO-ZrO_2 solid solution was not observed from the X-ray diffraction measurements in this study.

The decrease of lattice parameter with time at a fixed temperature can be assumed to be a rate process. The data were found to fit best the following empirical relation⁵⁸:

$$\frac{a_o - a_t}{a_o} = k t$$

where a_t = the lattice parameter at time t

a_o = the lattice parameter at time 0 (before annealing)

k = rate constant

t = annealing time

When $\frac{a_o - a_t}{a_o}$ versus t was plotted, a linear relation was obtained, as shown in Fig. 25. The slope of these lines is equal to the rate constant k . This empirical relation appeared to satisfy the kinetics of a "second order reaction".

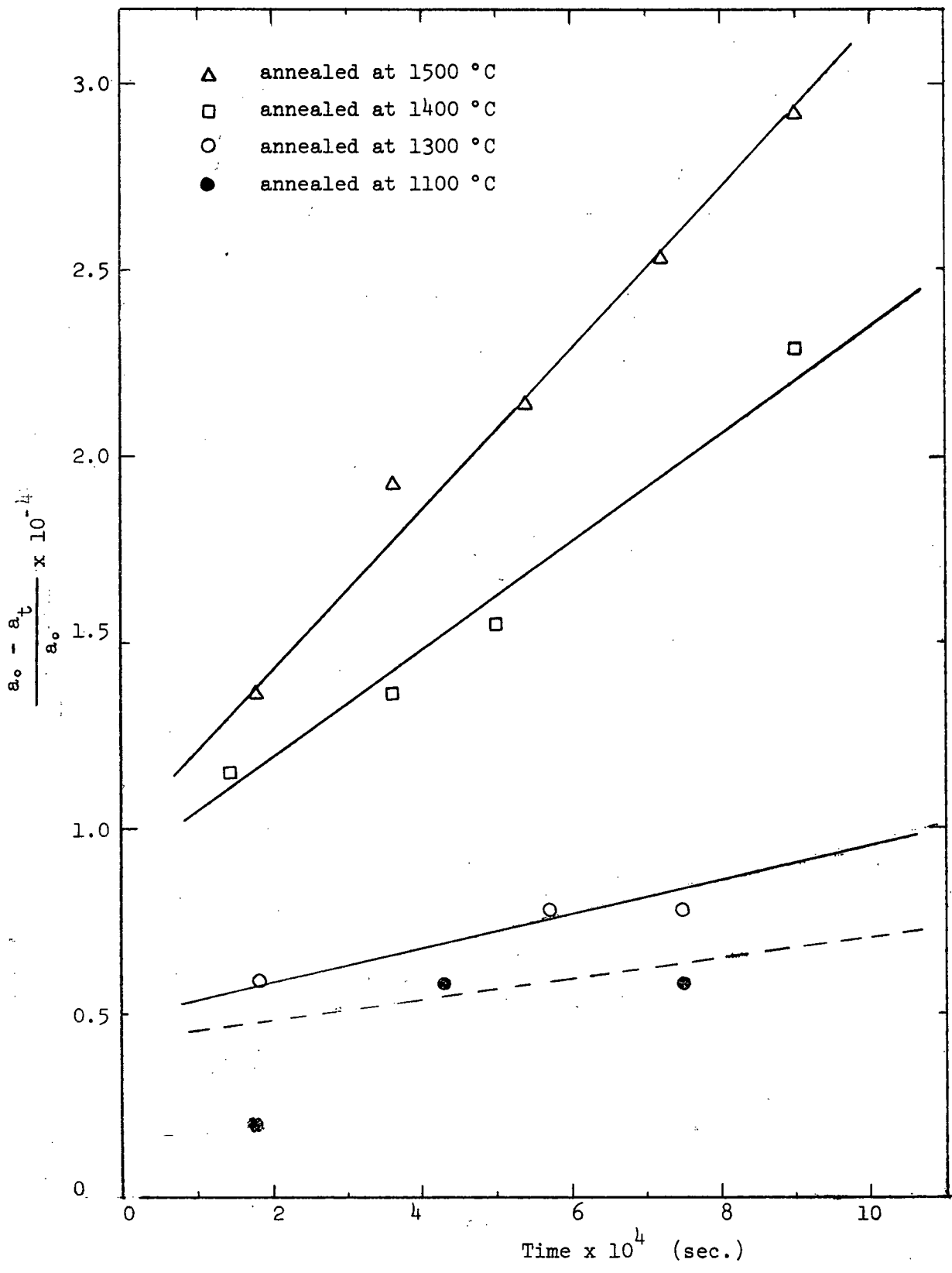


Figure 25. Relative Decrease of Lattice Parameter with Annealing Time.

Using the rate constants, the temperature coefficients for this process can be determined by an Arrhenius relation as follows⁵³:

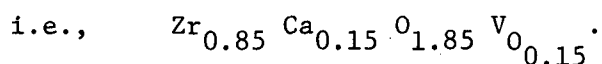
$$k = A \exp \left(\frac{-E}{KT} \right)$$

- where
- k = rate constant
 - A = pre-exponential constant
 - E = activation energy
 - K = Boltzman's constant
 - T = absolute temperature

When $\log(k)$ versus $\frac{1}{T}$ was plotted, a linear relation was obtained, as shown in Fig. 26. The activation energy calculated from this Arrhenius plot was found to be about 1.30 ± 0.20 eV. This value was observed to be in the same order of magnitude as the activation energy for oxygen ion diffusion in the CaO-ZrO₂ system or as the sum of energy for oxygen vacancy motion and the energy for dissociation of an oxygen vacancy from pairing or clustering with a Ca²⁺ ion.

The lattice contraction or shrinkage of the cubic unit cell could tentatively be interpreted by either of the following two mechanisms:

1. During the formation of the cubic solid solution of ZrO₂ with CaO by the hot-pressing process, it is possible that a very small fraction of the oxygen ions after being displaced to create the vacancies are trapped in the lattice as interstitials. As the hot-pressed specimens are subjected to further heat treatment, the oxygen ion interstitials are removed from the lattice thus causing a slight shrinkage of the unit cell. On the removal of all interstitials from the lattice, the solid solution would then be the final form of the oxygen vacancy material,



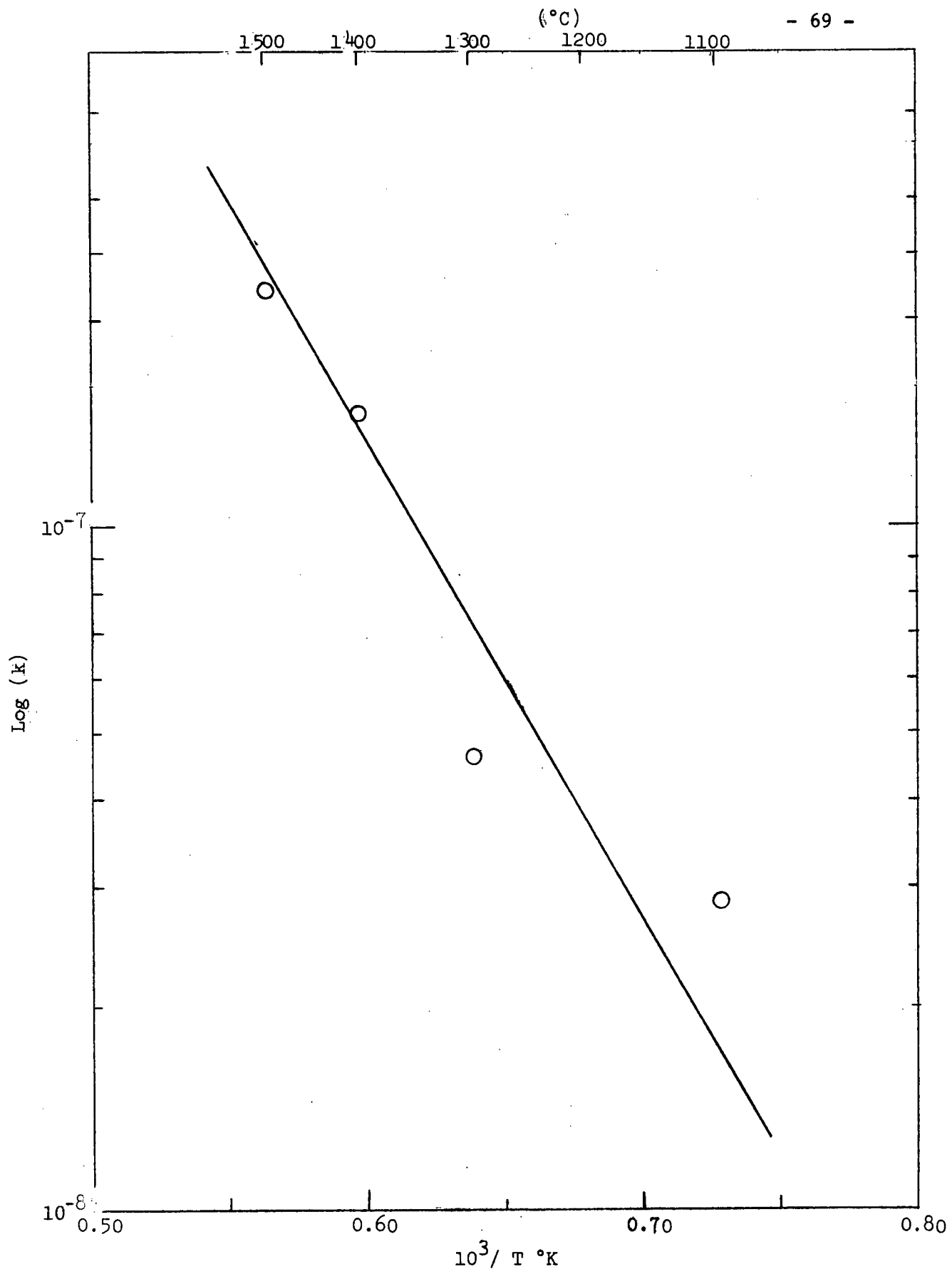


Figure 26. Arrhenius plot of the rate of relative decrease of lattice parameter and temperature.

2. During the formation of the cubic solid solution of CaO-ZrO_2 , the distribution of the CaO in the ZrO_2 lattice might not be completely uniform thus resulting in an inhomogeneous effect in the solid solution. As the specimens are subjected to further heat treatment after hot-pressing the material then becomes homogenized and attains the final form containing 15 mole % CaO .

In both mechanisms an equilibrium condition is reached at each temperature after a sufficient annealing time but this equilibrium value is dependent on the temperature of heat treatment. Judging from the activation energy obtained from the kinetic analysis, it appears that the lattice contraction of the cubic solid solution is controlled by a mechanism similar to that observed in the ionic conduction of the CaO-ZrO_2 system. However, the present data are insufficient to conclude which of the two mechanisms is a decisive one for explaining the shrinkage of the cubic unit cell.

(B) Effect of Annealing on the Electrical Properties of the $\text{Zr}_{0.85}\text{Ca}_{0.15}\text{O}_{1.85}$ Solid Solution.

The electrical conductivity of the $\text{Zr}_{0.85}\text{Ca}_{0.15}\text{O}_{1.85}$ cubic solid solution over the temperature range 500-1400°C obtained in the present investigation was found to be in good agreement with that reported in the literature. However, the activation energy for conduction obtained in this study was found to be significantly different from that obtained by other workers. The activation energy for conduction appeared to be dependent on the annealing temperature of the specimens after hot-pressing. A minimum activation energy was observed when the hot-pressed specimens were annealed at 1100°C for 24 hours. On the other hand, when the hot-pressed

specimens were annealed at 800°C and 1500°C for a similar period of time, the activation energy for conduction was observed to be slightly higher and comparable with those values reported by other workers. The following explanation is given for this variation.

In the cubic fluorite-type structure each cation has eight nearest neighbour oxygen ions. When Ca atoms diffuse into the ZrO_2 lattice by replacing Zr atoms, an equal number of oxygen vacancies are formed. This is necessary to maintain electronic neutrality in the system. Wachtman⁵⁹ has calculated that each vacancy is so tightly bound to a Ca ion that, to a good approximation, it can occupy only the eight nearest neighbour oxygen positions moving from one nearest position to another. Thus, each position is occupied with equal probability in the absence of a stress or electric field. On the other hand, a substitutional Ca ion can jump to an equivalent position only by interchanging with a Zr ion. Based on the proposed 8-position Nearest-Neighbour Model for ThO_2 containing CaO, which is also a solid solution of the cubic fluorite-type structure, he observed that the electrostatic attraction between an oxygen vacancy and substitutional Ca ion should cause association and that there is a difference of electrostatic energy of about 0.34 eV between nearest neighbour and next-neighbour positions. Furthermore, he estimated that the energy required to free an oxygen vacancy completely from a Ca ion would be in the order of about 0.71 eV, but he pointed out that the uncertainty in the electrostatic method of estimating the dissociation energy is so great that little weight should be attached to this value. From his study of the ThO_2 solid solution containing 1.5 mole % CaO, he calculated that the activation energy for the motion of an oxygen vacancy

neighbouring a Ca ion is about 0.93 eV and the activation energy of free oxygen-vacancy motion might well be slightly larger than for the motion of an oxygen vacancy neighbouring a foreign ion. It is generally believed that the volume electrical conductivity could be attributed to oxygen vacancies with an activation energy for motion alone, because the number of oxygen vacancies is fixed by the CaO content. However, Franklin⁶⁰ has pointed out that while the total number of oxygen vacancies is presumably fixed by the CaO content, most of these are bound to Ca ions and so do not contribute to volume conductivity. The number of free oxygen vacancies should still be thermally activated and conductivity by oxygen-vacancy motion should still require an activation energy which is the sum of an energy of motion and one half the energy of dissociation.

Since both CaO-ThO₂ and CaO-ZrO₂ solid solutions are of the cubic fluorite-type structure and the volume conductivity is based mostly on the motion of oxygen vacancies in the material, it is possible to interpret results obtained in the present investigation with the arguments outlined above. Assuming that the energy required for the motion of oxygen vacancy in the CaO-ZrO₂ system is very nearly the same as that in the CaO-ThO₂ system of 0.93 eV, any excess energy observed would be equal to one half of the energy of dissociation. The dissociation energy calculated from the observed activation energy for conduction is summarized in Table IV.

Table IV
 Energies for Oxygen Vacancy^C Motion and Dissociation in the CaO-ZrO₂ System

Annealing Temperature (°C)	Observed E in conduction (eV)	E for oxygen vacancy motion (eV)	Total E for dissociation (eV)
800	1.14	0.93	0.42
900	1.07	"	0.28
1000	1.00	"	0.14
1100	0.92	"	0
1200	1.03	"	0.20
1300	1.04	"	0.22
1400	1.09	"	0.32
1500	1.14	"	0.42

The relationship between the total energy and the heat treatment of the specimens is shown in Fig. 27. It can be seen that the activation energy for conduction obtained from specimens annealed at 1100°C is just the energy required for the motion of an oxygen vacancy, while the excess energy observed in the other specimens is one half the dissociation energy necessary for the vacancy-foreign ion to be dissociated before they could move under an electric potential.

The excess energy observed in the temperature range 800-1000°C can be considered in two aspects. It can be considered as the energy associated with the oxygen ion interstitials if they do exist in the lattice. In order to facilitate the migration of the oxygen vacancies during ionic conduction, it is necessary to remove all interstitial oxygen

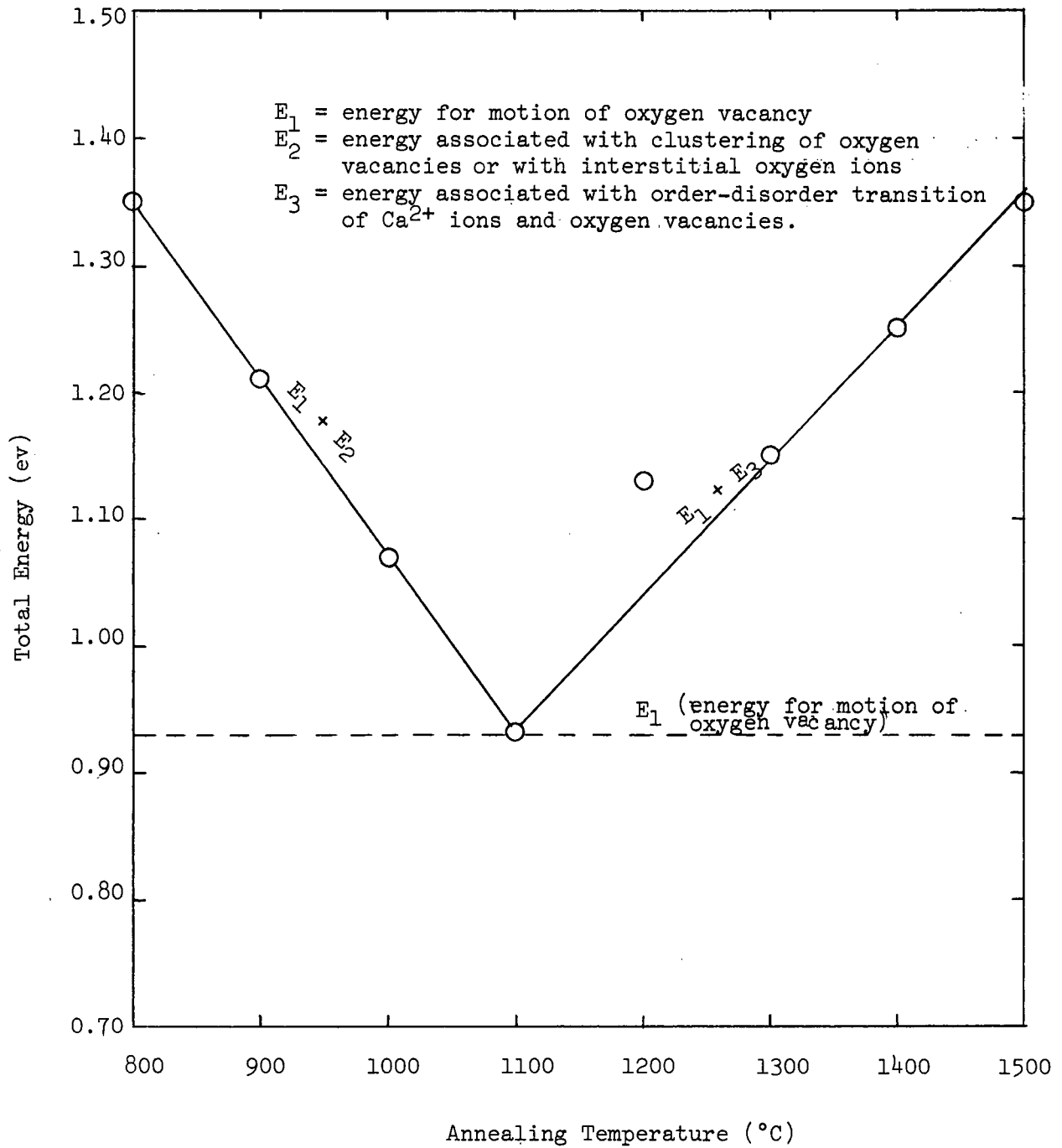


Figure 27. Change of Excess Energy for Conduction with Annealing Temperature.

ions from the lattice because they might be blocking the vacancy migration path. Thus, an extra amount of energy in addition to the energy for vacancy motion is required. On the other hand, this excess energy can also be regarded as the energy associated with localized pairing or clustering of the oxygen vacancies and Ca^{2+} ions due to the existence of an inhomogeneous distribution of CaO in the ZrO_2 lattice. Thus, an extra amount of energy is required to dissociate them for ionic conduction.

~~Wachtman~~⁵⁹ and Franklin⁶⁰ have pointed out that the oxygen vacancies are mostly bound to Ca ions in the CaO- ThO_2 system. This postulation was also supported by Kroger⁵² in his proposed imperfection model for the $\text{Zr}_{0.85}\text{Ca}_{0.15}\text{O}_{1.85}\text{V}_{0.15}$ solid solution. He maintained that the imperfections may interact by short-range forces through the formation of associates. The high binding energy, expected, combined with the high concentration in which Ca ions and oxygen vacancies are present in stabilized ZrO_2 , suggests that the majority of these imperfections are paired or clustered.

The effect of the heat treatment of the CaO- ZrO_2 solid solutions leading to the order-disorder transition of the Ca ions and oxygen vacancies in the system has been observed by Subbarao and Tien,²² Subbarao and Sutter,⁴⁶ and also by Wachtman and Corwin³⁸. Subbarao and his co-workers have observed that superlattice lines appeared in the X-ray diffraction pattern for specimens of the $\text{Zr}_{0.80}\text{Ca}_{0.20}\text{O}_{1.80}$ solid solution which had been annealed at 1000°C and that these superlattice lines disappeared when the specimens were reheated to 1400°C . They also observed that at temperatures below 1100°C , those specimens heated at 1000°C exhibited a lower conductivity than those heated at 1400°C . Beyond 1100°C , the

1000°C heat treated specimens exhibited a change in slope of the Arrhenius plot and became more conductive. On reheating the same specimens, the Arrhenius plot ^{has} ~~have~~ a straight line with a displacement of the curve to a higher conductivity at lower temperatures and joined the first curve at higher temperatures. They concluded that the ordered phase was less conductive and was transformed into the disordered phase at about 1100°C. Wachtman and Corwin have observed that there are variations in the internal friction peak height between unannealed specimens and specimens annealed at 1000°C for the CaO-ZrO₂ solid solutions. For ZrO₂ solid solutions containing 13 mole % or 16 mole % CaO, the internal friction peak height was decreased as the specimens were heated at 1000°C. These experimental observations have been interpreted as a consequence of the attraction of the oxygen vacancies to the Ca ions due to Coulombic forces.

The total dissociation energy observed in the present investigation varied from 0.22 to 0.42 eV, which is in the same order of magnitude as the energy calculated by Wachtman for the complete dissociation of an oxygen vacancy from the attraction of a Ca ion. A dissociation energy of 0.22 eV was also observed by Wachtman in his studies of the mechanical and electrical relaxation in ThO₂ solid solution containing 1.5 mole % CaO.

In view of the previous observations, it is apparent that the oxygen vacancies and the substitutional Ca ions in the CaO-ZrO₂ solid solution have a tendency to form pairs or clusters particularly at high temperatures. The true reaction temperature of the formation of solid solution during hot-pressing was found to be about 1750°C in the present investigation. Thus it is quite possible that due to the inhomogeneous

distribution of Ca ions, localized clustering effect in the solid solution would be predominant. As the specimens were annealed at about 1100°C, the clustering effect in the solid solution is minimized. The ionic conduction mechanism in the CaO-ZrO₂ solid solution is due to the migration of oxygen vacancies. In order to facilitate the migration of these vacancies, an extra amount of energy in addition to the energy of oxygen vacancy motion is therefore required to dissociate any pairs of clusters.

(C) Effect of Heat Treatment on the Oxygen Ion Diffusion in the CaO-ZrO₂ Cubic Solid Solution

The oxygen ion diffusion coefficients calculated from the electrical conductivity data for the Zr_{0.85}Ca_{0.15}O_{1.85} solid solution obtained in the present investigation were found to be comparable with those reported elsewhere. However, the activation energy for oxygen ion diffusion appeared to show a similar annealing temperature variation as that observed in the electrical conductivity measurements.

Kroger⁵² has pointed out that ionic conduction and oxygen diffusion probably take place by migration of the oxygen vacancy V_O's as neutral pairs (Ca_{Zr} V_O^x)_m; migration by way of the free vacancy centers V_O^{••} would introduce the association enthalpy into the activation energy of diffusion. For easy migration through the neutral defects to be possible, it is essential that the associated Ca ions and oxygen vacancies form a random pattern, but with the Ca ions near enough so that oxygen vacancies can jump from a position next to a calcium ion to another one. If ordering of the Ca ions and oxygen vacancies exists in the CaO-ZrO₂ solid solution it would decrease the oxygen diffusion coefficients.

Kroger has estimated that the association enthalpy has the form $(H_p / 2m)$. If the vibration entropy is not affected by the pairing and $m = 1$ for pairs, the value of $H_p = -2.7$ eV gives an association enthalpy of about -1.35 eV. However, if the ordering forms larger associates, (clusters instead of pairs), the value of m would be greater than 1, thus reducing the association enthalpy.

V. SUMMARY AND CONCLUSIONS

1. The cubic fluorite-type solid solution having composition 15 mole % CaO + 85 mole % ZrO₂ (Zr_{0.85} Ca_{0.15} O_{1.85}) can be prepared by hot-pressing the mixture of ZrO₂ and CaCO₃ powders at 1750°C and 4600 psi pressure for about 30 minutes.
2. The lattice parameter of the CaO-ZrO₂ cubic solid solution decreased in a linear relation with the annealing temperature as the specimens were annealed from 800°C to 1500°C.
3. At a constant temperature of 1100, 1300, 1400, and 1500°C, the lattice parameter of the cubic solid solution decreased rapidly with annealing time in the early stage and attained a constant value after sufficient time.
4. As the lattice parameter of the cubic solid solution decreased, the peak band frequency of the infrared absorption spectra of the same solid solution increased. A linear relationship between lattice parameter and band frequency was observed.
5. The peak band frequency of the infrared absorption spectra of the CaO-stabilized ZrO₂ solid solution shifted depending on the heat treatment of the specimen.
6. The lattice contraction or shrinkage of the unit cell in the CaO-ZrO₂ solid solution was attributed to the removal of interstitial oxygen ions from the lattice or possibly related to the existence of the inhomogeneous distribution of Ca ions in the solid solution.
7. In the temperature range 500-1400°C, the electrical conductivity can be represented by an Arrhenius-type expression $\sigma = \sigma_0 \exp\left(\frac{-E}{kT}\right)$ where the activation energy E for electric conduction varied depending on the heat treatment of the specimens after hot-pressing. The activation energy for conduction decreased as the specimens were annealed from 800°C

to 1100°C and increased as the specimens were annealed from 1200°C to 1500°C with a minimum activation energy for the specimens annealed at 1100°C.

8. Specimens annealed at 1100°C exhibited the lowest value of the activation energy for conduction. This value corresponded to the amount of energy required for the motion of the oxygen vacancy in the CaO-ZrO₂ system.
9. The excess energy observed in specimens annealed in other temperatures was interpreted as the extra amount of energy required to dissociate the oxygen vacancies from Ca ions forming pairs or clusters.
10. The dependence of the activation energy for the oxygen ion diffusion (diffusion coefficients, are calculated from the electrical conductivity data using the Nernst-Einstien equation) on the annealing temperature followed a trend similar to that observed in the electrical conductivity measurements.

VI. SUGGESTIONS FOR FUTURE WORK

The results obtained in the present investigation have, to some extent, been exploratory in nature. The various models proposed for explaining the experimental observations are hypotheses. In order to confirm these models or to extend the subject of this study, several topics are suggested. These topics include:

1. A more precise density measurement is required in order to confirm the oxygen interstitial model.
2. The annealing temperature can be extended up to 2000°C and substantiate the lattice contraction phenomenon observed in the temperature range of this study.
3. The effect of impurities on the kinetics of stabilization of ZrO_2 should be investigated.
4. A study of the reaction kinetics between CaO and ZrO_2 would be of interest to investigate using the reactive hot-pressing process for specimen preparation.

APPENDIX I

TABLE 1

Lattice Parameter-Annealing Temperature Data of the Three
Separate Series of Samples

Expt.No.	Specimen No.	Annealing		Lattice Parameter (Å)
		Temperature (°C)	Time (hrs.)	
4	30	800	1	5.1369
5	"	1100	14	5.1361
6	"	1400	14	5.1354
7	"	1500	14	5.1346
17	29	800	1	5.1358
18	"	1200	17	5.1353
19	"	1300	24	5.1352
20	"	1400	10	5.1351
42	73	800	1	5.1360
43	"	900	24	5.1358
44	"	1150	24	5.1355
45	"	1300	24	5.1353
46	"	1500	24	5.1350

Lattice Parameter - Annealing Temperature Data
of Most Measured Samples

Annealing		Specimen No.	Lattice Parameter (Å)			
Temperature (°C)	Time (hrs.)		Measured Values	Mean Values	Mean Deviation	Standard Deviation
800	1	29	5.1358	5.1363	-0.0005	± 0.0004
"	"	30	5.1369		+0.0006	
"	"	31	5.1359		-0.0004	
"	"	41	5.1365		+0.0002	
"	"	43	5.1359		-0.0004	
"	"	46	5.1363		0	
"	"	52	5.1368		+0.0005	
"	"	73	5.1360		-0.0003	
1100	14	30	5.1361	5.1356	+0.0005	± 0.0004
"	24	63	5.1354		-0.0002	
1200	17	29	5.1356	5.1356	0	± 0.00002
"	24	51	5.1357		+0.0001	
"	24	57	5.1356		0	
"	24	73	5.1355		-0.0001	
1300	24	29	5.1352	5.1352	0	± 0.0001
"	21	43	5.1353		+0.0001	
"	24	51	5.1349		-0.0003	
"	24	59	5.1353		+0.0001	
"	24	73	5.1353		+0.0001	
1400	25	31	5.1344	5.1349	-0.0005	± 0.0005
"	24	40	5.1354		+0.0005	
"	24	41	5.1344		-0.0005	
"	24	65	5.1352		+0.0003	
1500	14	30	5.1346	5.1350	-0.0004	± 0.0002
"	25	46	5.1351		+0.0001	
"	24	51	5.1350		0	
"	26	72	5.1352		+0.0003	
"	24	73	5.1350		0	

Lattice Parameter and Peak Band Frequency of the Infrared
Absorption Spectra of the CaO-Stabilized ZrO₂

Specimen No.	Annealing		Lattice Parameter (Å)	Band Frequency (cm ⁻¹)
	Temperature (°C)	Time (hrs.)		
31	800	1	5.1359	445
30	"	1	5.1369	440
41	"	1	5.1365	442
43	"	1	5.1359	445
56	"	25	5.1359	444
60	900	25	5.1356	446
62	1000	25	5.1354	448
63	1100	25	5.1354	448
57	1200	24	5.1355	447
43	1300	24	5.1353	449
59	"	24	5.1353	449
31	1400	15	5.1348	453
31	"	25	5.1344	455
30	1500	14	5.1346	454
51	"	24	5.1350	452

Lattice Parameter - Annealing Time Data
of Four Separate Series of Samples

Expt. No.	Specimen No.	Annealing		Lattice Parameter (\AA)
		Temperature ($^{\circ}\text{C}$)	Time (hrs.)	
59	67	no annealing	0	5.1361
60	"	1100	5	5.1360
61	"	"	12	5.1358
62	"	"	21	5.1358
63	"	"	48	5.1358
64	"	"	69	5.1359
21	43	800	1	5.1359
22	"	1300	5	5.1355
23	"	"	16	5.1355
24	"	"	21	5.1356
25	"	"	40	5.1356
26	"	"	61	5.1356
27	"	"	68	5.1355
28	46	800	1	5.1357
29	"	1400	4	5.1351
30	"	"	10	5.1350
31	"	"	14	5.1349
32	"	"	20	5.1345
33	"	"	25	5.1345
56	"	"	40	5.1345
55	"	"	65	5.1345
11	31	800	1	5.1359
12	"	1500	5	5.1352
13	"	"	10	5.1349
14	"	"	15	5.1348
15	"	"	20	5.1346
16	"	"	25	5.1344
57	"	"	44	5.1344
58	"	"	64	5.1344

Relative Decrease of Lattice Parameter with Annealing Time

Specimen No.	Tempera- ture (°C)	Lattice Parameter (Å)	Annealing Time		$\frac{a_0 - a_t}{a_0}$ $\times 10^{-4}$	Slope (k) 10^{-8} (sec. ⁻¹)
			(hrs.)	(sec. $\times 10^4$)		
67	1100	5.1361	0	0	0	2.86
		5.1360	5	1.80	0.1947	
		5.1358	12	4.32	0.5841	
		5.1358	21	7.56	0.5841	
43	1300	5.1359	0	0	0	4.72
		5.1356	5	1.80	0.5841	
		5.1355	16	5.76	0.7788	
		5.1355	21	7.56	0.7788	
40	1400	5.1357	0	0	0	14.50
		5.1351	4	1.44	1.1683	
		5.1350	10	3.60	1.3630	
		5.1349	14	5.04	1.5577	
		5.1345	25	9.00	2.3366	
31	1500	5.1359	0	0	0	21.00
		5.1352	5	1.80	1.3629	
		5.1349	10	3.60	1.9471	
		5.1348	15	5.40	2.1418	
		5.1346	20	7.20	2.5312	
		5.1344	25	9.00	2.9206	

Electrical Conductivity - Temperature Data Obtained at
Equilibrated Temperatures During the Heating Cycle

Spec. No.	Bulk Density (gm/cc)	Poro- sity (%)	Anneal- ing Temp. (°C)	Electrical Conductivity (ohm ⁻¹ -cm ⁻¹)					
				500°C	700°C	900°C	1100°C	1300°C	1400°C
61	4.466	17.0	800	1.54x10 ⁻⁵	2.84x10 ⁻⁴	2.83x10 ⁻³	1.95x10 ⁻²	7.66x10 ⁻²	1.60x10 ⁻¹
58	4.478	19.1	900	0.92x10 ⁻⁵	4.23x10 ⁻⁴	3.62x10 ⁻³	1.17x10 ⁻²	3.73x10 ⁻²	0.70x10 ⁻¹
64	4.489	19.4	1000	2.96x10 ⁻⁵	5.53x10 ⁻⁴	6.20x10 ⁻³	3.01x10 ⁻²	6.12x10 ⁻²	0.84x10 ⁻¹
66	4.504	18.8	1100	1.44x10 ⁻⁵	6.75x10 ⁻⁵	1.65x10 ⁻³	0.51x10 ⁻²	0.92x10 ⁻²	0.16x10 ⁻¹
69	4.429	18.8	1200	1.55x10 ⁻⁵	1.34x10 ⁻⁴	7.50x10 ⁻³	1.68x10 ⁻²	5.42x10 ⁻²	1.36x10 ⁻¹
70	4.500	18.3	1300	1.98x10 ⁻⁵	6.93x10 ⁻⁴	6.70x10 ⁻³	1.38x10 ⁻²	5.70x10 ⁻²	1.32x10 ⁻¹
74	4.593	17.8	1400	2.74x10 ⁻⁵	6.01x10 ⁻⁴	6.22x10 ⁻³	4.37x10 ⁻²	1.48x10 ⁻¹	1.23x10 ⁻¹
71	4.650	17.1	1500	1.95x10 ⁻⁵	1.32x10 ⁻³	1.13x10 ⁻²	3.38x10 ⁻²	1.65x10 ⁻¹	2.62x10 ⁻¹

Electrical Conductivity - Temperature Data With Measurements
Made Before and After Soaking at the Same Temperature

Spec. No.	Annealing Temp. (°C)	Soaking	Electrical Conductivity (ohm ⁻¹ - cm ⁻¹)					
			500 °C	700 °C	900 °C	1100 °C	1300 °C	1400 °C
61	800	before	1.39x10 ⁻⁵	2.79x10 ⁻⁴	2.89x10 ⁻³	1.92x10 ⁻²	7.76x10 ⁻²	1.55x10 ⁻¹
		after	1.54x10 ⁻⁵	2.84x10 ⁻⁴	2.83x10 ⁻³	1.95x10 ⁻²	7.66x10 ⁻²	1.60x10 ⁻¹
58	900	before	0.87x10 ⁻⁵	4.32x10 ⁻⁴	3.68x10 ⁻³	1.31x10 ⁻²	3.92x10 ⁻²	0.67x10 ⁻¹
		after	0.92x10 ⁻⁵	4.23x10 ⁻⁴	3.62x10 ⁻³	1.17x10 ⁻²	3.72x10 ⁻²	0.69x10 ⁻¹
64	1000	before	2.79x10 ⁻⁵	5.08x10 ⁻⁴	5.98x10 ⁻³	3.23x10 ⁻²	8.77x10 ⁻²	0.77x10 ⁻¹
		after	2.96x10 ⁻⁵	5.53x10 ⁻⁴	6.20x10 ⁻³	3.01x10 ⁻²	6.12x10 ⁻²	0.84x10 ⁻¹
66	1100	before	0.95x10 ⁻⁵	0.98x10 ⁻⁴	1.71x10 ⁻³	0.52x10 ⁻²	1.00x10 ⁻²	0.16x10 ⁻¹
		after	1.44x10 ⁻⁵	0.67x10 ⁻⁴	1.65x10 ⁻³	0.51x10 ⁻²	1.01x10 ⁻²	0.16x10 ⁻¹
69	1200	before	1.20x10 ⁻⁵	1.42x10 ⁻⁴	1.42x10 ⁻²	2.01x10 ⁻²	5.50x10 ⁻²	1.34x10 ⁻¹
		after	1.55x10 ⁻⁵	1.34x10 ⁻⁴	7.50x10 ⁻³	1.68x10 ⁻²	5.42x10 ⁻²	1.36x10 ⁻¹
70	1300	before	1.76x10 ⁻⁵	1.43x10 ⁻³	8.00x10 ⁻³	1.37x10 ⁻²	6.47x10 ⁻²	1.44x10 ⁻¹
		after	1.98x10 ⁻⁵	0.67x10 ⁻³	6.70x10 ⁻³	1.38x10 ⁻²	5.70x10 ⁻²	1.32x10 ⁻¹
74	1400	before	4.42x10 ⁻⁵	0.50x10 ⁻³	6.47x10 ⁻³	4.54x10 ⁻²	1.81x10 ⁻¹	3.06x10 ⁻¹
		after	2.74x10 ⁻⁵	0.60x10 ⁻³	6.22x10 ⁻³	4.37x10 ⁻²	1.48x10 ⁻¹	1.23x10 ⁻¹
71	1500	before	1.65x10 ⁻⁵	1.32x10 ⁻³	1.18x10 ⁻²	3.57x10 ⁻²	1.59x10 ⁻¹	2.82x10 ⁻¹
		after	1.91x10 ⁻⁵	1.32x10 ⁻²	1.13x10 ⁻²	3.38x10 ⁻²	1.65x10 ⁻¹	2.62x10 ⁻¹

Electrical Conductivity - Temperature Data With Measurements
Made During the Heating and Cooling Cycles

Spec No.	Anneal- ing Temp. (°C)	Cycle	Electrical Conductivity (ohm ⁻¹ - cm ⁻¹)					
			500 °C	700 °C	900 °C	1100 °C	1300 °C	1400 °C
61	800	Heating	1.54x10 ⁻⁵	2.84x10 ⁻⁵	2.83x10 ⁻³	1.95x10 ⁻²	7.66x10 ⁻²	1.60x10 ⁻¹
		Cooling	1.99x10 ⁻⁵	3.76x10 ⁻⁵	6.96x10 ⁻³	2.46x10 ⁻²	8.51x10 ⁻²	1.60x10 ⁻¹
58	900	Heating	0.92x10 ⁻⁵	4.23x10 ⁻⁴	3.62x10 ⁻³	1.17x10 ⁻²	3.73x10 ⁻²	0.70x10 ⁻¹
		Cooling	1.71x10 ⁻⁵	3.71x10 ⁻⁴	7.43x10 ⁻³	3.20x10 ⁻²	4.90x10 ⁻²	0.70x10 ⁻¹
64	1000	Heating	2.96x10 ⁻⁵	5.53x10 ⁻⁴	6.20x10 ⁻³	3.01x10 ⁻²	6.12x10 ⁻²	0.84x10 ⁻¹
		Cooling	0.53x10 ⁻⁵	3.26x10 ⁻⁴	4.74x10 ⁻³	0.82x10 ⁻²	4.73x10 ⁻²	0.84x10 ⁻¹
66	1100	Heating	1.44x10 ⁻⁵	0.67x10 ⁻⁴	1.65x10 ⁻³	0.51x10 ⁻²	0.91x10 ⁻²	0.16x10 ⁻¹
		Cooling	6.20x10 ⁻⁵	4.40x10 ⁻⁴	2.58x10 ⁻³	0.50x10 ⁻²	1.01x10 ⁻²	0.16x10 ⁻¹
69	1200	Heating	1.55x10 ⁻⁵	1.34x10 ⁻³	7.50x10 ⁻³	1.68x10 ⁻²	5.42x10 ⁻²	1.36x10 ⁻¹
		Cooling	1.21x10 ⁻⁵	1.40x10 ⁻³	7.60x10 ⁻³	1.72x10 ⁻²	5.94x10 ⁻²	1.36x10 ⁻¹
70	1300	Heating	1.98x10 ⁻⁵	6.93x10 ⁻⁴	6.70x10 ⁻³	1.38x10 ⁻²	5.70x10 ⁻²	1.32x10 ⁻¹
		Cooling	1.57x10 ⁻⁵	1.61x10 ⁻³	6.64x10 ⁻³	1.30x10 ⁻²	5.20x10 ⁻²	1.32x10 ⁻¹
74	1400	Heating	2.74x10 ⁻⁵	6.01x10 ⁻⁴	6.22x10 ⁻³	4.37x10 ⁻²	1.48x10 ⁻¹	1.23x10 ⁻¹
		Cooling	0.50x10 ⁻⁵	2.85x10 ⁻⁴	5.47x10 ⁻³	0.85x10 ⁻²	0.89x10 ⁻¹	1.23x10 ⁻¹
71	1500	Heating	1.95x10 ⁻⁵	1.32x10 ⁻³	1.13x10 ⁻²	3.38x10 ⁻²	1.65x10 ⁻¹	2.62x10 ⁻¹
		Cooling	1.20x10 ⁻⁵	1.39x10 ⁻³	0.86x10 ⁻²	2.61x10 ⁻²	1.24x10 ⁻¹	2.62x10 ⁻¹

Activation Energies for Electrical Conduction and for Oxygen Ion Diffusion in the $Zr_{0.85}Ca_{0.15}O_{1.85}$ Solid Solution

Specimen No.	Annealing		Activation Energy for Conduction (eV)		Activation Energy for Oxygen ion Diffusion (eV)
	Temperature (°C)	Time (hrs.)	Heating	Cooling	
34	800	1	1.14	1.28	
61	800	25	1.14	1.08	1.25
58	900	24	1.07	1.03	1.18
64	1000	24	1.00	1.12	1.12
66	1100	24	0.92	1.12	1.04
69	1200	24	1.03	1.07	1.14
70	1300	26	1.04	1.02	1.15
74	1400	24	1.09	1.23	1.20
76	1500	26	1.14	1.17	1.25

Summary of Lattice Parameter, Electrical Conductivity, Activation Energy for Electrical Conduction, and Method of Specimen Preparation of the $Zr_{0.85}Ca_{0.15}O_{1.85}$ Solid solution as Reported in the Literature

Author	Lattice Parameter (Å)	Electrical Conductivity at 1000 °C (ohm ⁻¹ cm ⁻¹)	Activation Energy (eV)	Method of Specimen Preparation
Hund ¹⁹	-	2.2×10^{-3}	1.21	Calcined ZrO_2 and $CaCO_3$ mixtures at 1200 °C for 2 hours, then sintered at 1460 °C for 5 hours.
Trombe & Foex ⁴¹	-	4.0×10^{-3}	-	Calcined ZrO_2 and $CaCO_3$ mixtures at 1300 °C.
Volechenkova & Pal'guev ²¹	-	2.7×10^{-3}	-	----
Kingery et al. ²⁵	5.131	2.3×10^{-2}	1.26	Calcined ZrO_2 and $CaCO_3$ mixtures at 1300 °C, then sintered at 2000 °C for 7 hours.
Rhodes & Carter ³⁰	-	2.6×10^{-2}	-	-----
Hathaway ⁴²	-	5.0×10^{-2}	1.17	Reacted 4.25 mole Zirconyl Chloride and 0.82 mole $CaCl_2$, precipitated solution and calcined at 870 °C for 3 hours.
Dixon et al. ⁴³	-	2.0×10^{-2}	1.30	Hot-pressed ZrO_2 and $CaCO_3$ mixtures at 1400 °C and 3000-5000 psi pressure.
Tien & Subbarao ²²	5.133	3.3×10^{-2}	1.17	Calcined ZrO_2 and $CaCO_3$ mixtures at 1350 °C for 24 hours, then sintered at 2000 °C for 2 hours followed by one week annealing at 1400 °C.
Present study	5.135	2.0×10^{-2}	1.14	Hot-pressed ZrO_2 and $CaCO_3$ at 1350 °C and 4600 psi pressure for 30 minutes and then annealed at 1500 °C for 24 hours.

Oxygen Ion Diffusion Coefficients Calculated from the
Electrical Conductivity Data.

Specimen No.	Annealing Temp. (°C)	Diffusion Coefficients (cm ² - sec ⁻¹)					
		500 °C	700 °C	900 °C	1100 °C	1300 °C	1400 °C
61	800	1.92×10^{-11}	4.46×10^{-10}	5.38×10^{-9}	4.33×10^{-8}	1.95×10^{-7}	4.34×10^{-7}
58	900	1.15×10^{-11}	6.64×10^{-10}	6.88×10^{-9}	2.60×10^{-8}	0.95×10^{-7}	1.89×10^{-7}
64	1000	3.69×10^{-11}	8.68×10^{-10}	1.18×10^{-8}	6.68×10^{-8}	1.56×10^{-7}	2.29×10^{-7}
66	1100	1.80×10^{-11}	1.06×10^{-10}	0.31×10^{-8}	1.14×10^{-8}	0.23×10^{-7}	0.44×10^{-7}
69	1200	1.94×10^{-11}	2.10×10^{-9}	1.42×10^{-8}	3.73×10^{-8}	1.38×10^{-7}	3.68×10^{-7}
70	1300	2.47×10^{-11}	1.09×10^{-9}	1.27×10^{-8}	3.06×10^{-8}	1.45×10^{-7}	3.58×10^{-7}
74	1400	3.42×10^{-11}	0.94×10^{-9}	1.18×10^{-8}	9.70×10^{-8}	3.77×10^{-7}	3.33×10^{-7}
71	1500	2.38×10^{-11}	2.07×10^{-9}	2.15×10^{-8}	7.52×10^{-8}	4.40×10^{-7}	7.10×10^{-7}

Apparent Porosity and Bulk Density of the Hot-pressed Specimens

Specimen No.	Annealing		Bulk Density (gm/cc)		Apparent Porosity (%)	
	Temperature(°C)	Time (hrs.)	Before Heat Treatment	After Heat Treatment	Before Heat Treatment	After Heat Treatment
51	800	1	4.641	-----	16.6	---
61*	800	26	4.489	4.506	17.0	18.0
45	900	20	4.374	4.341	21.8	21.7
58*	900	24	4.478	4.593	19.1	19.1
64*	1000	24	4.489	4.468	19.4	18.4
66*	1100	24	4.504	4.488	18.8	18.9
69*	1200	24	4.429	4.470	18.8	18.6
70*	1300	24	4.499	4.481	18.3	18.3
75	1300	23	-----	4.530	---	17.9
37	1400	10	4.520	4.547	17.0	16.9
74*	1400	24	4.593	4.544	17.8	17.3
71*	1500	24	----	4.650	----	17.1
53	900 + 1400	24 + 22	4.454	4.420	20.2	19.8
55	1100 + 1400	20 + 20	4.661	4.600	19.0	15.7

* Besides annealing, these specimens had been heated from 500 °C to 1400 °C for about 16 hours in electrical conductivity measurements.

True Density of the $Zr_{0.85}Ca_{0.15}O_{1.85}$ Solid Solution
Determined by the Pycnometric Method Using Distilled Water

Specimen No.	Annealing		True Density (grams/cc)			
	Temp. (°C)	Time (hrs.)	Measured values	Mean value	Deviation from mean	Standard deviation
56	800	26	5.635	5.588	+0.047	± 0.038
			5.619		+0.031	
			5.553		-0.035	
			5.548		-0.040	
60	900	25	5.596	5.563	+0.033	± 0.026
			5.563		0	
			5.530		-0.033	
62	1000	25	5.542	5.534	+0.008	± 0.007
			5.535		+0.001	
			5.525		-0.009	
63	1100	24	5.575	5.545	+0.030	± 0.027
			5.570		+0.025	
			5.524		-0.021	
			5.514		-0.031	
57	1200	24	5.583	5.566	+0.017	± 0.013
			5.563		-0.003	
			5.552		-0.014	
59	1300	24	5.558	5.534	+0.020	± 0.017
			5.533		-0.001	
			5.512		-0.022	
65	1400	25	5.609	5.545	+0.064	± 0.041
			5.560		+0.015	
			5.554		+0.009	
			5.457		-0.088	
72	1500	24	5.592	5.551	+0.041	± 0.044
			5.597		+0.046	
			5.510		+0.041	
			5.503		-0.048	

Theoretical Density Calculations from X-ray Data Assuming
 Oxygen Vacancy Model ($Zr_{0.85}Ca_{0.15}O_{1.85}$) and
 Oxygen Interstitial Model ($Zr_{0.85}Ca_{0.15}O_{2.00}$)

Specimen No.	Annealing Temp. (°C)	Lattice Parameter (Å)	Volume of Unit Cell (Å) ³	Theoretical Density (gm/cc)	
				Oxygen Vacancy Model	Oxygen Interstitial Model
56	800	5.1359	135.471	5.5465	5.6642
60	900	5.1356	135.450	5.5474	5.6651
62	1000	5.1354	135.432	5.5481	5.6658
63	1100	5.1354	135.432	5.5481	5.6658
57	1200	5.1354	135.432	5.5481	5.6658
59	1300	5.1353	135.424	5.5485	5.6661
65	1400	5.1352	135.416	5.5485	5.6661
72	1500	5.1352	135.4166	5.5485	5.6661

Estimation of Error

1. Lattice Parameter Values

The lattice parameter values obtained in this study were calculated according to Cohen's method. (see APPENDIX V). Because of the complexity of the calculation, it is difficult to determine the uncertainty in each step. However, an estimate of error has been obtained through the computer printed results. The accuracy of reading the positions of the diffracted lines was ± 0.05 mm. Thus two sets of data, one with addition of 0.05 mm to all readings and one with subtraction of 0.05 mm to all readings, were calculated using the same computer programme. The variation of printed values was about ± 0.0001 Å. The drift constant which is a measure of the total systematic error involved in the determination varied from 0.0001 to 0.0003 for all computations.

2. Electrical Conductivity Values

The electrical conductivity values obtained in this study were calculated according to the following equation: (see page 32 of this thesis)

$$\sigma = \frac{L I}{A V}$$

Now taking the natural logarithms and differentiating both sides the total error in the conductivity, which is additive is as follows:

$$\frac{\delta \sigma}{\sigma} = \frac{\delta L}{L} + \frac{\delta A}{A} + \frac{\delta I}{I} + \frac{\delta V}{V}$$

The possible uncertainties involved in the measurement of the above parameters are:

- a) the electrode separation in the specimen could be measured to within 0.1 mm in 5.0 mm long, hence

$$\frac{\delta L}{L} = \frac{0.1}{5.0} = 0.02$$

- b) the diameter of the specimen could be measured to within 0.1 mm in about 9.0 mm, hence

$$\frac{\delta A}{A} = \frac{2 \delta L}{L} = \frac{2(0.1)}{9.0} = 0.022$$

- c) the current passing through the circuit could be measured to within half a division in 30 divisions, hence

$$\frac{\delta I}{I} = \frac{0.5}{30} = 0.017$$

- d) the voltage drop across the specimen could be measured to within half a division in 30 divisions, hence

$$\frac{\delta V}{V} = \frac{0.5}{30} = 0.017$$

The total uncertainty in the electrical conductivity values is therefore approximately 0.076 or 7.6% in error.

3. Density Values

The density of the material was determined in grams/cc. The uncertainties involved in the density measurement are the weight and the volume of the material.

- a) The weight of the material could be obtained to within 0.001 gram in 2.500 grams, hence

$$\frac{\delta W}{W} = \frac{0.001}{2.500} = 0.0004$$

- b) the volume of the material could be determined to within 0.005 cc in about 0.450 cc, hence

$$\frac{\delta V}{V} = \frac{0.005}{0.450} = 0.0111$$

The total uncertainty in the density values is therefore approximately

$$\frac{\delta \rho}{\rho} = \frac{\delta W}{W} + \frac{\delta V}{V} = 0.0115 \text{ or } 1.2\%$$

Cohen's Method for Precise Lattice Parameter Calculation

(A) Cohen's Method

The precise lattice parameter of a cubic substance can be calculated in accordance with the Cohen's method⁵⁵.

If the X-ray diffraction pattern was made with a symmetrical back-reflection focusing camera, the correct extrapolation function is

$$\frac{\Delta d}{d} = k \phi \tan \phi \quad \dots\dots\dots(1)$$

By squaring the Bragg law and taking logarithms of each side and then differentiating, the following result is obtained:

$$\frac{\Delta \sin^2 \theta}{\sin^2 \theta} = \frac{-2 \Delta d}{d} \quad \dots\dots\dots(2)$$

substituting equation (1) into (2), the following is obtained:

$$\begin{aligned} \Delta \sin^2 \theta &= -2 k \phi \sin^2 \theta \tan \phi \\ &= -2 k \phi \cos^2 \phi \tan \phi \\ &= D \phi \sin 2\phi \quad \dots\dots\dots(3) \end{aligned}$$

Where D is a new constant.

The true value of $\sin^2 \theta$ for any diffraction line is given by the following expression:

$$\sin^2 \theta \text{ (true)} = \frac{\lambda^2}{4 a_0^2} (h^2 + k^2 + l^2) \quad \dots\dots\dots(4)$$

where a_0 , the true value of the lattice parameter, is the quantity to be determined, but

$$\sin^2 \theta \text{ (observed)} - \sin^2 \theta \text{ (true)} = \Delta \sin^2 \theta \quad \dots\dots\dots(5)$$

For each line on the pattern, by combining equations (3), (4), and (5), the following is obtained:

$$\sin^2 \theta \text{ (observed)} = \frac{\lambda^2}{4 a_0^2} (h^2 + k^2 + l^2) + D \phi \sin 2\phi$$

since $\sin^2 \theta = \cos^2 \phi$

therefore $\cos^2 \phi = C\alpha + A\delta \dots\dots\dots(6)$

where $C = \frac{\lambda^2}{4 a_0^2}$

$\alpha = (h^2 + k^2 + l^2)$

$A = \frac{D}{10}$

$\delta = 10\phi \sin 2\phi$

The experimental values of equation(6) are calculated for each of the n back-reflection lines used in the determination. The two normal equations needed to find C and A are found from equation (6) and are given as follows:

$\Sigma \alpha \cos^2 \phi = C \Sigma \alpha^2 + A \Sigma \alpha \delta$

$\Sigma \delta \cos^2 \phi = C \Sigma \alpha \delta + A \Sigma \delta^2$

The lattice parameter a_0 can therefore be computed from the C value. The value of A is a drift constant which is a measure of the total error involved in the determination.

Since $Cu K_{\alpha 1}$ and $K_{\alpha 2}$ are of different wavelengths, lines will consequently appear on the diffraction pattern as doublets. The wavelength λ varies from line to line, whereas in equation (6) λ is treated as a constant. The data must therefore be normalized to any wavelength by use of the proper multiplying factor before equation (6) can be used for calculation.

The normalizing factor for all lines to the $Cu K_{\alpha 1}$ wavelength is given as:

Normalizing factor = $\frac{\lambda^2 K_{\alpha 1}}{\lambda^2 K_{\alpha 2}} = \frac{(1.54051)^2}{(1.54433)^2} = 0.99505$

(B) Determination of the Reflecting Planes (hkl) in the X-ray Diffraction Photograph

The experimental values of $\alpha = (h^2 + k^2 + l^2)$ for each set of diffraction lines in the pattern were determined by the following formula:

$$\cos^2 \phi = \sin^2 \theta = \frac{\lambda^2}{4 a_0^2} (h^2 + k^2 + l^2)$$

$$\alpha = (h^2 + k^2 + l^2) = \frac{\cos^2 \phi}{\frac{\lambda^2}{4 a_0^2}}$$

Using Tien and Subbarao's data for $a_0 = 5.133 \text{ \AA}^{22}$, the reflecting planes obtained in the present investigation are given in the following Table. (results for Expt. # 2).

Line No.	ϕ	$\cos^2 \phi$	α	(hkl)
2	27° 11.9'	0.79107	35.1=(35)	(531)
4	25° 32.7'	0.81398	36.1=(36)	(442) (600)
6	17° 59.9'	0.90451	40.1=(40)	(620)
8	9° 36.3'	0.97219	43.2=(43)	(533)
10	3° 28.1'	0.99634	44.2=(44)	(622)

Derivation of the Nernst-Einstien Equation for the
Relationship Between Electrical Conductivity and
Diffusion Coefficient

(A) Derivation

The self-diffusion coefficient of an ion (or defect) i resulting from thermal agitation is given by the following expression:^{53,54}

$$d_i = \frac{u_i k T}{Z_i e} \dots\dots\dots(1)$$

where d_i = microscopic diffusion coefficient of ion i .

u_i = mobility (drift velocity per unit electric field)

Z_i = valence

e = electronic charge

k = Boltzman's constant

T = absolute temperature

The conductivity of ion i and its macroscopic diffusion coefficient are given by :

$$\sigma_i = Z_i e n_i u_i \dots\dots\dots(2)$$

$$D_i = \left(\frac{n_i}{N} \right) d_i \dots\dots\dots(3)$$

where σ_i = electrical conductivity due to motion of ion i

n_i = defect concentration (number of defects/unit vol.)

N = concentration of the kind of atoms involved in the defect motion

D_i = macroscopic diffusion coefficient

Combining equations (1), (2), and (3), the following is obtained:

$$\frac{D_i}{\sigma_i} = \frac{k T}{N (Z_i e)^2} \dots\dots\dots(4)$$

Since the macroscopic tracer diffusion coefficient D , as

determined from tracer experiments, is not identical to the macroscopic ionic diffusion coefficient, a correlation factor "f" in diffusion is therefore required, which is defined as:

$$f = \frac{D}{D_i} \dots\dots\dots(5)$$

The conductivity which is usually measured is the total conductivity σ , which is related to the conductivity due to motion of ions σ_i through a transport number t_i . The relation is expressed as :

$$\sigma_i = \sigma \cdot t_i \dots\dots\dots(6)$$

Combining equations (4), (5), and (6), the following is obtained:

$$\frac{D}{\sigma} = \frac{f t_i k T}{N (Z_i e)^2} \dots\dots\dots(7)$$

(B) Sample Calculation of Oxygen Ion Diffusion Coefficients from the Electrical Conductivity Data

f (correlation factor for fluorite structure) = 0.65

t_i (transport number for CaO-stabilized ZrO₂) = 1

k (Boltzman's constant) = 1.37×10^{-16} erg/°K

Z (oxygen valence) = 2

N (oxygen ions per cm³ for the Zr_{0.85} Ca_{0.15} O_{1.85} solid solution) = 5.5×10^{22}

e^2 (electronic charge, if conductivity is expressed in ohm⁻¹-cm⁻¹ the factor 10⁹ must be introduced to convert from the electromagnetic units) = $10^9 \times 2.5 \times 10^{-40}$

$$D = \frac{0.65 \times 1 \times 1.37 \times 10^{-16}}{5.5 \times 10^{22} \times 4 \times 10^9 \times 2.5 \times 10^{-40}} \sigma T$$

$$D = 1.62 \times 10^{-9} \sigma T \text{ cm}^2\text{-sec}^{-1}$$

Apparent Porosity and Bulk Density Determination
(ASTM-C20-46)⁵⁷

Apparent Porosity, (P)

The apparent porosity expresses as a percentage the relationship of the volume of the open pores of the specimen to its exterior volume and is calculated as follows:

$$P = \frac{W - D}{W - S} \times 100\%$$

Bulk Density, (B)

The bulk density, in grams per cubic-centimeter of a specimen is the quotient of its dry weight divided by the exterior volume, including pores and is calculated as follows:

$$B = \frac{D}{W - S}$$

Where W = saturated weight

S = suspended weight

D = dry weight

APPENDIX VIII

True Specific Gravity and True Density Determination

(ASTM-C135-47)⁵⁷

True Specific Gravity

The true specific gravity of a refractory material determined by pycnometer bottle is calculated in accordance with the following formula:

$$\text{Sp. Gr.} = \frac{(W - P)}{(W_1 - P) - (W_2 - W)}$$

where P = weight of the stoppered pycnometer

W = weight of the stoppered pycnometer and sample

W₁ = weight of the stoppered pycnometer filled with water

W₂ = weight of the stoppered pycnometer, sample, and water

True Density

The true density in grams per cubic-centimeter of the sample is calculated in accordance with the following relation:

True density = Specific Gravity x density of water

Theoretical Density Calculations of the CaO-ZrO₂
Solid Solutions for the Oxygen Vacancy Model and
the Oxygen Interstitial Model

The basic density equation for a cubic solid solution is expressed as ⁵⁵

$$\rho = \frac{1.66020 \cdot \Sigma A}{a^3}$$

$$\text{where } \Sigma A = n_{\text{Zr}} A_{\text{Zr}} + n_{\text{Ca}} A_{\text{Ca}} + n_{\text{O}} A_{\text{O}}$$

n = number of atoms per unit cell

A = atomic weight

a = lattice parameter of the unit cell.

The total number of cations (Zr⁴⁺ and Ca²⁺) per unit cell in the f.c.c. structure is

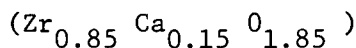
$$8 \left(\frac{1}{8}\right) + 6 \left(\frac{1}{2}\right) = 4$$

The total number of anions (oxygen ions) per unit cell in the fluorite structure is

$$4 \times 2 = 8$$

$$\text{Atomic weight of Zr} = 91.22; \text{Ca} = 40.08, \text{O} = 16.00$$

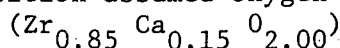
For the composition 15 mole% CaO + 85 mole% ZrO₂ assumed oxygen vacancy model



$$\begin{aligned} \Sigma A &= (4(0.85)) \times 91.22 + (4(0.15)) \times 40.08 + (4(1.85)) \times 16.00 \\ &= (3.4) \times 91.22 + (0.6) \times 40.08 + (7.4) \times 16.00 \\ &= 452.596 \end{aligned}$$

$$\rho = \frac{1.66020 \times 452.596}{(5.1359)^3} = 5.5465 \text{ grams/cc}$$

For the same composition assumed oxygen interstitial model.



$$\begin{aligned} \Sigma A &= (4(0.85)) \times 91.22 + (4(0.15)) \times 40.08 + (4(2.00)) \times 16.00 \\ &= (3.4) \times 91.22 + (0.6) \times 40.08 + (8.00) \times 16.00 \\ &= 462.196 \end{aligned}$$

$$\rho = \frac{1.66020 \times 462.196}{(5.1359)^3} = 5.6642 \text{ grams/cc}$$

1. A. E. Van Arkel, *Physica*, 4, 286 (1924).
2. O. Ruff and F. Ebert, *Z. auorg. U. allgem. chem.*, 180, 19 (1929).
3. W. M. Cohn, *J. Electrochem. Soc.*, 68, 65 (1935).
4. R. F. Domagala and D. J. McPherson, *J. Metals*, 6; *Trans. AIME*, 200, 238 (1954).
5. C. T. Lynch, F. W. Vahdiek, and L. B. Robinson, *J. Am. Ceram. Soc.*, 44(3), 147 (1961).
6. B. C. Weber and M. A. Schwartz, *Ber. deut. Keram. Ges.*, 34, 391 (1957).
7. F. A. Mumpton and R. Roy, *J. Am. Ceram. Soc.*, 43(5), 234 (1960).
8. P. Duwez and F. Odell, *J. Am. Ceram. Soc.*, 33, 274 (1950).
9. D. K. Smith and C. F. Cline, *J. Am. Ceram. Soc.*, 45(5), 249 (1962).
10. G. M. Wolten, *J. Am. Ceram. Soc.*, 46(9), 418 (1963).
11. E. Dow Whitney, *J. Electrochem. Soc.*, 112(1), 91 (1965).
12. G. M. Wolten, *J. Am. Ceram. Soc.*, 46(9), 420 (1963).
13. R. F. Geller and P. J. Yavorsky, *J. Research Natl. Bur. Standards*, 35(1), 87 (1945); RP 1662; *Ceram. Abstr.*, 24(10), 191 (1945).
14. R. S. Roth, *J. Am. Ceram. Soc.*, 39(7), 196 (1956).
15. P. Duwez, F. Odell, and F. H. Brown, Jr., *J. Am. Ceram. Soc.*, 35(5), 107 (1952).
16. B. C. Weber, H. J. Garrett, F. A. Mauer, and M. A. Schwartz, *J. Am. Ceram. Soc.*, 39(6), 197 (1956).
17. M. Hoch and Mool-Ray Mathen, *J. Am. Ceram. Soc.*, 45(8), 373 (1962).
18. T. W. Smoot and J. R. Ryan, *J. Am. Ceram. Soc.*, 46(12), 597 (1963).
19. F. Hund, *Z. Physik. Chem.*, 199, 142 (1952).
20. A. Dietzel and H. Tober, *Ber. Deut. Keram. Ges.*, 30(47), 71 (1953).
21. Z. S. Volchenkova and S. F. Pal'guez, *Trans. Inst. Electrochem.*, 1, 97 (1961).
22. T. Y. Tien and E. C. Subbarao, *J. Chem. Physics*, 39(4), 1041 (1963).
23. A. Cocco, *Chim. e ind. (Miland)*, 41, 882 (1959).
24. A. M. Diness and Rustum Roy, *Solid State Communication*, 3, 123 (1965).
25. W. D. Kingery, J. Pappis, M. E. Doty, and C. C. Hill, *J. Am. Ceram. Soc.*, 42(8), 393 (1959).
26. W. C. Hagel, "Oxygen Diffusion in Glasses and Oxide Crystals", presented at the Pittsburgh Meeting of the Electrochemical Society, April 17, 1963; Abstract: *J. Electrochem. Soc.*, 110(3), 63C (1963).
27. L. A. Simpson and R. E. Carter, *J. Am. Ceram. Soc.*, 49(3), 139 (1966).
28. R. J. Friauf, *J. Appl. Physics*, 33(1), 494 (1962).

29. John Crank, "Mathematics of Diffusion", Oxford Univ. Press, N.Y., 1956.
30. R. E. Carter and W. L. Roth, General Electric Report No. 63-R1-3479M, 1963.
31. R. E. Carter and W. H. Rhode, Bull. Am. Ceram. Soc., 41, 283 (1962).
32. H. Witzmann, H. H. Molbius and D. Gerlach, Z. Chem., 4(4), 154 (1964).
33. W. L. Baun and N. T. McDevitt, J. Am. Ceram. Soc., 46(6), 294 (1963).
34. W. L. Baun and N. T. McDevitt, J. Am. Ceram. Soc., 47(12), 622 (1964).
35. R. J. Dew, Jr., "Damping Capacity of Refractory Oxides Under Various Stress and Temperature Conditions", Sc. D. Thesis, MIT (1950), unpublished.
36. J. B. ^{Wachtman} ~~Watchman~~, Jr., W. E. Teft, D. G. Lam, Jr., and R. P. Stinchfield, Wright Patterson Air Development Center Technical Report 59-278 (1959).
37. Roger Chang, "Mechanical Properties of Engineering Ceramics", edited by W. W. Kriegel and H. Palmour III, (Interscience Publ. N.Y., 1961), p209.
38. J. B. ^{Wachtman} ~~Watchman~~, Jr., and W. C. Corwin, J. of Research of Natl. Bur. Standards -A, Physics and Chemistry 69A(5), 457 (1965).
39. K. Kiukkola & C. Wagner, J. Electrochem. Soc., 104(6), 379 (1957).
40. J. Weissbart and R. Ruka, J. Electrochem. Soc., 109(8), 723 (1962).
41. A. G. Buyers, J. Am. Ceram. Soc., 48(3), 122 (1965).
42. F. Trombe and M. Foex, Compt. Rend., 236, 1783 (1953).
43. J. M. Dixon, L. D. LaGrange, U. Merten, C. F. Miller, and J. T. Porter, II, J. Electrochem. Soc., 110(4), 276 (1963).
44. A. J. Hathaway, "Effect of Oxygen Vacancies on the Electrical Conductivity of Zirconia Solid Solutions", M. Sc. Thesis, Niagara University, Niagara Falls, N. Y., (1962).
45. H. A. Johansen and J. G. Cleary, J. Electrochem. Soc., 111(1), 100 (1964).
46. E. C. Subbarao and P. H. Sutter, J. Phys. Chem. Solids, 25, 148 (1964).
47. T. Y. Tien, J. Appl. Physics, 35(1), 122 (1964).
48. J. Weissbart and R. Ruka, Electrochem. Soc. Extended Abstract, #44, Oct. 1961.
49. Hermann Schmalzried, Z. Elektrochem., 66(7), 572 (1962).
50. C. B. Alcock and B. C. Steele, "Science in Ceramics", Vol. 2, edited by G. H. Stewart, (Academic Press, Inc., N. Y. 1965), p397.
51. R. W. Vest and N. M. Tallan, J. Appl. Physics, 36(2), 543 (1965).
52. F. A. Kroger, J. Am. Ceram. Soc., 49(4), 215 (1966).

53. W. D. Kingery, "Introduction to Ceramics", (John Wiley, Inc., N.Y., 1960), p647.
54. J. Bardeen and C. Herring, "Imperfections in Nearly Perfect Crystals", (John Wiley & Sons., Inc., N. Y., 1952), p261.
55. B. D. Cullity, "Elements of X-ray Diffraction", (Addison-Wesley Publishing Co., Inc., N. Y., 1956), p340.
56. K. Lark-Horovitz and V. A. Johnson, "Method of Experimental Physics, Vol. 6, part B, Solid State Physics", (Academic Press, Inc., N.Y., 1959), p33.
57. ASTM Standard, part 13, (American Society for Testing Materials, 1964 edition), p36 and p39.
58. K. J. Laidler, "Chemical Kinetics", (McGraw-Hill, Inc., 1965), p7.
59. J. B. ^{Watchman}~~Watchman~~, Jr., Physical Review, 13(12), 517 (1963).
60. A. D. Franklin, National Bureau of Standards, as cited by J. B. Watchman, Jr., in reference (59).